



Validation of GRASP algorithm product from POLDER/PARASOL data and assessment of multi-angular polarimetry potential for aerosol monitoring

5 Cheng Chen^{1, 2}, Oleg Dubovik¹, David Fuertes², Pavel Litvinov², Tatyana Lapyonok¹, Anton Lopatin²,
Fabrice Ducos¹, Yevgeny Derimian¹, Maurice Herman¹, Didier Tanré¹, Lorraine A. Remer³, Alexei
Lyapustin⁴, Andrew M. Sayer^{4, 5}, Robert C. Levy⁴, N. Christina Hsu⁴, Jacques Descloitres⁶, Lei Li^{1, 7},
Benjamin Torres¹, Yana Karol², Milagros Herrera¹, Marcos Herreras¹, Michael Aspetsberger⁸, Moritz
Wanzenboeck⁸, Lukas Bindreiter⁸, Daniel Marth⁸, Andreas Hangler⁸ and Christian Federspiel⁸

10

¹ Univ. Lille, CNRS, UMR 8518 - LOA - Laboratoire d'Optique Atmosphérique, F-59000 Lille, France

² GRASP-SAS, Villeneuve d'Ascq, France

³ Joint Center for Earth Systems Technology, University of Maryland, Baltimore, MD, USA

⁴ Universities Space Research Association, Columbia, MD, USA

15 ⁵ NASA Goddard Space Flight Center, Greenbelt, MD, USA

⁶ Univ. Lille, CNRS, CNES, UMS 2877 - AERIS/ICARE Data and Services Center, F-59000 Lille, France

⁷ State Key Laboratory of Severe Weather (LASW) and Key Laboratory of Atmospheric Chemistry (LAC),
Chinese Academy of Meteorological Sciences, CMA, Beijing, 100081, China

⁸ Cloudflight Austria GmbH, High Performance Computing, Linz, Austria

20

Correspondence to: Oleg Dubovik (oleg.dubovik@univ-lille.fr)

Abstract. Proven by multiple theoretical and practical studies, multi-angular spectral polarimetry is ideal
for comprehensive retrieval of properties of aerosols. Furthermore, a large number of advanced space
polarimeters have been launched recently or planned to be deployed in the coming few years (Dubovik et
25 al., 2019). Nevertheless, at present, practical utilization of aerosol products from polarimetry is rather
limited, due to the relatively small amount of polarimetric observations compared to photometric
observations, as well as challenges in making full use of the extensive information content available in
these complex observations. Indeed, while in recent years several new algorithms have been developed to
provide enhanced aerosol retrievals from satellite polarimetry, the practical value of available aerosol
30 products from polarimeters yet remains to be proven. In this regard, this paper presents the analysis of
aerosol products obtained by the Generalized Retrieval of Atmosphere and Surface Properties (GRASP)
algorithm from POLDER/PARASOL observations. After about a decade of development, GRASP has been
adapted for operational processing of polarimetric satellite observations and several aerosol products from



POLDER/PARASOL observations have been released. These updated PARASOL/GRASP products are
35 publicly available (e.g., <http://www.icare.univ-lille.fr>, www.grasp-open.com/products/), the dataset used in
the current study is registered under: <http://doi.org/10.5281/zenodo.3887265> (Chen et al., 2020).

The objective of this study is to comprehensively evaluate the GRASP aerosol products obtained
from POLDER/PARASOL observations. First, the validation of the entire 2005 - 2013 archive was
conducted by comparing to ground-based Aerosol Robotic Network (AERONET) data. The subjects of the
40 validation are spectral aerosol optical depth (AOD), aerosol absorption optical depth (AAOD) and single
scattering albedo (SSA) at 6 wavelengths, as well as Ångström exponent (AE), fine mode AOD (AODF)
and coarse mode AOD (AODC) interpolated to the reference wavelength 550 nm. Second, an inter-
comparison of PARASOL/GRASP products with the PARASOL/Operational, MODIS Dark Target (DT),
Deep Blue (DB) and Multi Angle Implementation of Atmospheric Correction (MAIAC) aerosol products
45 for the year 2008 was performed. Over land both satellite data validations and inter-comparisons were
conducted separately for different surface types, discriminated by bins of Normalized Difference
Vegetation Index (NDVI): <0.2 , $0.2 \leq$ and <0.4 , $0.4 \leq$ and <0.6 , and ≥ 0.6 . Three PARASOL/GRASP
products were analyzed: GRASP/HP (“High Precision”), Optimized, and Models. These different products
are consistent but were obtained using different assumptions in aerosol modeling with different accuracies
50 of atmospheric radiative transfer (RT) calculations. Specifically, when using GRASP/HP or Optimized
there is direct retrieval of the aerosol size distribution and spectral complex index of refraction. When using
GRASP/Models, the aerosol is approximated by a mixture of several aerosol components, each with their
own fixed size distribution and optical properties, and only the concentrations of those components are
retrieved. GRASP/HP employs the most accurate RT calculations, while GRASP/Optimized and
55 GRASP/Models are optimized to achieve the best trade-off between accuracy and speed. In all these
options, the underlying surface reflectance is retrieved simultaneously with the aerosol properties and the
radiative transfer calculations are performed “on line” during the retrieval.



All validation results obtained for the full archive of PARASOL/GRASP products show solid quality of retrieved aerosol characteristics. The GRASP/Models retrievals, however, provided the most solid AOD products, e.g. AOD (550 nm) is unbiased, has the highest correlation ($R \sim 0.92$) and the highest fraction of retrievals ($\sim 55.3\%$) satisfying the accuracy requirements of the Global Climate Observing System (GCOS) when compared to AERONET observations. GRASP/HP and GRASP/Optimized AOD products show a non-negligible positive bias (~ 0.07) when AOD is low (< 0.2). On the other hand, the detailed aerosol microphysical characteristics (AE, AODF, AODC and SSA, etc.) provided by GRASP/HP and GRASP/Optimized correlate generally better with AERONET than do the results of GRASP/Models. Overall, GRASP/HP processing demonstrates the high quality of microphysical characteristics retrieval versus AERONET. Evidently, GRASP/Models approach is more adapted for retrieval of total AOD, while the detailed aerosol microphysical properties are limited when a mixture of aerosol models with fixed optical properties are used.

The results of a comparative analysis of PARASOL/GRASP and MODIS products showed that, based on validation against AERONET, the PARASOL/GRASP AOD (550 nm) product is of similar and sometimes of higher quality compared to the MODIS products. All AOD retrievals are more accurate and in good agreement over ocean. Over land, especially over bright surfaces, the retrieval quality degrades and the differences in total AOD products increase. The detailed aerosol characteristics, such as AE, AODF and AODC from PARASOL/GRASP are generally more reliable, especially over land. The global inter-comparisons of PARASOL/GRASP versus MODIS showed rather robust agreement, though some patterns and tendencies were observed. Over ocean, PARASOL/Models and MODIS/DT AOD agree well with the correlation coefficient of 0.92. Over land, the correlation between PARASOL/Models and the different MODIS products is lower, ranging from 0.76 to 0.85. There is no significant global offset; though over bright surfaces MODIS products tend to show higher values compared to PARASOL/Models when AOD is low, and smaller values for moderate and high AODs. Seasonal means suggest that PARASOL/GRASP products show more biomass burning aerosol loading in central Africa and dust over the Taklamakan



Desert, but less AOD in the northern Sahara. It is noticeable also that the correlation for the data over AERONET sites is somewhat higher, suggesting that the retrieval assumptions generally work better over
85 AERONET sites than over the rest of the globe. One of the potential reasons may be that MODIS retrievals, in general, rely more on AERONET climatology than GRASP retrievals.

Overall, the analysis shows that the quality of AOD retrieval from multi-angular polarimetric observations like POLDER is at least comparable to those of single-viewing MODIS-like imagers. At the same time, the multi-angular polarimetric observations provide more information on other aerosol
90 properties (e.g. spectral AODF, AODC, AE), as well as additional parameters such as AAOD and SSA.

1 Introduction

Over the past few decades, satellite remote sensing has provided essential advances in understanding the global distribution of atmospheric aerosols (Kaufman et al., 2002; Remer et al., 2008) and constraining aerosol climate effects (Bellouin et al., 2005; Myhre, 2009; Yu et al., 2006). Nevertheless,
95 aerosol effects remain the largest contributor to forcing uncertainty according to the Intergovernmental Panel on Climate Change (IPCC) assessments (Boucher et al., 2013). Over the past few decades, satellite remote sensing techniques have developed rapidly and extensively, and various (primarily photometric) instruments have been developed and deployed to monitor atmospheric aerosols from space (Bréon et al., 2011; Dubovik et al., 2019; King et al., 1999; Kokhanovsky et al., 2015; Li et al., 2009; Tanré et al., 2011).
100 While the design and capabilities of the photometric observations are constantly evolving, the greatest improvement has been in the form of Multi-Angular multi-spectral Polarimetry (MAP) measurements (Hansen et al., 1995; Knobelspiesse et al., 2012; Mishchenko et al., 2004; Waquet et al., 2009; Tanré et al., 2011). MAP measurements have enough inherent information content to greatly improve our understanding about aerosol properties. Several space-borne polarimeters have already been deployed and more advanced
105 versions will be deployed soon (Dubovik et al., 2019). In addition, there are many airborne versions of orbital polarimeters that have operated during field campaigns, which can be used to verify and improve the



retrieval concepts (e.g. Knobelspiesse et al., 2020). Although the overall volume of polarimetric observations remains small compared to photometric observations, the potential for rapid advancement is large.

110 Several factors contribute to the current limited visibility of MAP observations and algorithms including: (i) limited amount of polarimetric observations in comparison to photometric ones, (ii) general complexity of polarimetric observations, and (iii) consequent challenges in developing capable retrieval algorithms. As a result, at present, there is a lack of extensive aerosol products from satellite MAPs that attract the aerosol science community. This tendency is especially evident by the contrast with the increase
115 of constantly improved aerosol products from mono- and bi- viewing photometric images. For example, the archive of most popular Moderate Resolution Imaging Spectroradiometer (MODIS) observations has been processed using many different algorithms, and NASA distributes three complementary MODIS aerosol products: Dark Target (DT) by Remer et al. (2005) and Levy et al., (2013), Deep Blue by Hsu et al. (2004, 2006, 2013) and Multi Angle Implementation of Atmospheric Correction (MAIAC) by Lyapustin et al.
120 (2018). Similarly, significant effort has been directed to improve aerosol products from European ENVISAT satellite platform observations in frame of Climate Change Initiative (CCI) projects of European Space Agency (e.g. see de Leeuw et al., 2015; Holzer-Popp et al., 2013; Popp et al., 2016). As a result, the product archives of MEdium Resolution Imaging Spectrometer (MERIS) and especially Advanced Along-Track Scanning Radiometer (AATSR) missions are constantly updated and improved.

125 To date, only one space-borne MAP has a long and wide enough coverage to advance aerosol science. The Polarization and Directionality of the Earth's Reflectances (POLDER) instrument was designed and developed by the French space agency Centre National d'Études Spatiales (CNES) to measure the spectral directional polarized solar radiation reflected by the Earth-atmosphere system (Deschamps et al., 1994). POLDER-1 and -2 flew on board of the Japanese Advanced Earth Observing
130 Satellites (ADEOS) platforms ADEOS-I and -II from November 1996 till June 1997 and from April 2003 till October 2003 correspondingly. Unfortunately, due to the failures of the platforms' solar panels, the



POLDER-1 and -2 have rather a limited time series of observations. POLDER-3 was launched in December 2004 on PARASOL (Polarization & Anisotropy of Reflectances for Atmospheric Sciences coupled with Observations from a Lidar) platform developed by CNES. POLDER-3/PARASOL (hereafter
135 PARASOL), was operational from March 2005 till October 2013 within the A-Train constellation, which is making nearly contiguous observations of many facets of the Earth system through a series of low-orbiting satellites (e.g. MODIS/AQUA, CALIOP/CALIPSO, OMI/AURA) (Parkinson, 2003; Schoeberl et al., 2006; Tanré et al., 2011; Winker et al., 2010). The PARASOL imager has 3 gaseous absorption channels (763, 765 and 710 nm), in addition to 6 channels (443, 490, 565, 670, 865 and 1020 nm) measuring the total
140 radiance, and 3 channels (490, 670 and 865 nm) measuring the polarization. The number of viewing angles is similar for all spectral channels varying from 14 to 16 depending on solar zenith angle and geographical location. PARASOL provided global coverage about every 2 days with a nadir spatial resolution ~6 km (Tanré et al., 2011).

Several POLDER-1, 2 and PARASOL aerosol products were developed by the science team at
145 LOA (Laboratoire d'Optique Atmosphérique, Lille, France). Hereafter, we refer to this aerosol product as POLDER/Operational or Operational. The initial POLDER/Operational aerosol retrieval over ocean by Deuzé et al. (1999) provided total Aerosol Optical Depth (AOD) from the measured total and polarized radiances at 670 and 865 nm with expected accuracy of $\pm 0.05 \pm 0.05 \text{AOD}$ (Goloub et al., 1999). The updated algorithm by Herman et al. (2005) provided AOD of fine and coarse modes and, when geometrical
150 conditions are optimal (scattering angle ranging between 90° - 160°), the spherical/non-spherical separation of coarse mode particles (Herman et al., 2005). Over land, the algorithm by Deuzé et al. (2001) retrieves only fine (“accumulation”) mode AOD (AODF) using only polarized light at two wavelengths (670 and 865 nm) to capitalize on the small and fairly neutral polarized reflectance typical of land surfaces (Deuzé et al., 2001; Herman et al., 1997). These algorithms were designed to utilize the benefits of MAP information
155 within the framework of a conventional MODIS like Look-up-Table (LUT) approach (Tanré et al., 1997; Kaufman et al. 1997) and did not intend to extend substantially the set of retrieved parameters. Moreover,



over land the POLDER/Operational retrieval provided only AODF while MODIS algorithms derives the total AOD.

The Generalized Retrieval of Atmosphere and Surface Properties (GRASP) algorithm considered

160 here was developed to further exploit the aerosol information content of POLDER spectral multi-angular polarization measurements (Dubovik et al., 2011, 2014). The algorithm allows for a large number of unknown parameters and retrieves a set of parameters affecting measurements at all wavelengths, all angles, and all states of polarization using the multi-term least square method (Dubovik, 2004). As will be later described in detail in section 2.1, GRASP does not utilize pre-calculated LUTs but instead searches in a
165 continuous space for the solutions and optimizes the statistical properties of the obtained retrieval. The GRASP algorithm derives an extended set of aerosol parameters from POLDER data, including spectral AOD, spectral Aerosol Absorption Optical Depth (AAOD), spectral AODF, spectral AODC, particle size distribution, Single Scattering Albedo (SSA), complex refractive index, fraction of spherical particles, etc. (see Table 1 and discussion in the next Section). The full archives of POLDER-1, 2 and PARASOL were
170 processed with GRASP and the resulting datasets are available for public at the official GRASP algorithm website (www.grasp-open.com) and the AERIS/ICARE Data and Services Center (<http://www.icare.univ-lille.fr>).

This paper presents and discusses new publicly-available aerosol products obtained from POLDER observations, which represent the longest to date satellite MAP record (Tanré et al., 2011; Dubovik et al.,
175 2019). Specifically, the discussion focuses on a new extended aerosol product generated by the recently developed GRASP algorithm (Dubovik et al., 2011, 2014). Here we perform quantitative analysis of PARASOL/GRASP aerosol products (the longest POLDER data set) through validation with AERONET reference data, as well as by comparisons with the POLDER/Operational product and the widely used MODIS DT, DB and MAIAC aerosol products. The analysis pursues two objectives. The first is to
180 understand the accuracy and value of each PARASOL/GRASP aerosol product. The second objective is to clarify the specifics, advantages, and shortcomings of MAP aerosol products compared to those from



photometric mono-viewing imagers. Thus, the analysis provides useful information for the aerosol community to meet the future challenge of accurate aerosol monitoring in the coming era of polarimetric missions. Over the next few years, we expect deployment of a number of new and existing satellite and
185 airborne MAPs including 3MI (Multi-View Multi-Channel Multi-Polarization Imaging), DPC (Directional Polarimetric Camera), Aerosol-UA (Ukraine), PACE (Plankton, Aerosol, Cloud, ocean Ecosystem), AirHARP (Airborne Hyper-Angular Rainbow Polarimeter), AirMSPI (Airborne Multi-angle SpectroPolarimeter Imager), **SPEX** (Spectro-Polarimetric Experiment), RSP (Research Scanning Polarimeter), etc. (Dubovik et al., 2019; Fougnie et al., 2018; Fu et al., 2020; Gao et al., 2020; Hasekamp et al., 2019; Knobelspiesse et al., 2020; Li et al., 2018; Milinevsky et al., 2019; Puthukkudy et al., 2020; Remer et al., 2019). **By providing a comprehensive analysis of PARASOL/GRASP products, we prove that the aerosol community can utilize the new era of MAP measurements.**

2 Data description and validation approach

The analysis compares several satellite data products. From POLDER, we have both the products of
195 the Operational algorithm and the GRASP retrieval. From MODIS, we utilize products generated by three different algorithms (DT, DB, and MAIAC). For all satellite products, validation is based on AERONET observations and retrievals.

2.1 POLDER/GRASP aerosol products

GRASP is a new-generation algorithm developed for deriving extensive aerosol properties from all
200 varieties of remote sensing instruments. The overall concept of the algorithm is described by Dubovik et al. (2014), while specific technical aspects are detailed in Dubovik et al. (2011). GRASP is based on highly advanced statistically optimized fitting implemented as multi-term least square minimization (Dubovik, 2004) which had earlier been successfully implemented for aerosol retrievals from ground-based AERONET radiometers (Dubovik and King, 2000; Dubovik et al., 2000, 2002a, 2002b, 2006). GRASP
205 inherits many methodological aspects in numerical inversion and aerosol modeling from the AERONET



retrieval developments. In fact, all retrieval set-ups including modeling of aerosol microphysical and optical properties, surface reflectance, numerical inversion, utilization of multiple a priori constraints, etc. can be realized using GRASP. At the same time, the GRASP concept and algorithm are highly flexible and versatile. GRASP includes several additional original features, and enables the implementation of advanced
210 retrieval scenarios. A unique aspect of GRASP is that it can perform radiative transfer (RT) computations fully accounting for multiple interactions of the scattered solar light in the atmosphere, and that it can perform it online without the use of traditional LUTs.

The GRASP retrieval can utilize whatever information content is available. If there is sufficient information content of the observations, GRASP will find the aerosol solutions. In the case of any currently
215 operational observations, GRASP can make optimal assumptions to constrain the solution. For example, GRASP can retrieve both aerosol and underlying surface properties simultaneously from satellite observations using additional a priori constraints on the spectral variability of land Bidirectional Reflection Distribution Function (BRDF). Or (probably the most essential methodological novelty) it can operate by relying on the multi-pixel concept wherein the statistically optimized retrieval is performed simultaneously
220 for a large group of pixels (Dubovik et al., 2011). This feature brings additional possibilities for improving the accuracy of satellite retrievals by using known constraints on the inter-pixel variability of retrieved aerosol and surface reflectance parameters. As a result, using this methodology GRASP provides reliable retrievals of detailed aerosol properties that traditionally have been difficult to obtain from satellites, for example, spectral AOD and AAOD over land including very bright deserts. The GRASP algorithm source
225 code and detailed documentation are available from <https://www.grasp-open.com>.

It should be noted that GRASP is a flexible inversion algorithm that can be applied to a wide variety of satellite, ground-based and laboratory observations. It has already been applied to ground-based AERONET photometers and LiDARs (Benavent-Oltra et al., 2017, 2019; Hu et al., 2019; Lopatin et al., 2013; Titos et al., 2019; Tsekeri et al., 2017), sky cameras (Román et al., 2017), polar-nephelometer data
230 (Espinosa et al., 2017, 2019; Schuster et al., 2019), and surface measurements of AOD (Torres et al., 2017).



In addition, GRASP is being used for several satellite instruments; aerosol products were generated for POLDER observations (discussed here) and for MERIS/Envisat, and there are ongoing developments for producing GRASP aerosol products from Sentinel-3 and -5P observations and operational aerosol retrievals for future Sentinel-4 and 3MI/Metop missions. GRASP is constantly being updated to produce many user-oriented products such as estimates of covariance matrices (Herrera et al., in preparation, 2020), direct radiative forcing (Derimian et al., 2016), and so on.

For POLDER, GRASP utilizes radiance and polarization observations from all available spectral channels with minor gaseous absorption, i.e. for total radiance 5 channels for POLDER-1 and -2, and 6 for PARASOL, and for polarized radiances (3 spectral channels for all instruments). The retrieval uses a unique global set of constraints (no location-specific assumptions) and a single initial guess globally. GRASP performs radiative transfer computations fully accounting for multiple interactions of the scattered solar light in the atmosphere on-line without using a traditional LUT. Since these RT computations are complex and time consuming, significant effort has been put into optimization and acceleration of the code for operational processing of voluminous datasets. At present, the speed of GRASP retrieval is appropriate for processing the full archive of POLDER observations at native resolution (POLDER-1 and -2 at ~7 km and PARASOL at ~6 km) using rather moderate computing resources, e.g. 3-4 sec/pixel for GRASP/HP, 0.3-0.5 sec/pixel for GRASP/Optimized and 0.1-0.2 sec/pixel for GRASP/Models, in a single core processor (the description of GRASP/HP, GRASP/Optimized and GRASP/Models will be detailed further in this section).

Since GRASP has been designed for use with different observations, it allows a variety of different possibilities on modeling aerosol scattering, surface reflectance and generally on implementing atmospheric radiative transfer calculations. As a result, different configurations of the atmospheric forward model can be used even for interpretation of the same data (as is the case here with POLDER). Currently, the full POLDER/PARASOL data archive is processed by GRASP using the three following retrieval configurations:



- 1) PARASOL/GRASP «optimized» (in the sense that radiative transfer calculations were optimized to find the best trade-off between speed of processing and accuracy of results);
- 2) PARASOL/GRASP «high-precision» (radiative transfer calculations with high precision were used).
- 260 3) PARASOL/GRASP «models» (the simplest, fastest processing; aerosol is assumed to be external mixture of several aerosol models).

The «optimized» and «high-precision» are different only by the precision of the RT calculations, while conceptually they are the same: aerosol size distribution, spectral values of complex index of refraction, fraction of spherical particles and the Aerosol Layer Height (ALH), are retrieved simultaneously with the
265 surface BRDF and Bidirectional Polarization Distribution Function (BPDF) parameters. The retrievals were performed using one aerosol component model with 5 bins of the size distribution and spectrally dependent complex refractive index. The aerosol vertical distribution was modeled using an exponential profile and scale height was retrieved. The details of implementation are discussed by Dubovik et al. (2011). The «models» approach uses different assumption for modeling aerosol properties (surface treatment is the
270 same as above): aerosol is assumed to be an external mixture of several aerosol components and only their concentrations are retrieved together with ALH and spectral BRDF/BPDF parameters. The size distribution, complex refractive index and non-sphericity parameter for each aerosol component are derived from the results of AERONET aerosol climatology for the main distinct aerosol types (Dubovik et al., 2002b) and improved in a series of sensitivity tests with satellite data. For retrievals over land, GRASP
275 retrieves the parameters of the Ross-Li BRDF (Li and Strahler, 1992; Ross, 1981) and BPDF (Maignan et al., 2009) models under assumption that the retrieved parameters are spectrally smooth (the strength of smoothness is different for each parameter) (Litvinov et al., 2011a, 2011b). For retrievals over ocean, the wind speed and a spectrally dependent Lambertian albedo are included in the state vector. It should be noted that “models” approach firstly was intended to be used for mono viewing satellite observations such
280 as those from MERIS/Envisat. However, once the approach was tested with PARASOL data, the obtained



results were quite appealing especially in conditions of low aerosol loading, motivating the generation of PARASOL/GRASP «models» archive that is included in the consideration here.

The three archives (Optimized, HP and Models) are released publicly and can be found at the AERIS/ICARE Data and Services Center (<http://www.icare.univ-lille.fr>) and at GRASP-OPEN website
285 (<https://www.grasp-open.com/products/>) in slightly different formats. The AERIS/ICARE is the official distributor of POLDER Level-1 and -2 data and allows the user to dive into the data using a web tool, which plots the results online. The AERIS/ICARE provides detailed visualization of the data, while GRASP-OPEN site is faster in releasing new products but with no visualization. The original PARASOL/GRASP retrievals are stored at Level-1, Level-2 and -3 products and are publicly available in
290 the form of daily, monthly, seasonal, yearly and climatological datasets. The Level-2 data contain full resolution data filtered following established quality criteria. Level 3 data is aggregated into a 0.1° and 1° grid box using the sinusoidal projection from Level-2 data. The list of retrieved aerosol parameters, as well as derived aerosol characteristics can be found in the Table 1. In this study, we adopt the current latest version of Optimized, HP (v1.2) and Models (v2.1) products.

295

[Table 1]

In addition to the PARASOL/GRASP products, all observations of POLDER-1 and -2 were also processed (using a single GRASP/Models approach). These data records are much shorter than PARASOL and therefore not included in the following analysis. However, based on limited comparisons (not presented here), the quality of the POLDER-1 and -2/GRASP retrievals is expected to be similar to those of
300 PARASOL/GRASP retrievals. Also, recently a new “GRASP/Component” approach has been developed (Li et al., 2019, 2020a, 2020b). This approach retrieved the size resolved fractions of aerosol components representing the different composition species, like black carbon, brown carbon, fine/coarse mode non-absorbing soluble and insoluble, coarse mode absorbing and aerosol water. The retrieved fractions drive the aerosol spectral index of refraction in modeling atmospheric radiances. This provides a fourth retrieval



305 archive; however, the results have not yet been fully analyzed and are not released in a user friendly format,
so the GRASP/Component data set will not be considered in this study.

PARASOL/GRASP aerosol products have already appeared in many studies, i.e. validation (Tan et al., 2019; Wei et al., 2019, 2020), data assimilation (Chen et al., 2018, 2019), AOD products merging (Li et al., 2020; Sogacheva et al., 2020). Despite these preliminary applications of the products, no systematic
310 evaluation of the global PARASOL/GRASP aerosol products has been published. Moreover, most early studies are based on the GRASP/Optimized products, which were released first. The evaluation of PARASOL/GRASP surface properties, as well as aerosol microphysical parameters (size distribution, complex refractive indices, fraction of spherical particles), and aerosol layer height, will be the subject of separate studies.

315 2.2 MODIS Dark Target, Deep Blue and MAIAC aerosol products

The MODIS sensors on board TERRA since 2000 (overpass ~10:30 local) and AQUA since 2002 (overpass ~13:30 local) provide near-global coverage twice per day. In this study, we will employ products from MODIS/AQUA only, which is on the same A-Train afternoon constellation orbit as PARASOL. MODIS has a wider swath of 2330 km compared to ~1600 km of PARASOL, 36 spectral channels ranging
320 from 410 to 15000 nm and higher spatial resolution for cloud mask. There are 3 mature aerosol products produced operationally and distributed by NASA: *Dark Target*, *Deep Blue* and *MAIAC*.

MODIS Dark Target

The Dark Target (DT) algorithm over land is based on an empirical surface reflectance relationship
325 between blue and red channels with the shortwave infrared (2113 nm) radiance. The AOD is retrieved by matching LUT values to observations at 466 nm, and then varying the weighting between two fixed aerosol models until the residual between LUT and observations are minimized at 645 nm. The main product is AOD at 553 nm with AOD reported at 466 nm, 645 nm and 2113 nm, consistent with the selected weighted aerosol model (Kaufman et al., 1997; Levy et al., 2007a, 2007b). Over ocean, the simplicity of the dark



330 ocean surface permits the retrieval of AOD and aerosol particle size (Tanré et al., 1997). In this situation
the algorithm chooses one fine mode out of four and one coarse mode out of five, along with the relative
weight between fine and coarse mode by minimizing the summed difference between LUT and
observations in six wavelengths (550, 660, 870, 1240, 1610, and 2130 nm) (Tanré et al., 1997; Remer et al.,
2005; Levy et al., 2013). The MODIS DT aerosol products are periodically updated to improve overall
335 performance (Levy et al., 2003, 2007a, 2007b, 2013; Remer et al., 2005; Gupta et al. 2016). The widely
recognized limitation of the DT algorithm is the complex spectral structure of bright land surfaces (e.g.
desert, bare soil, snow) that violates the assumptions of the empirical relationships between wavelengths
and increases uncertainty in the aerosol retrievals to unacceptable levels. Therefore, DT does not provide
coverage over these cases.

340

MODIS Deep Blue

The Deep Blue (DB) algorithm retrieves over both bright (except snow) and vegetated land
surfaces. It is able to retrieve over brighter surfaces than DT because it makes use of the much darker
surface reflectance in the deep blue (412 nm) channel (Hsu et al., 2004, 2006, 2013). Depending on the
345 processing path, determined by observed reflectance and vegetation indices, the algorithm will invoke
empirical spectral relationships of surface reflectance similar to DT (vegetation), rely on a pre-calculated
data base of surface reflectance (arid/deserts) or apply a hybrid method (urban surfaces). The MODIS DB
aerosol products have also gone through several version updates (Hsu et al., 2013; Sayer et al., 2015).
Within the MODIS official products, the DB algorithm is applied for only land aerosol retrieval. Over
350 vegetated surfaces DT tends to provide more retrievals in the tropics, and DB more retrievals at mid-
latitudes, due to different pixel selection and cloud screening criteria (Sayer et al., 2014).

MODIS MAIAC



The Multi Angle Implementation of Atmospheric Correction (MAIAC) algorithm has been
355 developed and applied to MODIS (Lyapustin et al., 2011a, 2011b, 2012, 2018), and is running
operationally in the NASA system. The MAIAC algorithm uses the minimum reflectance method to
dynamically characterize spectral ratios of the surface reflectance (which are prescribed in the DT) and
separate aerosol and surface contributions to the measurements. The accumulation of up to 16 days of the
last observations in the operational memory allows MAIAC to derive spectral surface BRDF. The MAIAC
360 aerosol product is available at higher spatial resolution of 1 km, in comparison to DT and DB that provide
aerosol products at 3 km and 10 km. As a more recent addition to the MODIS family of aerosol products
than DT and DB, MAIAC has shown itself to produce an AOD product as accurate or better than the older
algorithms over all types of land surfaces (Jethva et al., 2019), and thus offers a complementary/alternative
product to those from the original DT and DB algorithms.

365

All three MODIS algorithms (DT, DB and MAIAC) are developed based on LUT approaches with
a fixed certain number of aerosol models. Over ocean, DT assumes 9 aerosol models (4 fine models plus 5
coarse models); any retrieval corresponds to one of total 20 combinations of one fine mode and one coarse
mode (Levy et al., 2003; Remer et al., 2005; Tanré et al., 1997). Over land, DT algorithm adopts aerosol
370 models from AERONET retrievals, clustering down to three possible spherical fine-mode dominant models
(non-absorbing, moderately-absorbing and absorbing) and 1 spheroid coarse-mode dominant model (Levy
et al., 2007a). In addition, the fine- and coarse-mode dominant aerosol models over land are defined as a
function of season and location (Levy et al., 2013). The DB algorithm makes use of prescribed dust, and
smoke/sulfate aerosol models in the LUT (Hsu et al., 2013). For example, over vegetated surfaces, AE is
375 limited to some extent ($0.0 \leq AE \leq 1.8$), and fixed at 1.5 for low AOD conditions. Over bright arid/desert
surfaces the AE is limited to a maximum of 1.0 (Hsu et al., 2013; Sayer et al., 2013). A geographic
distribution of aerosol models is also adopted in the MAIAC algorithm, where the aerosol model
parameters are regionally, and may be parameterized as a function of AOD (dynamic models) for regions



with high humidity variations. The detailed description of the MAIAC regional aerosol models can be
380 found in Lyapustin et al., (2018). Hence, the MODIS aerosol products do not have the ability to retrieve
aerosol particle properties with known uncertainties, with the exceptions of size parameter (over ocean in
DT), SSA for dust (in DB), and AE (with known caveats).

In this study, MODIS Collection 6 aerosol products (MYD04_L2) from DT and DB algorithms
were acquired from the AERIS/ICARE Data and Services Center (<http://www.icare.univ-lille.fr>, last
385 [access: 30 August 2019](#)), where the unchanged NASA MODIS data are redistributed with enhanced
visualization. Note that the latest versions of DB and DT are Collection 6.1, although the differences
between the two versions are small on a large scale (Sayer et al., 2019) and do not significantly affect the
conclusions presented here. The latest MAIAC Collection 6 aerosol data (MAC19A2) is obtained from
NASA LAADS (Level-1 and Atmosphere Archive and Distribution System) DAAC (Distributed Active
390 Archive Center) (<https://ladsweb.modaps.eosdis.nasa.gov>, last access: 8 January 2020).

2.3 AERONET Dataset

The Aerosol Robotic Network (AERONET) is a global distributed network of well-calibrated sun-
sky photometers (Holben et al., 1998). By measuring direct Sun radiance, AERONET provides high
temporal (every 3 or 15 minutes in daytime depending on the operation mode of the instruments) multi-
395 wavelength AOD products with high reliable accuracy ($\sim\pm 0.01$ to ± 0.02) (Eck et al., 1999). Strict protocols
for the calibration and maintenance assure homogeneity among all its instruments. Due to its high data
quality, the AERONET AOD products are widely used as “ground truth” to evaluate satellite remote
sensing aerosol products (Bréon et al., 2011; Chu et al., 2002; Kahn et al., 2005; Liu et al., 2004; Remer et
al., 2005, 2002; Sayer et al., 2013).

400 In addition to direct Sun observations, AERONET radiometers conduct routine measurements of the
sky-scanning diffuse radiation. These observations are used to derive aerosol microphysical properties, e.g.
single scattering albedo, complex refractive index, size distribution and sphericity via Dubovik and King
(2000). The accuracy of the AERONET inversion products has been analyzed in many studies (Dubovik et



al., 2000; Sinyuk et al., 2020) and resulting recommendations were adopted for providing aerosol products
405 of highest quality (e.g. increase of quality of retrieval products with aerosol loading and range of observed
scattering angles). The microphysical properties provided by AERONET contribute to aerosol and climatic
applications. For example, the AERONET-derived aerosol particle property climatology (Dubovik et al.,
2002b), are used in some form in nearly in all satellite retrieval algorithms (including MODIS, see Levy et
al., 2007b; Lyapustin et al., 2018) and feed the climate models used to characterize aerosol climate effects
410 (Kinne et al., 2003; Sato et al., 2003).

In this study, the up-to-date AERONET Version 3 Level 2.0 dataset
(<http://www.aeronet.gsfc.nasa.gov>, last access: 3 September 2019) (Giles et al., 2019) with standard cloud
screening and quality control were used (Smirnov et al., 2000). We make use of all AERONET sites with
data during the POLDER/PARASOL archive (2005-2013). The AERONET direct-sun AOD, Ångström
415 Exponent, fine and coarse mode AOD from spectral deconvolution algorithm (SDA) (O'Neill et al., 2003),
AAOD and SSA products are chosen as references for satellite products validation.

2.4 Data quality assurance and matchup methodology

One of the main issues in satellite data validation is how to match the temporally-varying
AERONET point measurements with the spatially-varying satellite remote sensing aerosol products at over
420 pass time (Ichoku et al. 2002). This issue is compounded when multiple satellite products are involved that
vary from ~1 km to ~100 km pixel spatial resolution. There are some insightful studies (Kinne et al., 2013;
Schutgens et al., 2017) that quantify the AERONET sites spatial representativeness at the scales from ~50
km to ~300 km, which can be used for evaluation of chemical transport model simulations. However, the
spatial resolutions (~50 km to ~300 km) considered in those studies are seemingly too coarse for validation
425 of satellite products of 1 km for MAIAC, 10 km for DB and DT and ~6 km data from PARASOL/GRASP.

This study considers aerosol products at 10 km spatial resolution; that is the native resolution of
MODIS DB and DT products and seems to be the best compromise for comparing PARASOL/GRASP,
MODIS DT, DB and MAIAC results. Also, 10 km is utilized by the aerosol community and other datasets



(e.g. ESA CCI products mentioned earlier). That also was a reason for the generation of
430 PARASOL/GRASP Level 3 products. Thus, we adopted PARASOL/GRASP Level 3 daily 0.1° gridded
aerosol products, MODIS/AQUA Level 2 daily DT and DB 10 km products and the 1 km MODIS MAIAC
aggregated to 0.1° (MAIAC_0.1) and 0.01° (MAIAC_0.01) resolution for the inter-comparisons.
MAIAC_0.01 essentially represents the single 1 km pixel retrieval. The PARASOL/Operational L2 daily
aerosol product is directly used for validation, which is at 18.5 km x 18.5 km spatial resolution.

435 The strategies to select PARASOL/GRASP retrieval products with highest quality are presented in
Table 2. The land pixel is defined only if 100% of the 0.1° by 0.1° grid box has been identified as land, so
an ocean pixel must contain 0% land. Also, to guarantee proper coast elimination, the first pixel bordering
ocean and land is removed (see Fig. 1). We selected the more reliable retrievals using “Residual Relative”
(mean-root-square of relative error in fitting the measurements by the algorithm) for PARASOL/GRASP
440 products. We adopted the same threshold for GRASP/Optimized and GRASP/HP (0.05 over land and 0.1
over ocean). These thresholds are suggested for general users. For GRASP/Models approach, we did not
use any filter, since L3 products were generated from L2 using filtering. GRASP data filtering and quality
assurance schemes are likely to be improved in the future. Nonetheless, in this study we tried to avoid
additional filtering of PARASOL/GRASP L3 products, since most of users would utilize the data with no
445 screening or with a very straightforward filtering. For MODIS DT, DB and MAIAC products, we select the
data only with the highest Quality Assurance (QA) flag. The highest “Quality Index” was selected for
PARASOL/Operational products (Bréon et al., 2011). Any pixel with fitting residual higher than the
threshold for PARASOL or QA lower than the highest flag for MODIS will be set to “no data”.

[Table 2]

450 For validation with AERONET over land, we averaged all land satellite retrievals in a 3x3 window
for the gridded satellite data centered over the AERONET station. For ocean sites, in order to select pure
ocean pixels and keep reasonably high number of validation points, we decided to use a 9x9 window over
the AERONET site, using only pure ocean pixels. Any ocean pixels adjacent to land or land-ocean mixed



pixels were omitted as represented in Figure 1. The minimal number of accepted satellite data pixels within
455 the window is 1 over land and 41 over ocean; otherwise, the data were excluded from comparison. The
PARASOL/Operational product is treated a bit differently over ocean due to its relatively coarse resolution
(~18.5 km), with a similar land-like 3x3 window centered over the AERONET station.

The AERONET direct-sun AOD, AE, AODF and AODC data were averaged within ± 30 minutes of
the MODIS/AQUA and PARASOL overpass time, while AERONET SSA and AAOD (which have a lower
460 sampling frequency) are averaged within ± 180 minutes. In addition, AERONET station elevations greater
than 3600 m above mean sea level, satellite 3x3 or 9x9 data sets with AOD standard deviation greater than
0.05 between window pixels were excluded.

[Figure 1]

2.5 Considered metrics for comparison statistics

465 For quantifying the validation results, we used standard statistical parameters, including Pearson's
linear correlation coefficient (R), root mean square error (RMSE), slope and offset of linear regression and
bias.

$$R = \frac{\sum(O_{i,\text{satellite}} - \overline{O_{\text{satellite}}})(O_{i,\text{AERONET}} - \overline{O_{\text{AERONET}}})}{\sqrt{\sum(O_{i,\text{satellite}} - \overline{O_{\text{satellite}}})^2 \sum(O_{i,\text{AERONET}} - \overline{O_{\text{AERONET}}})^2}} \quad (1)$$

$$\text{RMSE} = \sqrt{\frac{\sum_{i=1}^N (O_{i,\text{satellite}} - O_{i,\text{AERONET}})^2}{N}} \quad (2)$$

470 $\text{BIAS} = \frac{1}{N} \sum_{i=1}^N (O_{i,\text{satellite}} - O_{i,\text{AERONET}})$ (3)

where N is the number of matched data points i ; $O_{\text{satellite}}$ represents the observations from satellite, and
 O_{AERONET} represents the referenced observations from AERONET; $\overline{O_{\text{satellite}}}$ and $\overline{O_{\text{AERONET}}}$ are the mean
value for satellite and AERONET observations.

For MODIS validation, a commonly-used metric is the fraction agreeing within and Expected Error
475 (EE) envelope such as $\pm 0.05 \pm 0.15 \text{AOD}$ (Remer et al., 2005) or $\pm 0.05 \pm 0.1 \text{AOD}$ (Lyapustin et al., 2018). In



this study, we adopted stricter requirements proposed by the Global Climate Observing System (GCOS) (the greater of 0.03 or 10%), which have been adopted in the Aerosol_cci study (Popp et al., 2016) as well as the latest DB validation (Sayer et al., 2019). Following the Aerosol_cci study by Popp et al. (2016), the uncertainty of 0.01 for AERONET AOD has been taken into account and GCOS is defined as:

$$480 \quad \text{GCOS} = \max(\pm 0.04, \pm 0.1 \text{AOD}) \quad (4)$$

Hence, the GCOS fraction (%) is the percentage of satellite retrieved AOD satisfying the GCOS requirement.

3 Validation of satellite observation by comparison with AERONET data: results and discussion

In order to characterize the quality of the retrieved aerosol parameters from PARASOL, the set of
485 main aerosol parameters including AOD, AE, AODF, AODC, SSA and AAOD were evaluated for the entire PARASOL ~9 years (2005-2013) data archive. This list includes all main aerosol parameters expected to be retrieved from MAP instruments in general (Dubovik et al., 2019). In addition, the validation results of AOD, AE, AODF and AODC were compared with the results of validation of these (where available) from the standard MODIS products for the year 2008.

490 PARASOL/GRASP retrievals are available and validated at six wavelengths (443, 490, 565, 670, 865 and 1020 nm). The MODIS retrievals and even PARASOL/Operational have different spectral coverage and, therefore, the comparisons of the GRASP product focused on the aerosol properties at midvisible (550 nm) that is commonly used in the satellite data comparisons and analysis (e.g. Sayer et al., 2018; Sogacheva et al., 2020). Therefore, for PARASOL/GRASP and PARASOL/Operational data the
495 aerosol products were generated at 550 nm by interpolations in log-log space from the closest channels available from the products. Similarly, AERONET aerosol products were also interpolated to 550 nm since the ground-based radiometers do not have a 550 nm channel.

3.1 Global validation of POLDER/GRASP aerosol products

Aerosol Optical Depth



500 Fig. 2 shows scatter plots of co-located PARASOL/GRASP AOD against AERONET AOD at 550 nm for the entire POLDER/PARASOL archive; Fig. 2a for GRASP/Optimized; Fig. 2b for GRASP/HP; and Fig. 2c for GRASP/Models. Validation metrics for total spectral AOD (443, 490, 550, 565, 670, 865 and 1020 nm), as well as AOD separated for land and ocean, are presented in Table 3. As can be seen from Fig. 2 and Table 3, all retrievals present good agreement with AERONET spectrally. Overall, based on 505 these metrics the quality of the comparison with AERONET is best for GRASP/Models. For example, for AOD (550 nm) GRASP/Models shows better performance than GRASP/Optimized and GRASP/HP: $R=0.923$ as compared to 0.877 and 0.899 and $RSME=0.119$ for GRASP/Models as compared to 0.160 and 0.161 for GRASP/Optimized and GRASP/HP respectively at 550 nm (see in Fig. 2). GRASP/Optimized and GRASP/HP show a positive overall bias of 0.06-0.07 for all AOD conditions, that remains for low 510 AOD conditions ($AOD < 0.2$) and even increases to 0.08 (GRASP/Optimized). In comparison, GRASP/Models has small overall bias (of 0.01 for AOD at 550 nm) that slightly increases to 0.03 for high AOD conditions ($AOD > 0.7$). Because of the bias in GRASP/HP and GRASP/Optimized AOD, GCOS fraction for them is much lower than for GRASP/Models AOD: e.g. 55.3% (AOD at 550 nm) for land + ocean vs. 28.2% and 34.4% respectively. Over ocean, all three archives show good correlation with 515 coefficients $R > 0.93$ at 550 nm. Nevertheless, GRASP/Models over ocean has the highest $R=0.950$ and offers the best performance for the other statistical metrics.

It is very important to note the robust performance of PARASOL/GRASP AOD retrieval in all spectral channels. For example, GRASP/Models product shows only minor spectrally independent bias of 0.01 over land, and over ocean the bias is about 0.02 at 440 nm and decreases to zero at longer wavelengths, 520 and the GCOS fraction for all wavelengths is at least ~50% over land and ~60% over ocean.

[Figure 2]

[Table 3]

Ångström Exponent



AE was determined from AOD at two different wavelengths ($AE = \frac{\ln[\tau(\lambda_1)/\tau(\lambda_2)]}{\ln(\lambda_2/\lambda_1)}$). The accuracy of
525 AE decreases for low AOD because even a small spectral bias the AOD affects AE strongly (e.g., Wagner
and Silva, 2008). Therefore, the threshold of PARASOL AOD (550 nm) > 0.2 was used in AE validation.
For calculating the PARASOL AE (440/870), the AOD retrieved at 443 nm and 865 nm are interpolated to
nominal 440 nm and 870 nm wavelengths. Fig. 3 shows the scatter plots of PARASOL/GRASP AE against
AERONET AE (440/870) for the whole archive (Fig. 3a: for GRASP/Optimized, Fig. 3b: for GRASP/HP
530 and Fig. 3c: for GRASP/Models). GRASP/HP has a higher correlation R (0.845) than GRASP/Optimized
(0.800) and GRASP/Models (0.692). In addition, GRASP/HP shows a lower RMSE (0.334) than
GRASP/Optimized (0.356) and GRASP/Models (0.415). The statistics of separated land and ocean AE
validation are presented in Table 4. Over ocean, the correlation coefficients are significantly higher
($R > 0.93$) than over land for all three datasets. Overall, the AE correlation statistical metrics is the best for
535 GRASP/HP both over land and ocean. GRASP/Models product has the smallest BIAS over land, which is
counterpoised by overestimation of low and underestimation of high AE values due to assumed size
distributions in the aerosol model-based approach. Both GRASP/Optimized and GRASP/HP capture AE
well when large particles are dominant ($AE < 1.0$), while the products tend to slightly underestimate AE
when small particles are dominant ($AE > 1.0$).

540 **[Figure 3]**

[Table 4]

Fine- and Coarse- mode Aerosol Optical Depth

Fig. 4 shows the validation of PARASOL/GRASP AODF against SDA AODF provided by
AERONET. AERONET SDA products (O'Neill et al, 2003) reported only at 500 nm, therefore here were
545 interpolated to AODF at 550 nm based on AE using a quadratic fit in log-log space (Eck et al., 1999). Over
land + ocean, GRASP/HP AODF shows the best validation statistics with correlation $R=0.925$, $BIAS=0.01$
and $Slope=0.892$ compared to $R=0.922$, $BIAS=0.02$ and $Slope=0.840$ for GRASP/Optimized and $R=0.867$,
 $BIAS=-0.02$, and $Slope=0.662$ for GRASP/Models. GRASP/Models AODF product has a slightly smaller



RMSE (0.092) than GRASP/HP (0.097) and GRASP/Optimized (0.099). Even though, the GCOS
550 requirement is initially defined for total AOD, here we also applied GCOS fraction on AODF validation
based on max (± 0.04 , $\pm 0.1AODF$). The GCOS fraction for all AODF products is at least ~55% over land +
ocean. The GCOS fraction is highest for GRASP/Models (65.2%), which is dominant for low aerosol
loading cases ($AODF < 0.2$). For moderate and high aerosol loadings ($AODF \geq 0.2$), GRASP/Optimized and
GRASP/HP show better performance than GRASP/Models, in terms of GCOS fraction and biases. The
555 linear regression slope for GRASP/Models is weakest 0.662 compared to 0.892 and 0.840 for GRASP/HP
and GRASP/Optimized respectively. These facts suggest a possible underestimation of fine-mode aerosol
in high AOD conditions for GRASP/Models. Caution is required in the interpretation of the regression
slope as these data may not meet the assumptions behind the technique; however, the results are useful in a
comparative sense. The statistics for separated land and ocean are presented in Table 5. As can be seen,
560 overall, PARASOL/GRASP AODF products show very good agreement with AERONET SDA products.
GRASP/HP AODF demonstrates best performance in terms of the highest correlation and smallest bias.

[Figure 4]

[Table 5]

The coarse-mode AOD (AODC) traditionally a difficult parameter to derive from satellite
565 observations especially over bright land surfaces, since nadir -looking satellite measurements are not very
sensitive to large particles. The validation of all archived PARASOL/GRASP AODC with AERONET
SDA AODC is presented in Fig. 5. Generally, the global (land + ocean) statistical metrics for AODC are
less convincing than that for AODF but still reasonable: GRASP/HP has higher correlation R (0.745) and
Slope (0.936) than GRASP/Optimized (R=0.689, Slope=0.748) and GRASP/Models (R=0.579,
570 Slope=0.657). GRASP/Models retrievals show a smaller bias (0.02) and RMSE (0.109) than
GRASP/Optimized (BIAS=0.04, RMSE=0.116) and GRASP/HP (BIAS=0.05, RMSE=0.123). The GCOS
fraction of AODC max (± 0.04 , $\pm 0.1AODC$) for GRASP/Models (65.4%) is higher than GRASP/Optimized
(44.3%) and GRASP/HP (48.4%). In line with AODF, GRASP/Models has better performance for low



aerosol loading cases, which account for ~90% of the number of points. The statistics of separated land and
575 ocean AODC validation, presented in Table 6, show a much higher correlation of retrieved AODC with
AERONET over ocean. It is also interesting to note that the validation statistics for AODF seems to be
superior to that for AODC over land, and the situation is reversed. This can be explained by the fact that the
fine mode aerosols have higher abundance over land while coarse mode aerosol is dominant over ocean, i.e.
dynamic ranges are difference. Also, at longer wavelengths where the contribution of coarse particles to
580 radiation is significant, the land surface is very bright while ocean surface is practically dark. Over land
AODC in GRASP/HP and GRASP/Optimized products exhibit rather high BIAS of 0.05 and 0.03
correspondingly, that probably dominates the bias for the total AOD in both. For GRASP/Models product
biases in AODF and AODC over land have comparable magnitudes and different signs, and therefore
compensate each other in the total AOD.

585

[Figure 5]

[Table 6]

Single Scattering Albedo

Fig. 6 shows the validation of PARASOL/GRASP SSA (670 nm) with AERONET L2 inversion
products. The SSA products in AERONET L2 database provide the values only for moderate and high
590 AOD cases (AOD at 440 nm ≥ 0.4) to assure the highest quality of the inversion products (Dubovik et al.,
2000, 2002b). Following the same strategy, PARASOL/GRASP L2 and L3 products of SSA for low AOD
cases are also filtered out (Land: AOD 443 nm < 0.3 ; Ocean: AOD 443 nm < 0.02). The threshold for filtering
SSA over ocean is very low because using higher values would eliminate a significant fraction of the
retrievals. This low-AOD filtering is done over L2 products, and then L3 SSA is generated from filtered L2
595 products. The validation shows convincing correlation of all SSA PARASOL/GRASP products with those
from AERONET, although due to a rather small dynamic range (mostly 0.7-1.0) of SSA, the correlation
coefficients for SSA (670 nm) in Fig. 6 are notably lower than for other parameters. The highest correlation
is for GRASP/HP with $R=0.536$ and RMSE (0.056) compared with GRASP/Optimized ($R=0.511$;



RMSE=0.065) and GRASP/Models (R=0.324; RMSE=0.057), while GRASP/Models has a smallest BIAS
600 (-0.02) compared to GRASP/HP (BIAS=-0.03) and GRASP/Optimized (BIAS=-0.04).

Table 7 shows the statistics of PARASOL/GRASP spectral SSA (443, 670, 865, and 1020 nm)
against AERONET SSA at four wavelengths (440, 675, 870, and 1020 nm). The statistics are given for
combined land and ocean, because of the limited amount of validation points over ocean. The SSA
correlation coefficients for GRASP/Optimized and GRASP/HP L3 products increase from 440 nm (~0.25)
605 to 1020 nm (~0.60), which is likely due to the increased dynamic range of SSA at longer wavelengths (e.g.
see Dubovik et al., 2002b, SSA at 1020 can change from very low values for biomass burning aerosol to
nearly unity for desert dust). Consequently, the RMSE also increases from 440 to 1020 nm.

In addition, Table 7 reports the statistics of SSA validation at different PARASOL AOD levels. The
results clearly illustrate the improvement of retrieved SSA with the increase of aerosol abundance, in
610 agreement with the results of AERONET sensitivity studies by Dubovik et al., (2000). For example, the
correlation coefficient for GRASP/Models SSA at 670 nm with AERONET significantly improves from
0.321 for all L3 products to 0.814 for AOD greater than 1.5.

[Figure 6]

[Table 7]

615 *Aerosol absorption optical depth*

Aerosol absorption optical depth (AAOD) is related to SSA and total AOD as:

$$AAOD(\lambda) = AOD(\lambda) \times [1 - SSA(\lambda)] \quad (5)$$

In the current PARASOL/GRASP L3 dataset, the AAOD value of each grid box (0.1° or 1° degree) is
calculated based on Eq. (5) using average AOD(λ) and SSA(λ) of the grid box. Note that the
620 PARASOL/GRASP L3 SSA(λ) values are aggregated based on moderate and high AOD cases (Land: AOD
443 nm \geq 0.3; Ocean: AOD 443 nm \geq 0.02), and again the very low threshold (\geq 0.02) for filtering SSA over
ocean was chosen in order to retain sufficient number of SSA and AOD retrievals. Choosing even slightly
higher values would eliminate the majority of retrieval over ocean. Thus, the direct use of L3 climatology



of AAOD may lead to overestimation of the global aerosol absorption, because the low AOD cases are
625 filtered. Similarly, the AERONET L2 database provides AAOD products only for moderate and high AOD
cases (AOD at 440 nm \geq 0.4) to assure their highest quality (Dubovik et al., 2000).

The statistics of PARASOL/GRASP spectral AAOD (443, 670, 865 and 1020 nm) validation versus
AERONET AAOD (440, 675, 870, and 1020 nm) are shown in Table 8. The correlation coefficients of
AAOD are relatively low (0.4-0.55), which is certainly due to the low absolute value of AAOD, most cases
630 are less than 30% of total AOD. GRASP/HP and GRASP/Models AAOD products show the RMSE equal
to 0.042-0.018 from 443 nm to 1020 nm for Models, and 0.047-0.025 for HP. The BIAS is lowest for
PARASOL/Models AAOD: 0.00 at 440, 870 and 1020 nm and 0.01 at 670. Thus, PARASOL/GRASP
AAOD provide rather useful information about global AAOD values, even the uncertainties are rather
significant given the generally low magnitudes of AAOD. In contrast with SSA, the attempts to analyze the
635 AAOD accuracy for different AOD levels did not show any consistent improvement in accuracy with
increase of abundance.

[Table 8]

3.2 Comparison of results obtained from validation of PARASOL and MODIS aerosol products against AERONET

640 In order to place the PARASOL/GRASP validation results into perspective, here we compare
PARASOL/GRASP ability to retrieve AOD, AE, AODF and AODC with other satellites. Specifically,
these products from MODIS, PARASOL/Operational and PARASOL/GRASP products are validated using
the same approach for the entire 2008 year and validation results were compared. MODIS aerosol products
have been extensively evaluated globally by the MODIS team in multiple studies (Gupta et al., 2018; Levy
645 et al., 2010, 2013, 2018; Lyapustin et al., 2018; Sayer et al., 2013, 2014, 2019) and PARASOL/Operational
aerosol products have been evaluated in Bréon et al. (2011); the present analyses is performed for reader
convenience and consistency of methodology across products. We confirmed that the statistic metrics that
we found for MODIS and PARASOL/Operational aerosol products validation in 2008 is similar to these
studies. This section is therefore focusing on a comprehensive evaluation of the consistencies and



650 differences between PARASOL and MODIS aerosol products using examples from one year. The year
2008 was chosen because it presents a generally good statistics of observations and all types of aerosol are
clearly present. The validation figures for the satellite products over land and ocean are presented
separately, because over land there are three MODIS products (DT, DB, and MAIAC), while only DT
product is provided over ocean. MAIAC products cover some land-containing ocean tiles, though as these
655 are spatially complete we do not consider MAIAC ocean products here. PARASOL/Operational AODF
products are provided over land and ocean, and total AOD products only over ocean.

Fig. 7 shows validation results for AOD at 550 nm for 3 PARASOL/GRASP products over land
with collocated AERONET measurements. Fig. 8 shows the validation results for MODIS DT, DB and
MAIAC AOD products over land. The products called MAIAC_0.1 and MAIAC_0.01 correspond to the
660 MODIS MAIAC original product aggregated to 0.1° and 0.01° grid boxes, respectively. In general MODIS
products have more matched points than PARASOL products due to MODIS' wider swath and higher
spatial resolution of measurements allowing better cloud detection. From low to high values the sequence
of obtained global correlation coefficients is: 0.870 (DB), 0.874 (MAIAC_0.01), 0.875
(GRASP/Optimized), 0.895 (MAIAC_0.1), 0.898 (DT), 0.908 (GRASP/HP) and 0.924 (GRASP/Models).
665 The GCOS fraction sequence is 28.8% (GRASP/Optimized), 32.4% (GRASP/HP), 46.1% (DT), 48.1%
(MAIAC_0.01), 48.8% (DB), 52.8% (MAIAC_0.1), and 53.2% (GRASP/Models). The high to low RMSE
sequence is: 0.157 (GRASP/HP), 0.150 (GRASP/Optimized), 0.126 (DB), 0.121 (GRASP/Models), 0.120
(DT), and 0.112 (MAIAC_0.1). The large to small total BIAS sequence is: 0.06 (GRASP/HP), 0.04
(GRASP/Optimized), -0.03 (MAIAC_0.01 and MAIAC_0.1), 0.02 (DT), -0.01 (DB) and 0.00
670 (GRASP/Models). The low to high sequence of regression slope values is: 0.780 (GRASP/Optimized),
0.793 (MAIAC_0.1), 0.794 (MAIAC_0.1), 0.841 (DB), 0.938 (GRASP/HP), 0.988 (DT), and 0.989
(GRASP/Models). The results illustrate that the overall accuracy of these AOD products are generally
comparable on a global scale. Note, however, that different products may have different regional strengths
and weaknesses (e.g. Sayer et al., 2014), motivating the mapped analysis later. The GRASP/Models AOD



675 yields overall the largest number of the best statistical indicators over land: with the highest correlation (R=0.924), the highest GCOS fraction (53.2%), correlation slope (0.989) and the smallest total bias (BIAS=0.00). The detailed statistics of PARASOL and MODIS AOD products against referenced collocated AERONET AOD at 550 nm over land and ocean are presented in Table 9.

[Figure 7]

680

[Figure 8]

Fig. 9 presents validation of PARASOL/GRASP (Optimized, HP and Models), PARASOL/Operational and MODIS/DT AOD products versus collocated AERONET measurements over ocean in 2008. The detailed statistic metrics are presented in Table 9. The matching methodology is the same as described in section 2.4. The total matched points in 2008 are ranging from minimum
685 GRASP/Optimized 116 to maximum MODIS/DT 218. In general, all AOD products show high correlation over ocean, of which GRASP/Models has the highest R (0.963), following by Operational (0.954), DT (0.952), GRASP/Optimized (0.950) and GRASP/HP (0.947). The high to low sequence of RMSE is 0.092 (GRASP/HP), 0.089 (GRASP/Optimized), 0.081 (DT), 0.077 (Operational) and 0.061 (GRASP/Models). The slopes are quite similar: 1.165 (Operational), 1.145 (GRASP/Optimized), 1.074 (GRASP/HP), 0.965
690 (GRASP/Models) and 0.974 (DT). Overall, GRASP/Models show slightly better bias (0.02) and GCOS fraction (62.9%), following by DT (BIAS=0.03, GCOS fraction=55.0%), Operational (BIAS=0.03, GCOS fraction=52.2%), GRASP/Optimized (BIAS=0.06, GCOS fraction=42.2%) and GRASP/HP (BIAS=0.07, GCOS fraction=26.6%). Altogether, GRASP/Models, PARASOL/Operational and DT AOD yield quite similar performance over ocean with a better correlation statistics than GRASP/Optimized and GRASP/HP
695 AODs that correlate well with AERONET measurements but present a significant positive bias (0.06-0.07).

[Figure 9]

[Table 9]

In order to obtain more information about the quality of the retrieval products over different land surfaces, the statistics of satellite validation against AERONET were also analyzed separately for different
700 land covers. Table 10 shows the statistic metrics for land surfaces with different Normalized Difference



Vegetation Index (NDVI). The statistics are presented for several categories: bare soil/desert surfaces (NDVI<0.2); mixture of bare soil and vegetated surfaces ($0.2 \leq \text{NDVI} < 0.4$); surfaces covered different types of vegetation ($0.4 \leq \text{NDVI} < 0.6$ and $\text{NDVI} \geq 0.6$). The global NDVI dataset is adopted from GRASP/Models L3 annual mean products for year 2008 (Fig. 10). The correlation metrics in Table 10 show that, in general, all products show better performance over surface type with $0.2 \leq \text{NDVI} < 0.6$ than bright, bare surfaces (NDVI<0.2), and somewhat better than for dense vegetation surface ($\text{NDVI} \geq 0.6$). Overall the AOD product of GRASP/Models seems to show the best correlation with AERONET, with highest R over 3 of 4 surface classes. Over bright surfaces (NDVI<0.2), GRASP/HP has a highest R (0.915), but also rather high BIAS of 0.06. The GRASP/Models AOD also has zero BIAS for 3 surface classes except the dense vegetation surface ($\text{NDVI} \geq 0.6$), where GRASP/Models AOD has total BIAS of 0.03, higher than that in any MODIS AODs.

[Figure 10]

[Table 10]

Fig. 11 shows the validation of AE for PARASOL/GRASP and MODIS DT and DB products over land versus collocated AERONET measurements. The MODIS AE for DT and DB products were calculated based on 470 and 660 nm that are reported in both products; an equivalent for AERONET was calculated using AOD interpolated to 470 and 660 nm. PARASOL/GRASP products contain AOD at 440 and 870 nm, therefore AE (440/870) was directly used for validation PARASOL/GRASP results. MAIAC AE was not included because MAIAC reports AOD at two rather close wavelengths 470 and 550 nm and calculation of AE using these such close channels could produce substantial uncertainties in AE. The threshold of satellite AOD (550 nm) > 0.2 was used in validation of AE over land and ocean. In general, PARASOL/GRASP (Optimized, HP and Models) AE correlate notably better with AERONET than MODIS (DT and DB), which is likely caused by the lower information content in regards to aerosol size in mono-viewing MODIS observations. In addition, both DT and DB algorithms rely on climatology for the aerosol model selection, i.e. AE is rather predetermined than retrieved to some extent. For example, although AOD over land is reported by DT at 470 nm and 660 nm, the spectral dependence of the DT land



retrieval is mostly imposed by assumed aerosol models. The DT team makes a specific point of not reporting AE over land for that reason, and at best the spectral dependence might allow a binary inference of either fine mode or coarse mode dominated particles, but not a quantitative measure of the true spectral
730 dependence. The DT over ocean algorithm has greater flexibility in its mixing of models and does return a quantitative AE. The weaker performance of GRASP/Models approach compare to GRASP/HP and Optimized is caused by the limitation of maximum and minimum AE values allowed by the mixture of aerosol components used, even though GRASP/Models approach allows mixing of different components freely with no location specific constraints. As a result, GRASP/Models tends to overestimate AE for large
735 particles (low AE values), and underestimate AE for small particles (high AE values). Hence, GRASP/Models AE products are less appealing than those from GRASP/Optimized and GRASP/HP in terms of evaluation metrics. GRASP/HP tends to provide the best AE products over land.

[Figure 11]

[Figure 12]

740

[Table 11]

Fig. 12 presents the validation of AE over ocean from PARASOL/GRASP, PARASOL/Operational and MODIS/DT products against AERONET measurements. PARASOL/Operational AE was calculated based on 670 and 870 nm that are reported in the product, and AE (670/870) of AERONET was calculated using AOD interpolated to 670 and 870 nm. Although there are not many available points the satellite
745 derived AE over ocean are much better than that over land. GRASP/Models show R (0.949) higher than Operational (0.891), GRASP/HP (0.890), GRASP/Optimized (0.840) and DT (0.832). GRASP/Models and MODIS DT AE show an overestimation for large particles. Operational AE tends to overestimate both for large and small particles. At the same time, GRASP/HP AE correlation has the slope closer to 1:1 line with AERONET AE than other products, with the best linear fitting slope (0.810) and intercept (0.051). The
750 statistic metrics of AE validation over land and ocean are listed in Table 11.

AODF is often used to estimate anthropogenic aerosol climate effects (Bellouin et al., 2005) and surface air quality (e.g. PM_{2.5}) (Zhang and Li, 2015). MODIS started to report fine mode weighting



parameter (η) in the products from the second generation DT operational algorithm (Levy et al., 2007b), though η is weighted for reflectance not for AOD. Consequently η over land is a diagnostic that has little physical meaning and the resulting AODF and AODC do not have physical meaning and generally are not recommended to be used. Therefore, it is not considered in the analysis. However, over ocean, based on single scattering approximation, η is also weighted for AOD (Remer et al., 2005). Therefore, MODIS fine and coarse mode AOD at 550 nm over ocean are derived according to the equations below:

$$\text{AODF} = \text{AOD} \times \eta \quad (6)$$

$$\text{AODC} = \text{AOD} \times (1.0 - \eta) \quad (7)$$

Fig. 13 shows the validation of AODF at 550 nm for PARASOL/GRASP and PARASOL/Operational AODF products over land against AERONET AODF products from the SDA algorithm. It's noticeable that the AODF products over land are only available from PARASOL MAP measurements. The results in Fig. 13 indicate the PARASOL/GRASP and PARASOL/Operational AODF products are in good agreement with AERONET SDA products, for example, $R > 0.86$. The GCOS fraction of AODF for PARASOL/GRASP and PARASOL/Operational products are at least 50%. GRASP/HP AODF shows the best correlation among all four AODF products over land, with rather similar performance for GRASP/Optimized AODF.

The AODF validation over ocean is shown in Fig. 14, and statistical metrics over land and ocean are presented in Table 12. GRASP/Optimized and GRASP/HP AODF show generally consistent performance over ocean and over land, with correlation R around 0.9, while the BIAS for GRASP/Optimized and GRASP/HP AODF is higher over ocean than over land. At the same time, GRASP/Models AODF shows significant improvement over ocean, for example, the fitting line is much closer to 1:1 (dotted line), and the RMSE decreased dramatically. PARASOL/Operational AODF shows a slight decrease of R from land ($R=0.886$) to ocean ($R=0.780$), also reported in Bréon et al. (2011), while the fitting line, RMSE and BIAS show improvement from land to ocean. This is likely due to higher information content about aerosols in satellite observations over dark ocean surfaces compared to brighter land surfaces.



[Figure 13]

[Figure 14]

780

[Table 12]

The validation of AODC over land and ocean are shown in Figs. 15 and 16, respectively. Even though AODC products over land are only provided for PARASOL/GRASP, for completeness we present this over land for year 2008 in Fig. 15. Similarly to the results from the total PARASOL/GRASP archive, AODC over ocean is more accurate than over land. The overall best results of AODC are provided by GRASP/HP with highest R (0.771) and the best linear fitting (slope is reaching 1 and intercept is close to 0) over land. Yet, the BIAS of GRASP/HP AODC is 0.05, which is higher than GRASP/Models (0.01) and GRASP/Optimized (0.03), which results in higher GCOS fraction for GRASP/Models AODC (63.7%) than GRASP/HP (45.8%) and GRASP/Optimized (45.6%). At the same time, as mentioned above, over dark ocean the sensitivity of the observed signal to aerosol is stronger allowing for retrieval of particle size information that is more challenging over land. The GRASP/Models AODC shows the best R (0.966) and RMSE (0.040) while MODIS/DT AODC has the smallest bias (0.00) against AERONET over ocean, following by Operational (0.01), GRASP/Models (-0.01), GRASP/Optimized (0.03), and GRASP/HP (0.05). Although AODC is not included in PARASOL/Operational product list, over ocean we subtract AODF from total AOD to obtain Operational AODC, which shows a rather good agreement with AERONET (R=0.936, Slope=0.971, RMSE=0.045, BIAS=0.01). However, over land, only AODF is provided in the PARASOL/Operational product.

790

795

[Figure 15]

[Figure 16]

[Table 13]

800

The statistics in comparison of each single product vary due to the differences in product coverage: coverage of MODIS/AQUA is wider than PARASOL; at the same time, the products have different limitations and availability:



- MODIS/DT has limited products over bright land surfaces, and AODF and AODC are only available over ocean;
- 805 - MODIS/DB and MAIAC AOD products are only over land, and do not include AODF and AODC;
- PARASOL/Operational over land provides only AODF;
- Quality screening is different (even between PARASOL/GRASP products).

Therefore, the approaches chosen in this paper for considering all above factors could have some effects on
810 the results and their interpretation. At the same time, the correlations with AERONET obtained in these studies for known products including MODIS DT, DB and MAIAC and PARASOL/Operational in general agree with the results of previously mentioned studies.

3.3 Evaluation of PARASOL and MODIS validation results over different AERONET sites

In this section, we compare the validation metrics of PARASOL/GRASP and MODIS aerosol
815 products over spatially distributed AERONET sites. PARASOL/Operational AOD products are provided over ocean only, hence are not included in this section. The AOD validation was conducted over all AERONET sites that had available data in 2008. At the same time, and to increase statistical robustness only sites with at least 10 matchup points were included in the analysis. However, the different products can also have different number of matchup points over different AERONET sites due to various factors (as
820 discussed previously). Therefore, to evaluate the validation performance of different products, the percentage (%) of the cases when the product of each algorithm showed the best statistic metrics, observed among all the products (e.g. the highest R, GCOS Fraction, and the lowest RMSE, BIAS, etc.) was used as an indicator for the performance evaluation.

Fig. 17 shows the percentage score for each algorithm at AERONET sites for statistical metrics R,
825 RMSE, BIAS and GCOS Fraction respectively. The detailed statistics for the performance of each AOD products is shown in Fig. 18 (only the 1st ranking statistics over each site are present in the maps.). All PARASOL/GRASP products have fewer sites with at least 10 matchup points than MODIS AOD products.



There are 102, 124, and 95 sites having sufficient matchup points for GRASP/Optimized, GRASP/HP and GRASP/Models respectively, lower than DT (153), DB (172), MAIAC_0.1 (169) and MAIAC_0.01 (172) 830 by 20%~45%. Regarding the correlation coefficient R, GRASP/Models, DT and MAIAC_0.1 are the 3 algorithms showing higher scores for 37.9%, 28.1% and 24.9% sites where respective products were provided. As shown in Fig. 18a, these 3 algorithms show good performance worldwide, e.g. North America, Europe and East Asia. There are no MODIS AOD products showing the best R over Australia (only 4 sites are available there). The 3 GRASP algorithms show high percentage for products over dust and biomass 835 burning regions, e.g. South America, southern Africa, central Africa, central Australia, etc. At the same time, the GRASP/Optimized and GRASP/HP AOD products performed less well over North America.

[Figure 17]

[Figure 18]

In terms of the percentage of sites with the best RMSE, GRASP/Models and MAIAC_0.1 are the 840 top 2 algorithms showing the best RMSE results over 60.0% and 33.1% of AERONET sites with available GRASP/Models and MAIAC_0.1 retrievals. Thus, overall, all these results indicate that GRASP/Models presents a strong ability to provide AOD that agrees well with AERONET measurements. Both GRASP/Models and MAIAC_0.1 show the best RMSE over Europe and North America (Fig. 18b), which also have the highest density of AERONET sites. GRASP/Models shows the best BIAS over 36.8% sites, 845 followed by DB (27.3%) and MAIAC_0.01 (23.3%). For the best GCOS Fraction, GRASP/Models leads this for 57.9% over its total 95 sites. After, MAIAC_0.1 has the highest GCOS Fraction for 30.8% over total 169 sites. In Fig. 18d, the best GRASP/Models sites are globally distributed. Over the Eastern United States, DB and MAIAC_0.1 products tend to have more sites with the best GCOS Fraction.

Using a similar concept as the AOD analysis above, the PARASOL/GRASP and MODIS (DT and 850 DB) AE validation over AERONET sites were compared. Only cases with satellite AOD (550 nm) > 0.2 were included in the analysis; due to the reduced data volume from this threshold, the requirement on minimum matchups was reduced to 5. Fig. 19 shows the detailed statistics for the performance of each AE products. Fig. 20 shows the best performing algorithm at each site according to R and RMSE respectively.



In general, GRASP/HP and GRASP/Optimized AE products outperform the other AE products in the site
855 level validation. The best sites are globally distributed (see Fig. 20). There are 44.1%, 38.6% and 34.7%
sites showing the best R for GRASP/Optimized, GRASP/HP and GRASP/Models, somewhat higher than
DT (12.0%) and DB (8.2%). GRASP/HP AE has the best RMSE over 43.0% AERONET sites, higher than
GRASP/Optimized (34.3%), DB (28.6%), GRASP/Models (24.5%) and DT (17.0%).

[Figure 19]

860

[Figure 20]

4 Inter-comparison of satellite products at global scale

This section presents the inter-comparison of different satellite products for the year 2008 data on a
global scale, i.e. not only over AERONET sites. Specifically, we want to know if the consistency of the
satellite products remains the same in the areas where no AERONET observations are available. In the first
865 part, we compare PARASOL/GRASP and PARASOL/Operational at a spatial resolution of $0.2^\circ \times 0.2^\circ$,
which represents a compromise between PARASOL/Operational (18.5 km) and PARASOL/GRASP Level
3 (0.1°) resolutions. In the second part of this section, the global inter-comparison is done between
PARASOL/GRASP and MODIS aerosol products in a spatial resolution of $0.1^\circ \times 0.1^\circ$, close to the DT and
DB product native resolution of 10 km, and only use MAIAC_0.1 data that is of similar resolution. Only
870 GRASP/HP and GRASP/Models products for PARASOL/GRASP are used in the consideration of this
section since GRASP/Optimized shows rather similar results to GRASP/HP. Since the focus of this section
is global pixel-to-pixel comparison of satellite aerosol products, we use all available data of the highest
quality for each dataset (Table 2).

4.1 Comparisons between PARASOL/GRASP and PARASOL/Operational aerosol products

875 To begin, we investigate two independent aerosol products derived from PARASOL measurements,
PARASOL/GRASP and PARASOL/Operational, globally for 2008. As mentioned above,
PARASOL/Operational provides only AODF over land, while over ocean AOD, AE and AODF are
available. We subtract AODF from total AOD to obtain Operational AODC over ocean.



Table 14 presents the pixel-to-pixel statistic metrics (R, Slope, Intercept, RMSE and BIAS) between
880 Operational and GRASP aerosol products (note here the BIAS should be interpreted as an offset rather than
true bias as the “truth” is unknown; we retain the name of the metric for consistency with the earlier
analysis). We took Operational products as a reference as these were the original PARASOL aerosol
products released by AERIS/ICARE; hence, the BIAS is defined as GRASP - Operational. All the statistics
for AOD, AODF and AODC are given for the midvisible wavelength (550 nm), while AE is calculated
885 based on 670 and 870 nm. The statistical metrics are reported both for global comparisons and over
AERONET pixels only (the numbers in the brackets). It can be seen from Table 14 the global comparison
between PARASOL/GRASP and PARASOL/Operational is rather consistent for AOD over ocean and
AODF over land, for which, the global pixel-to-pixel correlations between GRASP/HP, GRASP/Models
and Operational products are generally higher than 0.85 based on more than 5 million pairs. However, the
890 agreement of AODF over ocean decreases to 0.63-0.73 for R. The slight decreasing of correlation against
AERONET from land to ocean for Operational AODF products is also recorded in Table 12 and previous
study by Bréon et al. (2011). The AODC over ocean for the Operational product is derived from AOD and
AODF, hence, the number of matched pairs is lower than for AODF. The overall agreement has a
correlation coefficient of ~ 0.7 . GRASP/HP AODC is ~ 0.05 higher than Operational, but the difference
895 between GRASP/Models and Operational is ~ 0.0 , which are in line with the validation against AERONET
in Table 13. The pixel-to-pixel agreement for PARASOL/GRASP and PARASOL/Operational AE is less
convincing ($R < 0.6$) than any other parameters, even though they are all well correlated with AERONET
($R > 0.8$) over ocean. One possible reason is that the AE here is calculated at different wavelengths (670 and
870 nm) than for the comparisons with AERONET (470/660 nm and 440/870 nm). Besides, the **increase** of
900 AE agreement for global correlation (R) compared to that over AERONET pixels is more notable than
other parameters. This may explain that the AE products resulting from LUT-based algorithms are more
determined by climatological assumptions about the aerosol models than retrieved.

[Table 14]



4.2 AOD comparisons between PARASOL/GRASP and MODIS products

905 In order to further clarify the level of consistency of satellite products (PARASOL/GRASP and MODIS), the global correlations of different satellite products were extensively analyzed for the year 2008 at a spatial resolution of $0.1^\circ \times 0.1^\circ$. Fig. 21 shows the seasonal pattern of AOD (550 nm) from PARASOL (GRASP/HP and GRASP/Models) and MODIS (DT, DB, and MAIAC) products. Any grid box with less than 3 measurements for a season was omitted. Fig. 22 shows the differences of AOD (550 nm) by season
910 between PARASOL and MODIS aerosol products using GRASP/Models as the reference. A positive value indicates that the MODIS product had a higher mean value. Note that Fig. 22 is not a simple difference of the seasonal means shown in Fig. 21. Instead, to decrease sampling-related differences, a difference between the products was calculated at the pixel level, and these pixel-to-pixel differences were then averaged for a season. In addition, we require at least three matched points in a season to be plotted on the
915 map. Since the analysis in Section 3 suggested that the AOD products over land and ocean from the GRASP/Models processing have the lowest biases, this was used as a reference product in Fig. 22. It should be noted that in order to show the intrinsic difference between the products, the overall bias from AERONET values (using validation metrics in Table 9) were subtracted from the AOD products before obtaining the seasonal differences shown in Fig. 22.

920 In addition, the global correlations between different satellite products and GRASP/Models data at 550 nm were calculated for the complete year 2008. Also, in order to evaluate the consistency of different MODIS products over land, the inter-comparisons were done against MAIAC AOD (Land) product chosen as a reference, as MAIAC provides the most universal coverage over land. Table 15 presents the pixel-to-pixel statistic metrics (R, Slope, Intercept, RMSE and BIAS) between AOD products compared to the
925 reference of GRASP/Models (Land and Ocean) and MAIAC AOD (Land) products. The statistical metrics are reported both for global comparisons and over AERONET pixels only (numbers in brackets).

[Figure 21]

[Figure 22]

[Table 15]



930 Each of these global correlations was based on several dozens of millions of pairs, and less noisy compared to the AERONET correlations (based on only a few thousand points). In spite of this significant difference in volume, the outcome of the global satellite comparisons is rather consistent with the results of validation against AERONET. For example, all AOD products are in close agreement over ocean, with the correlation coefficients above 0.9 and slope lines close to 1:1 (Table 15). Specifically, the three aerosol
935 products (GRASP/HP, GRASP/Models and DT) over ocean agree with $R > 0.92$ for any two products. Also, in line with the validation over AERONET sites, GRASP/HP AOD (550 nm) consistently has a positive offset ~ 0.05 - 0.16 from low to high AOD conditions with respect to GRASP/Models. DT and GRASP/Models AOD show good agreement over ocean, $R = 0.92$ for all points and $R = 0.97$ for AERONET pixels, in addition, the BIAS (DT-GRASP/Models) equals to -0.01 for all points and 0.00 for low AOD
940 (< 0.2), while the negative BIAS of -0.06 appears when AOD is greater than 0.7 . Statistics over ocean rely on ~ 65 million pairs between GRASP/HP and GRASP/Models, and ~ 32 million pairs between DT and GRASP/Models.

However, over land surfaces the situation is quite different, and MODIS/MAIAC and DB AOD products show evidently better agreement with GRASP/Models over AERONET pixels than the rest of
945 globe. The correlations over AERONET pixels both for MAIAC versus GRASP/Models and DB versus GRASP/Models are of ~ 0.89 that is generally in line with the correlation coefficient values with AERONET shown in Table 9. In a contrast, the corresponding correlation coefficients decrease to 0.76 and 0.77 for global statistics. The other statistical parameters (e.g. Slope, Offset, RMSE and BIAS) showed the same trend, indicating a better agreement over AERONET pixels. For comparisons of GRASP/HP and DT
950 versus GRASP/Models AOD such tendency is not evident. Even though, the correlation coefficient drops from 0.90 over AERONET to 0.85 globally, the rest of statistical indicators do not show significant changes, whether over an AERONET site or elsewhere. It is interesting to note that MODIS products show better agreement (especially in correlations) with other MODIS products over AERONET stations and globally than between PARASOL and MODIS products over AERONET stations and globally (Table 15).



955 This phenomenon can be explained by several factors. First, the inputs from the two satellites differ significantly. The multi-angle polarization information from PARASOL offers algorithms many more degrees of freedom from which to constrain environmental factors and invert aerosol parameters than does a single view radiometer like MODIS. Second, because of this extra information the PARASOL/GRASP retrievals do not have location specific assumption about aerosol and conduct their retrievals in the exactly
960 the same manner globally. In contrast, all three MODIS retrievals use some regional assumptions over land about aerosol types, surface properties, etc. Even though each algorithm's assumptions are different, the need for a priori constraints could draw the MODIS products closer together. Therefore, the similarities in global performance of three algorithms can probably be explained by somewhat similar a priori assumptions about aerosol types, etc. used in MODIS algorithms. Third, as can be seen from the Table 15
965 and Fig. 21, GRASP/Models, GRASP/HP and MAIAC have wider coverage over land than DB and DT, because of the lack of retrievals over bright surfaces for DT and reduced number of retrievals over dark vegetation for DB (although some of this was improved in DB Collection 6.1; Sayer et al., 2019). Specifically, for the year 2008, there are more than 64 millions of pairs MAIAC/GRASP/Models AOD over land, which is much higher than the number of pairs obtained with other two AOD products. Thus, the
970 collocation statistics for MAIAC/GRASP, DT/GRASP, DB/GRASP as well as MAIAC/DT and MAIAC/DB were based on different data sets. Fourth, the different representation of various natural conditions in the global statistics and statistics over AERONET can be non-identical and, therefore, the average performance indications can differ. For example, there is only a certain fraction of AERONET sites in desert areas while land cover with bright surface may have notably higher or lower fraction in global
975 statistics. Correspondingly, if the product agreement is non-identical over different land surfaces, then the statistics with different representations of various surfaces can differ.

In order to explore the last factor, the statistics of the comparisons were sorted by land surface type. The Tables 16 and 17 show pixel-to-pixel statistic metrics with reference AOD from GRASP/Models and



MAIAC respectively, over different land coverage using four classes of land surface by NDVI (as before,
980 NDVI<0.2, $0.2 \leq \text{NDVI} < 0.4$, $0.4 \leq \text{NDVI} < 0.6$, and $\text{NDVI} \geq 0.6$).

[Table 16]

[Table 17]

Tables 16 and 17 show that over very bright land surfaces ($\text{NDVI} < 0.2$), the global correlations
between MODIS (especially DB and MAIAC) with PARASOL/Models products were significantly lower
985 than over other surfaces and showed a most notable drop (>0.1) in global correlations compared to the
correlation over AERONET sites. Such a large drop was not seen between different PARASOL products or
between different MODIS products. Therefore, these differences are likely related to the fact that MODIS
retrievals rely on regional climatological aerosol assumptions or surface assumptions derived from
atmospheric correction at (unevenly-distributed) AERONET sites while in PARASOL/GRASP retrievals
990 no location specific assumptions are used. Another issue maybe related is that MODIS has much higher
spatial resolution for cloud detection than PARASOL. The possible sub-pixel cloud contamination for
PARASOL may affect the global inter-comparison statistics, since the validation against AERONET brings
additional cloud clearing filter from AERONET. As a result, PARASOL/GRASP retrievals are expected to
be rather consistent globally, while MODIS retrievals are more closely tied to AERONET statistics and
995 may perform less well in the areas with a lack of AERONET sites. At the same time, the fraction of pairs
over bright surfaces in inter-satellite product comparisons is higher than in AERONET statistics since there
are only a limited number of AERONET sites in desert areas. This latter statement does not necessarily
apply to MODIS DT because it often does not retrieve over deserts; however, although the sample size is
very small, Table 16 shows that it actually matches GRASP/Models less well at AERONET sites than
1000 globally for $\text{NDVI} < 0.2$.

Interestingly, the maps in Fig. 22 of seasonal AOD difference indicate lower AOD (550 nm) for
PARASOL/Models over bright surfaces compared to MODIS products, while the global comparisons of
PARASOL/Models and MODIS DB and MAIAC products did not show significant BIAS in AOD (550
nm). At the same time, the global comparisons (Table 16) between PARASOL/Models and MODIS DB,



1005 MAIAC show a significant BIAS for different ranges of AODs. MODIS DB and MAIAC had a positive
BIAS of ~ 0.06 - 0.04 for the situation with lower aerosol loadings ($\text{AOD } 550 \text{ nm} < 0.2$) and a notable
negative BIAS ($0.02 \sim 0.06$) for moderate ($0.2 < \text{AOD } 550 \text{ nm} < 0.7$) and especially large for high aerosol
loadings ($\text{AOD } 550 \text{ nm} > 0.7$) that reached ~ 0.3 . A very similar tendency can be seen from the statistics of
validation against AERONET in Table 10: both PARASOL/Models and MODIS/DB have very small BIAS
1010 of -0.01 , while the distribution of BIAS is quite different for the situations with different loadings: 0.01 and
 0.03 for low AODs, -0.03 and -0.05 for moderate AODs and for high AOD 0.01 and -0.16 . This suggests
that the observed positive differences when MODIS/DB and MAIAC show higher AOD over bright
surfaces occurs mainly during low AOD conditions. This conclusion is supported by the fact that seasonal
means from all products do not show high AOD over the northern Sahara between 20°N and 30°N latitude.
1015 Also, both DB and MAIAC show significant underestimation of AOD over the Taklamakan desert where
seasonal mean AOD retrieved by PARASOL is high, which agrees with the negative offset between
MODIS DB, MAIAC and PARASOL/Models products over bright and bare soil land surfaces ($\text{NDVI} < 0.4$).

The negative BIAS between MODIS and PARASOL products is clearly seen on the maps of
seasonal AOD from different products for African biomass burning events. The results of correlation
analysis over green vegetation ($\text{NDVI} \geq 0.6$) in Table 16 also show a significant negative BIAS in all
1020 MODIS products compared to PARASOL/Models over green vegetation that increases for medium and
high aerosol loading. The validation against AERONET in Table 10 shows the highest BIAS of 0.06 to
 0.07 for PARASOL/Models is over green vegetation ($\text{NDVI} \geq 0.6$) when $0.2 < \text{AOD} < 0.7$, while the
MODIS products tend to be less biased (DT BIAS = 0.03) or negatively biased (MAIAC BIAS = -0.04 to -
1025 0.06 , and DB BIAS = -0.04) for this surface type and AOD range. This pattern continues for DB and
MAIAC through all the vegetated surfaces with $\text{NDVI} > 0.2$. MODIS DB and MAIAC continue to be more
negatively biased against AERONET for moderate to high aerosol loading than PARASOL/Models is.
Thus, the results suggest that observed differences for African biomass burning events can be explained by
two potential reasons: a combination of overestimations of AOD by PARASOL/GRASP retrievals and



1030 underestimation of AOD by MODIS products for cases of moderate to high aerosol loading. However, the
DT retrievals also show this negative bias against PARASOL/GRASP in the African biomass burning
(Figure 22), but do not follow the same trends against MODIS as DB and MAIAC. Other factors, such as
differences in cloud-screening, data amount, aggregation and quality screening approaches must also
contribute to these differences and need to be investigated in future analysis.

1035 **4.3 AE comparisons between PARASOL/GRASP and MODIS products**

The seasonal pattern of AE from PARASOL (GRASP/HP and GRASP/Models) and MODIS (DT
and DB) products is presented in Fig. 23, as well as, AE differences by season between PARASOL and
MODIS aerosol products in Fig. 24. Table 18 shows the global pixel-to-pixel statistic metrics between AE
products based on references of GRASP/HP; in the brackets, the values corresponding to validation results
1040 over AERONET pixels only. As before, the statistic metrics split into four classes of land surface by NDVI
are presented in Table 19. The GRASP/HP AE products are chosen to be a reference taking into account
the highest obtained correlation in the validation with AERONET in the Section 3. Again, note that
although AOD over land is reported by DT at 470 nm and 660 nm, the spectral dependence of the DT land
retrieval is mostly imposed by assumed aerosol models, and thus DT AE over land is at most a binary
1045 indication of fine and coarse particles, and not a quantitative parameter. We expect no correlation with
GRASP/HP over land. AE over land from DB is similarly prescribed, not retrieved, when $AOD < 0.2$ (Hsu
et al., 2013). On the other hand, the DT AE over ocean is a true quantitative measure.

[Figure 23]

[Figure 24]

1050

[Table 18]

[Table 19]

The differences between PARASOL/GRASP and MODIS DT and DB AE products are pronounced
in all comparisons. From Fig. 23, the seasonal variations for DB and DT are minor, which likely implies
utilization of similar climatological information in the DB and DT algorithms. Even though the differences



1055 for GRASP/Models and GRASP/HP shown in Fig. 24 are not small (mainly due to the limited dynamic
range of aerosol components used in the GRASP/Models approach), the overall pixel-to-pixel correlation
between GRASP/Models and GRASP/HP is the highest between any two products (0.70 over land, 0.74
over ocean). The correlations for AE over land between MODIS DT and DB AE versus GRASP/HP are
lower than 0.5 for all land surface types (Table 19), which is not surprising for the aforementioned reasons.
1060 Over ocean, all available products (GRASP/HP, GRASP/Models and DT) show good agreement with
AERONET measurements, with $R > 0.8$ (Fig. 11 and Table 11), however, the pixel-to-pixel correlation
between DT and GRASP/HP for ocean pixels globally decreases to 0.46. The cause of the drop in
correlation for global statistics is presently unknown. It could be due to assumptions in the DT retrieval, but
could also be linked to differences in calibration between POLDER and MODIS, as AE is particularly
1065 sensitive to nuanced spectral changes in calibration in the lower-AOD conditions often seen over ocean.

4.4 AODF and AODC comparisons between PARASOL/GRASP and MODIS products

This section compares AODF and AODC at 550 nm from PARASOL/GRASP (GRASP/HP and
GRASP/Models) and MODIS DT algorithms. As discussed earlier, the quantitative fine mode fraction (η)
provided by the DT algorithm can be used to derive AODF and AODC only over ocean. Therefore, the
1070 comparison of AODF and AODC over land is between GRASP/HP and GRASP/Models. The seasonal
distribution of AODF and AODC are shown in Fig. 25 and Fig. 27 respectively. The seasonal differences
between GRASP/Models, DT and GRASP/HP are shown in Fig. 26 (AODF) and Fig. 28 (AODC).
GRASP/Models AODF is higher than GRASP/HP over dust source and downwind regions, while it is
lower than GRASP/HP over biomass burning and urban areas, which is consistent with the validation
1075 versus AERONET measurements in Figs. 13-16.

[Figure 25]

[Figure 26]

[Figure 27]

[Figure 28]



1080 Globally, GRASP/Models and GRASP/HP AODF show a consistent agreement over land ($R=0.87$)
and ocean ($R=0.89$), as presented in Table 20. MODIS/DT AODF and AODC over ocean have good
agreement with GRASP/HP with R 0.86 and 0.84 respectively. GRASP/Models AODC shows a better
agreement with GRASP/HP over ocean than over land, while differences are less pronounced, R of 0.89
and 0.71, respectively. As was mentioned above, this tendency can be explained by a stronger sensitivity of
1085 the observed signal to aerosol over dark ocean surface. Another interesting tendency is that correlations for
AODF over land are generally higher than for AODC, while over ocean the situation is inverse and the
correlations are higher for AODC, especially over AERONET. This can probably be explained by the two
facts that dominating oceanic aerosol has a pronounced coarse mode and that at the longer wavelengths,
where the contribution of coarse mode is the strongest, the ocean is practically dark. The land reflectance is,
1090 however, higher than ocean at long wavelengths, even for relatively dark vegetated surfaces. The statistics
of pixel-to-pixel comparison (GRASP/HP and GRASP/Models) over different land surface types, as
discriminated by different NDVI categories, are also reported in Table 22 (AODF) and Table 23 (AODC).

[Table 20]

[Table 21]

1095 [Table 22]

[Table 23]

In conclusion, the differences in more detailed aerosol characteristics including AE, AODF and
AODC (Tables 18-23) derived from PARASOL and MODIS are pronounced over both land and ocean.
This is in contrast to the results for the total AOD from PARASOL and MODIS, which are close over
1100 ocean and in a reasonable agreement over land. This conclusion can likely be generalised by the fact that
retrieval accuracy of detailed aerosol properties is expected to be significantly higher from MAP products
than from mono-viewing photometric imagery.



5 Summary and conclusions

The new PARASOL/GRASP products were extensively evaluated using validations against
1105 AERONET and comparisons with the original POLDER algorithm (PARASOL/Operational), and MODIS
Collection 6 aerosol products. The study was focused on the main aerosol parameters AOD, AE, AODF,
AODC, SSA and AAOD included in all PARASOL/GRASP products. Level 3 data quality filtered and
aggregated to 0.1 degree spatial resolution were used. The validation of PARASOL/GRASP spectral
products (443 – 1020 nm) was done for the full PARASOL archive (2005-2013) against all available
1110 AERONET products. In addition to the direct validation of the full archive of PARASOL satellite products,
the PARASOL/GRASP products were intensively inter-compared with the widely used MODIS/AQUA
aerosol products from DT, DB and MAIAC (land only) algorithms and PARASOL/Operational aerosol
products for one full year, 2008, at 0.1 degree (~10 km) resolution. A global comparison with AERONET
for the year 2008 was performed for all products and the results inter-compared. The percentage of the
1115 cases when the product of each algorithm showed the best statistical metrics among all the products was
used as an indicator for the performance evaluation. In addition, in order to further clarify the level of
consistency of the satellite products, the comparisons of seasonal means as well as the global correlations
of different satellite products at 0.1 degree or 0.2 degree were comprehensively analyzed for the year 2008.
In terms of data volume and geographic extent, the global comparisons analyses are more representative of
1120 the global aerosol system than the subset based on collocations with AERONET.

The results show that the PARASOL/GRASP retrieval provided reliable aerosol products, and
important advancement over the reference MODIS aerosol products:

- Total AOD

- the PARASOL spectral products including AOD for six wavelengths in the range 443 to 1020 nm
1125 agree well with AERONET AOD measurements, e.g. for PARASOL/Models AOD correlation
coefficients R are ≥ 0.86 over land and ≥ 0.94 over ocean with BIAS not exceeding 0.01 over land
and 0.02 over ocean for all wavelengths;



1130 • the AOD (550 nm) products from PARASOL/GRASP (especially GRASP/Models) correlate with AERONET generally similar or better than the correlations of MODIS AOD (550 nm) results both over ocean and land:

- over ocean: all PARASOL (including Operational) and MODIS DT algorithms provide comparable and well correlated retrieval results;
- over land: PARASOL/GRASP provides full land coverage products that correlate generally better with AERONET; MAIAC shows the highest percentage falling with the GCOS
1135 criteria and lowest RMSE among MODIS products, but greater overall BIAS than either DT or DB.

1140 • the correlation between different PARASOL/GRASP products obtained only over AERONET sites and globally are rather consistent, while the correlations between PARASOL and MODIS products for global analysis over land notably degrade compared for those obtained only over AERONET sites, especially for MAIAC and DB. This finding suggests possible dependence of MODIS retrievals on AERONET regional assumptions of aerosol types or AERONET-assisted atmospheric correction to determine surface reflectance, while GRASP retrievals do not use any location specific aerosol or surface assumptions.

- AE:

- 1145
- the PARASOL products agree with AERONET generally similar to the MODIS DT product over ocean and significantly better over land;
 - all PARASOL/GRASP products (Optimized, HP and Models) provide AE values globally over land and ocean that agree between themselves consistently over AERONET sites and globally;

- AODF and AODC:

- 1150
- all PARASOL/GRASP products (Optimized, HP and Models) provide spectral AODF and AODC values globally over ocean and all land covers including bright surfaces, and the different products agree between themselves consistently over AERONET sites and globally;



1155 • the PARASOL/GRASP uniquely provides AODF and AODC with global coverage;
PARASOL/Operational provides only AODF over land, while MODIS AODF and AODC products
are only available over ocean;

- the PARASOL/GRASP AODF and AODC products agree with AERONET as well as MODIS (and PARASOL/Operational) and somewhat better over ocean;

- Aerosol absorption:

- 1160
- all PARASOL/GRASP products (Optimized, HP and Models) provide SSA and AAOD spectral values that are generally not accessible from MODIS and other satellite products;
 - the validation of PARASOL/GRASP shows robust correlation of the retrieved SSA and AAOD spectral values with AERONET (440–1020 nm), correlations increase for retrievals corresponding to the events with higher AOD. For AAOD retrievals overall the BIAS does not exceed 0.01, suggesting that PARASOL products can be used for making global estimations of AAOD at such
1165 level of uncertainty.

Analysis presented in this paper suggests that the data from PARASOL, and therefore from multi-angle polarimeters (MAP) in general, allow not only solid retrievals of conventional aerosol products (e.g. AOD at 550 nm), but also detailed aerosol properties such as AOD for the whole spectrum of observations (e.g. for PARASOL from 443 to 1020 nm), and aerosol SSA and AAOD that are practically not accessible from
1170 mono- and bi- viewing photometric satellite observations, as well as improved AE, AODF, and AODC at a global scale. It is also important to emphasize that PARASOL/GRASP retrievals are based on rigorous optimized inversion that searches for statistically optimized fitting in a continuous space of solution without using widely used Look-up-Tables. As a result, it provides a globally-consistent product using exactly the same aerosol modeling approach over land and ocean, unique set of a priori constraints and
1175 initial guess, while retrieving surface reflectance properties simultaneously with aerosol. It is expected that similar type of approaches will become more common and evolve further in the coming era of multiple MAP instruments, e.g. 3MI, DPC, Aerosol-UA, SPEXone and HARP2, etc. (see more in Dubovik et al.,



2019). The multi-dimensional aerosol information derived from MAPs is expected to improve quality and utility of atmospheric aerosol characterization from space.

1180 One key finding of this work is that the best retrieval of total AOD is provided by the GRASP/Models approach, which restrains the retrieval to a priori aerosol model components, vastly reducing the number of free parameters for retrieval. The more complex GRASP/HP retrieval with many more retrieval parameters seemed to offer more accurate detailed aerosol parameters such as AE, AODF, AODF and SSA. Future efforts on improving the GRASP retrieval will be aimed at achieving accurate
1185 retrievals within one approach. However, this situation also reveals the challenge of a developing unique approach that can provide a retrieval of all parameters with highest accuracy from MAP observations. Indeed, multi-angular polarimetric observations have sensitivity to different aerosol properties, and therefore the MAP algorithms tend to be designed for the retrieval of large number of parameters, while in the situations with low aerosol presence the information may be not sufficient to retrieve all parameters
1190 reliably. Nonetheless, the presented results demonstrate an overall clear advantages of MAP aerosol retrievals compare with photometric mono-viewing product and support high expectations from future MAP missions with improved instrumental and algorithmic developments.

Data availability

The PARASOL/GRASP Optimized, HP and Models products are publicly available the official GRASP
1195 algorithm website (<https://www.grasp-open.com/products>) and the AERIS/ICARE Data and Services Center (<http://www.icare.univ-lille.fr>). The dataset used in the current study is registered under: <http://doi.org/10.5281/zenodo.3887265> (Chen et al., 2020).

Author contribution

The GRASP aerosol products evaluation exercise has been implemented and investigated by the GRASP
1200 team (OD, DF, PL, TL AL, CC). CC and OD carried out this study and analysis. The results were widely



discussed with POLDER/Operational and MODIS (DT, DB and MAIAC) aerosol team, who are co-authors of this paper. CC and OD wrote the manuscript with contributions from all authors. FD, JD, MA, LB, DM, AH and CF carried through the POLDER data processing based on the GRASP-OPEN software.

Competing interests

1205 The authors declare that they have no conflict of interest.

Acknowledgements

The authors would like to acknowledge the use of POLDER data, POLDER/PARASOL Level-1 data originally provided by CNES and AERIS/ICARE Data and Services Center (<http://www.icare.univ-lille.fr/>). The PARASOL/GRASP results are generated by Laboratoire d'Optique Atmosphérique and
1210 Cloudflight Austria GmbH with the GRASP-OPEN software (<https://www.grasp-open.com>). We would like to thank the AERONET team and all PIs of AERONET stations for maintaining the instrument and making the data available for the community. The authors are also grateful to the MODIS aerosol team, especially DT, DB and MAIAC groups, for providing the data used in this study. We would like to acknowledge to the CaPPA (Chemical and Physical Properties of the Atmosphere) project funded by ANR
1215 (ANR-II-LABX-0005-01), AERIS/ICARE Data and Services Center and GRASP-SAS for data.

References

- Anderson, T. L., Wu, Y., Chu, D. A., Schmid, B., Redemann, J. and Dubovik, O.: Testing the MODIS satellite retrieval of aerosol fine-mode fraction, *J. Geophys. Res.*, 110(D18), D18204, doi:10.1029/2005JD005978, 2005.
- 1220 Bellouin, N., Boucher, O., Haywood, J. and Reddy, M. S.: Global estimate of aerosol direct radiative forcing from satellite measurements, *Nature*, 438(7071), 1138–1141, doi:10.1038/nature04348, 2005.
- Benavent-Oltra, J. A., Román, R., Granados-Muñoz, M. J., Pérez-Ramírez, D., Ortiz-Amezcuca, P., Denjean, C., Lopatin, A., Lyamani, H., Torres, B., Guerrero-Rascado, J. L., Fuertes, D., Dubovik, O., Chaikovsky, A., Olmo, F. J., Mallet, M. and Alados-Arboledas, L.: Comparative assessment of GRASP algorithm for a dust event over Granada (Spain) during



- 1225 ChArMEx-ADRIMED 2013 campaign, *Atmos. Meas. Tech.*, 10(11), 4439–4457, doi:10.5194/amt-10-4439-2017, 2017.
- Benavent-Oltra, J. A., Román, R., Casquero-Vera, J. A., Pérez-Ramírez, D., Lyamani, H., Ortiz-Amezcuca, P., Bedoya-Velásquez, A. E., de Arruda Moreira, G., Barreto, Á., Lopatin, A., Fuertes, D., Herrera, M., Torres, B., Dubovik, O., Guerrero-Rascado, J. L., Goloub, P., Olmo-Reyes, F. J. and Alados-Arboledas, L.: Different strategies to retrieve aerosol properties at night-time with the GRASP algorithm, *Atmos. Chem. Phys.*, 19(22), 14149–14171, doi:10.5194/acp-19-1230-2019, 2019.
- Boucher, O., Randall, D., Artaxo, P., Bretherton, C., Feingold, G., Forster, P., Kerminen, V., Kondo, Y., Liao, H., Lohmann, U., Rasch, P., Satheesh, S., Sherwood, S., Stevens, B., Zhang, X., Qin, D., Plattner, G., Tignor, M., Allen, S., Boschung, J., Nauels, A., Xia, Y., Bex, V. and Midgley, P.: Clouds and Aerosols, in *Climate Change 2013: The Physical Science Basis. Contribution of Working Group I to the Fifth Assessment Report of the Intergovernmental Panel on Climate Change*, 1235 Stocker, T.F., D. Qin, G.-K. Plattner, M. Tignor, S.K. Allen, J. Boschung, A. Nauels, Y. Xia, Cambridge University Press, Cambridge, United Kingdom and New York, NY, USA. [online] Available from: http://www.ipcc.ch/pdf/assessment-report/ar5/wg1/WG1AR5_Chapter07_FINAL.pdf, 2013.
- Bréon, F.-M., Vermeulen, A. and Descloitres, J.: An evaluation of satellite aerosol products against sunphotometer measurements, *Remote Sens. Environ.*, 115(12), 3102–3111, doi:10.1016/J.RSE.2011.06.017, 2011.
- 1240 Chen, C., Dubovik, O., Henze, D. K., Lapyonok, T., Chin, M., Ducos, F., Litvinov, P., Huang, X. and Li, L.: Retrieval of desert dust and carbonaceous aerosol emissions over Africa from POLDER/PARASOL products generated by the GRASP algorithm, *Atmos. Chem. Phys.*, 18(16), 12551–12580, doi:10.5194/acp-18-12551-2018, 2018.
- Chen, C., Dubovik, O., Henze, D. K., Chin, M., Lapyonok, T., Schuster, G. L., Ducos, F., Fuertes, D., Litvinov, P., Li, L., Lopatin, A., Hu, Q. and Torres, B.: Constraining global aerosol emissions using POLDER/PARASOL satellite remote sensing observations, *Atmos. Chem. Phys.*, 19(23), 14585–14606, doi:10.5194/acp-19-14585-2019, 2019.
- 1245 Chen, C., Dubovik, O., Fuertes, D., Litvinov, P., Lapyonok, T., Lopatin, A., Ducos, F., Derimian, Y., Herman, M., Tanré, D., Remer, L. A., Lyapustin, A., Sayer, A. M., Levy, R. C., Hsu, N. C., Descloitres, J., Li, L., Torres, B., Karol, Y., Herrera, M., Herreras, M., Aspetsberger, M., Wanzenboeck, M., Bindreiter, L., Marth, D., Hangler, A. and Federspiel, C.: Dataset used for PARASOL/GRASP aerosol products validation with AERONET and comparison with MODIS, doi:10.5281/ZENODO.3887265, 2020.
- Chu, D. A., Kaufman, Y. J., Ichoku, C., Remer, L. A., Tanré, D. and Holben, B. N.: Validation of MODIS aerosol optical depth retrieval over land, *Geophys. Res. Lett.*, 29(12), doi:10.1029/2001GL013205, 2002.
- Derimian, Y., Dubovik, O., Huang, X., Lapyonok, T., Litvinov, P., Kostinski, A. B., Dubuisson, P. and Ducos, F.: Comprehensive tool for calculation of radiative fluxes: illustration of shortwave aerosol radiative effect sensitivities to the



- 1255 details in aerosol and underlying surface characteristics, *Atmos. Chem. Phys.*, 16(9), 5763–5780, doi:10.5194/acp-16-5763-2016, 2016.
- Deschamps, P.-Y., Breon, F.-M., Leroy, M., Podaire, A., Bricaud, A., Buriez, J.-C. and Seze, G.: The POLDER mission: instrument characteristics and scientific objectives, *IEEE Trans. Geosci. Remote Sens.*, 32(3), 598–615, doi:10.1109/36.297978, 1994.
- 1260 Deuzé, J. L., Herman, M., Goloub, P., Tanré, D. and Marchand, A.: Characterization of aerosols over ocean from POLDER/ADEOS-1, *Geophys. Res. Lett.*, 26(10), 1421–1424, doi:10.1029/1999GL900168, 1999.
- Deuzé, J. L., Bréon, F. M., Devaux, C., Goloub, P., Herman, M., Lafrance, B., Maignan, F., Marchand, A., Nadal, F., Perry, G. and Tanré, D.: Remote sensing of aerosols over land surfaces from POLDER-ADEOS-1 polarized measurements, *J. Geophys. Res. Atmos.*, 106(D5), 4913–4926, doi:10.1029/2000JD900364, 2001.
- 1265 Dubovik, O.: Optimization of Numerical Inversion in Photopolarimetric Remote Sensing, in *Photopolarimetry in Remote Sensing*, pp. 65–106, Kluwer Academic Publishers, Dordrecht., 2004.
- Dubovik, O. and King, M. D.: A flexible inversion algorithm for retrieval of aerosol optical properties from Sun and sky radiance measurements, *J. Geophys. Res. Atmos.*, 105(D16), 20673–20696, doi:10.1029/2000JD900282, 2000.
- Dubovik, O., Smirnov, A., Holben, B. N., King, M. D., Kaufman, Y. J., Eck, T. F. and Slutsker, I.: Accuracy assessments of aerosol optical properties retrieved from Aerosol Robotic Network (AERONET) Sun and sky radiance measurements, *J. Geophys. Res. Atmos.*, 105(D8), 9791–9806, doi:10.1029/2000JD900040, 2000.
- 1270 Dubovik, O., Holben, B. N., Lapyonok, T., Sinyuk, A., Mishchenko, M. I., Yang, P. and Slutsker, I.: Non-spherical aerosol retrieval method employing light scattering by spheroids, *Geophys. Res. Lett.*, 29(10), 54-1-54-4, doi:10.1029/2001GL014506, 2002a.
- 1275 Dubovik, O., Holben, B., Eck, T. F., Smirnov, A., Kaufman, Y. J., King, M. D., Tanré, D. and Slutsker, I.: Variability of Absorption and Optical Properties of Key Aerosol Types Observed in Worldwide Locations, *J. Atmos. Sci.*, 59(3), 590–608, doi:10.1175/1520-0469(2002)059<0590:VOAAOP>2.0.CO;2, 2002b.
- Dubovik, O., Sinyuk, A., Lapyonok, T., Holben, B. N., Mishchenko, M., Yang, P., Eck, T. F., Volten, H., Muñoz, O., Veihelmann, B., van der Zande, W. J., Leon, J.-F., Sorokin, M. and Slutsker, I.: Application of spheroid models to account for aerosol particle nonsphericity in remote sensing of desert dust, *J. Geophys. Res.*, 111(D11), D11208, doi:10.1029/2005JD006619, 2006.
- 1280 Dubovik, O., Herman, M., Holdak, A., Lapyonok, T., Tanré, D., Deuzé, J. L., Ducos, F., Sinyuk, A. and Lopatin, A.: Statistically optimized inversion algorithm for enhanced retrieval of aerosol properties from spectral multi-angle polarimetric satellite observations, *Atmos. Meas. Tech.*, 4(5), 975–1018, doi:10.5194/amt-4-975-2011, 2011.



- 1285 Dubovik, O., Lapyonok, T., Litvinov, P., Herman, M., Fuertes, D., Ducos, F., Torres, B., Derimian, Y., Huang, X., Lopatin, A., Chaikovskiy, A., Aspetsberger, M. and Federspiel, C.: GRASP: a versatile algorithm for characterizing the atmosphere, SPIE Newsroom, doi:10.1117/2.1201408.005558, 2014.
- Dubovik, O., Li, Z., Mishchenko, M. I., Tanré, D., Karol, Y., Bojkov, B., Cairns, B., Diner, D. J., Espinosa, W. R., Goloub, P., Gu, X., Hasekamp, O., Hong, J., Hou, W., Knobelspiesse, K. D., Landgraf, J., Li, L., Litvinov, P., Liu, Y., Lopatin, A.,
- 1290 Marbach, T., Maring, H., Martins, V., Meijer, Y., Milinevsky, G., Mukai, S., Parol, F., Qiao, Y., Remer, L., Rietjens, J., Sano, I., Stammes, P., Stamnes, S., Sun, X., Tabary, P., Travis, L. D., Waquet, F., Xu, F., Yan, C. and Yin, D.: Polarimetric remote sensing of atmospheric aerosols: Instruments, methodologies, results, and perspectives, *J. Quant. Spectrosc. Radiat. Transf.*, 224, 474–511, doi:10.1016/J.JQSRT.2018.11.024, 2019.
- Eck, T. F., Holben, B. N., Reid, J. S., Dubovik, O., Smirnov, A., O'Neill, N. T., Slutsker, I. and Kinne, S.: Wavelength
- 1295 dependence of the optical depth of biomass burning, urban, and desert dust aerosols, *J. Geophys. Res. Atmos.*, 104(D24), 31333–31349, doi:10.1029/1999JD900923, 1999.
- Espinosa, W. R., Remer, L. A., Dubovik, O., Ziemba, L., Beyersdorf, A., Orozco, D., Schuster, G., Lapyonok, T., Fuertes, D. and Martins, J. V.: Retrievals of aerosol optical and microphysical properties from Imaging Polar Nephelometer scattering measurements, *Atmos. Meas. Tech.*, 10(3), 811–824, doi:10.5194/amt-10-811-2017, 2017.
- 1300 Espinosa, W. R., Martins, J. V., Remer, L. A., Dubovik, O., Lapyonok, T., Fuertes, D., Puthukkudy, A., Orozco, D., Ziemba, L., Thornhill, K. L. and Levy, R.: Retrievals of Aerosol Size Distribution, Spherical Fraction, and Complex Refractive Index From Airborne In Situ Angular Light Scattering and Absorption Measurements, *J. Geophys. Res. Atmos.*, 124(14), 7997–8024, doi:10.1029/2018JD030009, 2019.
- Fougnie, B., Marbach, T., Lacan, A., Lang, R., Schlüssel, P., Poli, G., Munro, R. and Couto, A. B.: The multi-viewing multi-
- 1305 channel multi-polarisation imager – Overview of the 3MI polarimetric mission for aerosol and cloud characterization, *J. Quant. Spectrosc. Radiat. Transf.*, 219, 23–32, doi:10.1016/j.jqsrt.2018.07.008, 2018.
- Fu, G., Hasekamp, O., Rietjens, J., Smit, M., Di Noia, A., Cairns, B., Wasilewski, A., Diner, D., Seidel, F., Xu, F., Knobelspiesse, K., Gao, M., da Silva, A., Burton, S., Hostetler, C., Hair, J. and Ferrare, R.: Aerosol retrievals from different polarimeters during the ACEPOL campaign using a common retrieval algorithm, *Atmos. Meas. Tech.*, 13(2),
- 1310 553–573, doi:10.5194/amt-13-553-2020, 2020.
- Gao, M., Zhai, P.-W., Franz, B., Knobelspiesse, K., Ibrahim, A., Cairns, B., Craig, S., Fu, G., Hasekamp, O., Hu, Y. and Werdell, P. J.: Inversion of multi-angular polarimetric measurements from the ACEPOL campaign: an application of improving aerosol property and hyperspectral ocean color retrievals, *Atmos. Meas. Tech.*, 13(7), 3939–3956, doi:10.5194/amt-13-3939-2020, 2020.



- 1315 Giles, D. M., Sinyuk, A., Sorokin, M. G., Schafer, J. S., Smirnov, A., Slutsker, I., Eck, T. F., Holben, B. N., Lewis, J. R., Campbell, J. R., Welton, E. J., Korkin, S. V. and Lyapustin, A. I.: Advancements in the Aerosol Robotic Network (AERONET) Version 3 database – automated near-real-time quality control algorithm with improved cloud screening for Sun photometer aerosol optical depth (AOD) measurements, *Atmos. Meas. Tech.*, 12(1), 169–209, doi:10.5194/amt-12-169-2019, 2019.
- 1320 Goloub, P., Tanré, D., Deuzé, J. L., Herman, M., Marchand, A. and Breon, F.-M.: Validation of the first algorithm applied for deriving the aerosol properties over the ocean using the POLDER/ADEOS measurements, *IEEE Trans. Geosci. Remote Sens.*, 37(3), 1586–1596, doi:10.1109/36.763270, 1999.
- Gupta, P., R.C. Levy, S. Mattoo, L. Remer, and L.A. Munchak, (2016): A surface reflectance scheme for retrieving aerosol optical depth over urban surfaces in MODIS Dark Target retrieval algorithm. *Atmos. Meas. Tech.*, 9, 3293-3308, DOI: 10.5194/amt-9-3293-2016.
- 1325 Gupta, P., L.A. Remer, R.C. Levy and S. Mattoo, 2018: Validation of MODIS 3 km land aerosol optical depth from NASA’s EOS Terra and Aqua missions. *Atmos. Meas. Tech.*, 11, 3145-3159, doi: 10.5194/amt-11-3145-2018.
- Hansen, J., Rossow, W., Carlson, B., Lacis, A., Travis, L., Del Genio, A., Fung, I., Cairns, B., Mishchenko, M. and Sato, M.: Low-cost long-term monitoring of global climate forcings and feedbacks, *Clim. Change*, 31(2–4), 247–271, doi:10.1007/BF01095149, 1995.
- 1330 Hasekamp, O. P., Fu, G., Rusli, S. P., Wu, L., Di Noia, A., Brugh, J. aan de, Landgraf, J., Martijn Smit, J., Rietjens, J. and van Amerongen, A.: Aerosol measurements by SPEXone on the NASA PACE mission: expected retrieval capabilities, *J. Quant. Spectrosc. Radiat. Transf.*, 227, 170–184, doi:10.1016/j.jqsrt.2019.02.006, 2019.
- Herman, M., Deuzé, J. L., Devaux, C., Goloub, P., Bréon, F. M. and Tanré, D.: Remote sensing of aerosols over land surfaces including polarization measurements and application to POLDER measurements, *J. Geophys. Res. Atmos.*, 102(D14), 17039–17049, doi:10.1029/96JD02109, 1997.
- 1335 Herman, M., Deuzé, J. L., Marchand, A., Roger, B. and Lallart, P.: Aerosol remote sensing from POLDER/ADEOS over the ocean: Improved retrieval using a nonspherical particle model, *J. Geophys. Res.*, 110(D10), D10S02, doi:10.1029/2004JD004798, 2005.
- 1340 Holben, B. N., Eck, T. F., Slutsker, I., Tanré, D., Buis, J. P., Setzer, A., Vermote, E., Reagan, J. A., Kaufman, Y. J., Nakajima, T., Lavenue, F., Jankowiak, I. and Smirnov, A.: AERONET—A Federated Instrument Network and Data Archive for Aerosol Characterization, *Remote Sens. Environ.*, 66(1), 1–16, doi:10.1016/S0034-4257(98)00031-5, 1998.
- Holzer-Popp, T., de Leeuw, G., Griesfeller, J., Martynenko, D., Klüser, L., Bevan, S., Davies, W., Ducos, F., Deuzé, J. L., Grainger, R. G., Heckel, A., von Hoyningen-Hüne, W., Kolmonen, P., Litvinov, P., North, P., Poulsen, C. A., Ramon, D.,



- 1345 Siddans, R., Sogacheva, L., Tanré, D., Thomas, G. E., Vountas, M., Descloitres, J., Griesfeller, J., Kinne, S., Schulz, M. and Pinnock, S.: Aerosol retrieval experiments in the ESA Aerosol_cci project, *Atmos. Meas. Tech.*, 6(8), 1919–1957, doi:10.5194/amt-6-1919-2013, 2013.
- Hsu, N. C., Tsay, S.-C., King, M. D. and Herman, J. R.: Aerosol Properties Over Bright-Reflecting Source Regions, *IEEE Trans. Geosci. Remote Sens.*, 42(3), 557–569, doi:10.1109/TGRS.2004.824067, 2004.
- 1350 Hsu, N. C., Tsay, S.-C., King, M. D. and Herman, J. R.: Deep Blue Retrievals of Asian Aerosol Properties During ACE-Asia, *IEEE Trans. Geosci. Remote Sens.*, 44(11), 3180–3195, doi:10.1109/TGRS.2006.879540, 2006.
- Hsu, N. C., Jeong, M.-J., Bettenhausen, C., Sayer, A. M., Hansell, R., Seftor, C. S., Huang, J. and Tsay, S.-C.: Enhanced Deep Blue aerosol retrieval algorithm: The second generation, *J. Geophys. Res. Atmos.*, 118(16), 9296–9315, doi:10.1002/jgrd.50712, 2013.
- 1355 Hu, Q., Goloub, P., Veselovskii, I., Bravo-Aranda, J.-A., Popovici, I. E., Podvin, T., Haeffelin, M., Lopatin, A., Dubovik, O., Pietras, C., Huang, X., Torres, B. and Chen, C.: Long-range-transported Canadian smoke plumes in the lower stratosphere over northern France, *Atmos. Chem. Phys.*, 19(2), 1173–1193, doi:10.5194/acp-19-1173-2019, 2019.
- Ichoku, C., Chu, D. A., Mattoo, S., Kaufman, Y. J., Remer, L. A., Tanré, D., Slutsker, I. and Holben, B. N.: A spatio-temporal approach for global validation and analysis of MODIS aerosol products, *Geophys. Res. Lett.*, 29(12), 8006, doi:10.1029/2001GL013206, 2002.
- 1360 Jethva, H., Torres, O., and Yoshida, Y.: Accuracy assessment of MODIS land aerosol optical thickness algorithms using AERONET measurements over North America, *Atmos. Meas. Tech.*, 12, 4291–4307, <https://doi.org/10.5194/amt-12-4291-2019>, 2019.
- Kahn, R. A., Gaitley, B. J., Martonchik, J. V., Diner, D. J., Crean, K. A. and Holben, B.: Multiangle Imaging Spectroradiometer (MISR) global aerosol optical depth validation based on 2 years of coincident Aerosol Robotic Network (AERONET) observations, *J. Geophys. Res.*, 110(D10), D10S04, doi:10.1029/2004JD004706, 2005.
- Kaufman, Y. J., Tanré, D., Remer, L. A., Vermote, E. F., Chu, A. and Holben, B. N.: Operational remote sensing of tropospheric aerosol over land from EOS moderate resolution imaging spectroradiometer, *J. Geophys. Res. Atmos.*, 102(D14), 17051–17067, doi:10.1029/96jd03988, 1997.
- 1370 Kaufman, Y. J., Tanré, D. and Boucher, O.: A satellite view of aerosols in the climate system, *Nature*, 419(6903), 215–223, doi:10.1038/nature01091, 2002.
- King, M. D., Kaufman, Y. J., Tanré, D. and Nakajima, T.: Remote Sensing of Tropospheric Aerosols from Space: Past, Present, and Future, *Bull. Am. Meteorol. Soc.*, 80(11), 2229–2259, doi:10.1175/1520-0477(1999)080<2229:RSOTAF>2.0.CO;2, 1999.



- 1375 Kinne, S., Lohmann, U., Feichter, J., Schulz, M., Timmreck, C., Ghan, S., Easter, R., Chin, M., Ginoux, P., Takemura, T., Tegen, I., Koch, D., Herzog, M., Penner, J., Pitari, G., Holben, B., Eck, T., Smirnov, A., Dubovik, O., Slutsker, I., Tanré, D., Torres, O., Mishchenko, M., Geogdzhayev, I., Chu, D. A. and Kaufman, Y.: Monthly averages of aerosol properties: A global comparison among models, satellite data, and AERONET ground data, *J. Geophys. Res.*, 108(D20), 4634, doi:10.1029/2001JD001253, 2003.
- 1380 Kinne, S., O'Donnel, D., Stier, P., Kloster, S., Zhang, K., Schmidt, H., Rast, S., Giorgetta, M., Eck, T. F. and Stevens, B.: MAC-v1: A new global aerosol climatology for climate studies, *J. Adv. Model. Earth Syst.*, 5(4), 704–740, doi:10.1002/jame.20035, 2013.
- Knobelspiesse, K., Cairns, B., Mishchenko, M., Chowdhary, J., Tsigaridis, K., van Diedenhoven, B., Martin, W., Ottaviani, M. and Alexandrov, M.: Analysis of fine-mode aerosol retrieval capabilities by different passive remote sensing instrument designs, *Opt. Express*, 20(19), 21457, doi:10.1364/oe.20.021457, 2012.
- 1385 Knobelspiesse, K., J Barbosa, H. M., Bradley, C., Bruegge, C., Cairns, B., Chen, G., Chowdhary, J., Cook, A., Di Noia, A., van Diedenhoven, B., Diner, D. J., Ferrare, R., Fu, G., Gao, M., Garay, M., Hair, J., van Harten, G., Hasekamp, O., Helmlinger, M., Hostetler, C., Kalashnikova, O., Kupchock, A., Longo De Freitas, K., Maring, H., Vanderlei Martins, J., McBride, B., McGill, M., Norlin, K., Puthukkudy, A., Rheingans, B., Rietjens, J., Seidel, F. C., da Silva, A., Smit, M., Stamnes, S., Tan, Q., Val, S., Wasilewski, A., Xu, F., Xu, X. and Yorks, J.: The Aerosol Characterization from Polarimeter and Lidar (ACEPOL) airborne field campaign, *Earth Syst. Sci. Data Discuss.*, doi:10.5194/essd-2020-76, 2020.
- 1390 Kokhanovsky, A. A., Davis, A. B., Cairns, B., Dubovik, O., Hasekamp, O. P., Sano, I., Mukai, S., Rozanov, V. V., Litvinov, P., Lapyonok, T., Kolomiets, I. S., Oberemok, Y. A., Savenkov, S., Martin, W., Wasilewski, A., Di Noia, A., Stap, F. A., Rietjens, J., Xu, F., Natraj, V., Duan, M., Cheng, T. and Munro, R.: Space-based remote sensing of atmospheric aerosols: The multi-angle spectro-polarimetric frontier, *Earth-Science Rev.*, 145, 85–116, doi:10.1016/j.earscirev.2015.01.012, 2015.
- 1395 de Leeuw, G., Holzer-Popp, T., Bevan, S., Davies, W. H., Descloitres, J., Grainger, R. G., Griesfeller, J., Heckel, A., Kinne, S., Klüser, L., Kolmonen, P., Litvinov, P., Martynenko, D., North, P., Ovigneur, B., Pascal, N., Poulsen, C., Ramon, D., Schulz, M., Siddans, R., Sogacheva, L., Tanré, D., Thomas, G. E., Virtanen, T. H., von Hoyningen Huene, W., Vountas, M. and Pinnock, S.: Evaluation of seven European aerosol optical depth retrieval algorithms for climate analysis, *Remote Sens. Environ.*, 162, 295–315, doi:10.1016/j.rse.2013.04.023, 2015.
- 1400 Levy, R. C., Remer, L. A., Tanré, D., Kaufman, Y. J., Ichoku, C., Holben, B. N., Livingston, J. M., Russell, P. B. and Maring, H.: Evaluation of the moderate-resolution imaging spectroradiometer (MODIS) retrievals of dust aerosol over the ocean during PRIDE, *J. Geophys. Res. D Atmos.*, 108(19), doi:10.1029/2002jd002460, 2003.



- 1405 Levy, R. C., Remer, L. A. and Dubovik, O.: Global aerosol optical properties and application to Moderate Resolution Imaging Spectroradiometer aerosol retrieval over land, *J. Geophys. Res. Atmos.*, 112(13), doi:10.1029/2006JD007815, 2007a.
- Levy, R. C., Remer, L. A., Mattoo, S., Vermote, E. F. and Kaufman, Y. J.: Second-generation operational algorithm: Retrieval of aerosol properties over land from inversion of Moderate Resolution Imaging Spectroradiometer spectral reflectance, *J. Geophys. Res. Atmos.*, 112(D13), doi:10.1029/2006JD007811, 2007b.
- 1410 Levy, R. C., Remer, L. A., Kleidman, R. G., Mattoo, S., Ichoku, C., Kahn, R. and Eck, T. F.: Global evaluation of the Collection 5 MODIS dark-target aerosol products over land, *Atmos. Chem. Phys.*, 10(21), 10399–10420, doi:10.5194/acp-10-10399-2010, 2010.
- Levy, R. C., Mattoo, S., Munchak, L. A., Remer, L. A., Sayer, A. M., Patadia, F. and Hsu, N. C.: The Collection 6 MODIS aerosol products over land and ocean, *Atmos. Meas. Tech.*, 6(11), 2989–3034, doi:10.5194/amt-6-2989-2013, 2013.
- 1415 Levy, R.C., S. Mattoo, V. Sawyer, Y. Shi, P.R. Colarco, A.I. Lyapustin, Y. Wang and L.A. Remer, 2018: Exploring systematic offsets between aerosol products from the two MODIS sensors. *Atmos. Meas. Tech.*, 11, 4073-4092, doi: 10.5194/amt-11-4073-2018.
- Li, J., Kahn, R. A., Wei, J., Carlson, B. E., Lacis, A. A., Li, Z., Li, X., Dubovik, O. and Nakajima, T.: Synergy of Satellite and Ground-Based Aerosol Optical Depth Measurements Using an Ensemble Kalman Filter Approach, *J. Geophys. Res. Atmos.*, 125(5), doi:10.1029/2019JD031884, 2020.
- 1420 Li, L., Dubovik, O., Derimian, Y., Schuster, G. L., Lapyonok, T., Litvinov, P., Ducos, F., Fuertes, D., Chen, C., Li, Z., Lopatin, A., Torres, B. and Che, H.: Retrieval of aerosol components directly from satellite and ground-based measurements, *Atmos. Chem. Phys.*, 13409–13443, doi:10.5194/acp-19-13409-2019, 2019.
- Li, L., Che, H., Derimian, Y., Dubovik, O., Schuster, G. L., Chen, C., Li, Q., Wang, Y., Guo, B., Zhang, X., Key, S., Weather, S., Lac, C. and Academy, C.: Remote Sensing of Environment Retrievals of fine mode light-absorbing carbonaceous aerosols from POLDER/PARASOL observations over East and South Asia, *Remote Sens. Environ.*, 247, doi:10.1016/j.rse.2020.111913, 2020a.
- 1425 Li, L., Che, H., Derimian, Y., Dubovik, O. and Luan, Q.: Climatology of fine and coarse mode aerosol optical thickness over East and South Asia derived from POLDER / PARASOL satellite, *J. Geophys. Res. Atmos.*, doi:10.1029/2020JD032665, 2020b.
- 1430 Li, X. and Strahler, A. H.: Geometric-Optical Bidirectional Reflectance Modeling of the Discrete Crown Vegetation Canopy: Effect of Crown Shape and Mutual Shadowing, *IEEE Trans. Geosci. Remote Sens.*, 30(2), 276–292, doi:10.1109/36.134078, 1992.
- Li, Z., Zhao, X., Kahn, R., Mishchenko, M., Remer, L., Lee, K.-H., Wang, M., Laszlo, I., Nakajima, T. and Maring, H.:



- 1435 Uncertainties in satellite remote sensing of aerosols and impact on monitoring its long-term trend: a review and perspective, *Ann. Geophys.*, 27(7), 2755–2770, doi:10.5194/angeo-27-2755-2009, 2009.
- Li, Z., Hou, W., Hong, J., Zheng, F., Luo, D., Wang, J., Gu, X. and Qiao, Y.: Directional Polarimetric Camera (DPC): Monitoring aerosol spectral optical properties over land from satellite observation, *J. Quant. Spectrosc. Radiat. Transf.*, 218, 21–37, doi:10.1016/J.QSRT.2018.07.003, 2018.
- 1440 Litvinov, P., Hasekamp, O. and Cairns, B.: Models for surface reflection of radiance and polarized radiance: Comparison with airborne multi-angle photopolarimetric measurements and implications for modeling top-of-atmosphere measurements, *Remote Sens. Environ.*, 115(2), 781–792, doi:10.1016/J.RSE.2010.11.005, 2011a.
- Litvinov, P., Hasekamp, O., Cairns, B. and Mishchenko, M.: Semi-empirical BRDF and BPDF models applied to the problem of aerosol retrievals over land: testing on airborne data and implications for modeling of top-of-atmosphere measurements, in book: *Polarimetric Detection, Characterization and Remote Sensing*, Springer, Dordrecht., 2011b.
- 1445 Liu, L., Mishchenko, M. I., Geogdzhayev, I., Smirnov, A., Sakerin, S. M., Kabanov, D. M. and Ershov, O. A.: Global validation of two-channel AVHRR aerosol optical thickness retrievals over the oceans, *J. Quant. Spectrosc. Radiat. Transf.*, 88(1–3), 97–109, doi:10.1016/j.jqsrt.2004.03.031, 2004.
- Lopatin, A., Dubovik, O., Chaikovskiy, A., Goloub, P., Lapyonok, T., Tanré, D. and Litvinov, P.: Enhancement of aerosol characterization using synergy of lidar and sun-photometer coincident observations: the GARRLiC algorithm, *Atmos. Meas. Tech.*, 6(8), 2065–2088, doi:10.5194/amt-6-2065-2013, 2013.
- 1450 Lyapustin, A., Wang, Y., Laszlo, I., Kahn, R., Korkin, S., Remer, L., Levy, R. and Reid, J. S.: Multiangle implementation of atmospheric correction (MAIAC): 2. Aerosol algorithm, *J. Geophys. Res.*, 116(D3), D03211, doi:10.1029/2010JD014986, 2011a.
- 1455 Lyapustin, A., Wang, Y., Korkin, S. and Huang, D.: MODIS Collection 6 MAIAC algorithm, *Atmos. Meas. Tech.*, 11, 5741–5765, doi:10.5194/amt-11-5741-2018, 2018.
- Lyapustin, A. I., Martonchik, J. V., Wang, Y., Laszlo, I. and Korkin, S.: Multiangle implementation of atmospheric correction (MAIAC): 1. Radiative transfer basis and look-up tables, *J. Geophys. Res.*, 116(D3), D03210, doi:10.1029/2010JD014985, 2011b.
- 1460 Lyapustin, A. I., Wang, Y., Laszlo, I., Hilker, T., Hall, F. G., Seller, P. J., Tucker, C. J. and Korin, S. V.: Multi-angle implementation of atmospheric correction for MODIS (MAIAC): 3. Atmospheric correction, *Remote Sens. Environ.*, 127, 385–393, doi:10.1016/J.RSE.2012.09.002, 2012.
- Maignan, F., Bréon, F. M., Fédèle, E. and Bouvier, M.: Polarized reflectances of natural surfaces: Spaceborne measurements and analytical modeling, *Remote Sens. Environ.*, 113(12), 2642–2650, doi:10.1016/j.rse.2009.07.022, 2009.



- 1465 Milinevsky, G., Oberemok, Y., Syniavskiy, I., Bovchaliuk, A., Kolomiets, I., Fesianov, I. and Wang, Y.: Calibration model of polarimeters on board the Aerosol-UA space mission, *J. Quant. Spectrosc. Radiat. Transf.*, 229, 92–105, doi:10.1016/j.jqsrt.2019.03.007, 2019.
- Mishchenko, M. I., Cairns, B., Hansen, J. E., Travis, L. D., Burg, R., Kaufman, Y. J., Martins, J. V. and Shettle, E. P.: Monitoring of aerosol forcing of climate from space: Analysis of measurement requirements, *J. Quant. Spectrosc. Radiat. Transf.*, 88(1–3), 149–161, doi:10.1016/j.jqsrt.2004.03.030, 2004.
- 1470 Myhre, G.: Consistency between satellite-derived and modeled estimates of the direct aerosol effect., *Science (80-.)*, 325(5937), 187–90, doi:10.1126/science.1174461, 2009.
- O'Neill, N. T., Eck, T. F., Smirnov, A., Holben, B. N. and Thulasiraman, S.: Spectral discrimination of coarse and fine mode optical depth, *J. Geophys. Res. Atmos.*, 108(17), doi:10.1029/2002jd002975, 2003.
- 1475 Parkinson, C. L.: Aqua: An earth-observing satellite mission to examine water and other climate variables, *IEEE Trans. Geosci. Remote Sens.*, 41(2 PART 1), 173–183, doi:10.1109/TGRS.2002.808319, 2003.
- Popp, T., de Leeuw, G., Bingen, C., Brühl, C., Capelle, V., Chedin, A., Clarisse, L., Dubovik, O., Grainger, R., Griesfeller, J., Heckel, A., Kinne, S., Klüser, L., Kosmale, M., Kolmonen, P., Lelli, L., Litvinov, P., Mei, L., North, P., Pinnock, S., Povey, A., Robert, C., Schulz, M., Sogacheva, L., Stebel, K., Stein Zweers, D., Thomas, G., Tilstra, L., Vandenbussche, S., Veefkind, P., Vountas, M. and Xue, Y.: Development, Production and Evaluation of Aerosol Climate Data Records from European Satellite Observations (Aerosol_cci), *Remote Sens.*, 8(5), 421, doi:10.3390/rs8050421, 2016.
- 1480 Puthukkudy, A., Martins, J. V., Remer, L. A., Xu, X., Dubovik, O., Litvinov, P., McBride, B., Burton, S. and Barbosa, H. M. J.: Retrieval of aerosol properties from Airborne Hyper Angular Rainbow Polarimeter (AirHARP) observations during ACEPOL 2017, *Atmos. Meas. Tech. Discuss.*, doi:10.5194/amt-2020-64, 2020.
- 1485 Remer, L. A., Tanré, D., Kaufman, Y. J., Ichoku, C., Mattoo, S., Levy, R., Chu, D. A., Holben, B., Dubovik, O., Smirnov, A., Martins, J. V., Li, R. R. and Ahmad, Z.: Validation of MODIS aerosol retrieval over ocean, *Geophys. Res. Lett.*, 29(12), 8008, doi:10.1029/2001GL013204, 2002.
- Remer, L. A., Kaufman, Y. J., Tanré, D., Mattoo, S., Chu, D. A., Martins, J. V., Li, R.-R., Ichoku, C., Levy, R. C., Kleidman, R. G., Eck, T. F., Vermote, E., Holben, B. N., Remer, L. A., Kaufman, Y. J., Tanré, D., Mattoo, S., Chu, D. A., Martins, J. V., Li, R.-R., Ichoku, C., Levy, R. C., Kleidman, R. G., Eck, T. F., Vermote, E. and Holben, B. N.: The MODIS Aerosol Algorithm, Products, and Validation, *J. Atmos. Sci.*, 62(4), 947–973, doi:10.1175/JAS3385.1, 2005.
- 1490 Remer, L. A., Kleidman, R. G., Levy, R. C., Kaufman, Y. J., Tanré, D., Mattoo, S., Martins, J. V., Ichoku, C., Koren, I., Yu, H. and Holben, B. N.: Global aerosol climatology from the MODIS satellite sensors, *J. Geophys. Res.*, 113(D14), D14S07, doi:10.1029/2007JD009661, 2008.



- 1495 Remer, L. A., Davis, A. B., Mattoo, S., Levy, R. C., Kalashnikova, O. V., Coddington, O., Chowdhary, J., Knobelspiesse, K.,
Xu, X., Ahmad, Z., Boss, E., Cairns, B., Dierssen, H. M., Diner, D. J., Franz, B., Frouin, R., Gao, B.-C., Ibrahim, A.,
Martins, J. V., Omar, A. H., Torres, O., Xu, F. and Zhai, P.-W.: Retrieving Aerosol Characteristics From the PACE
Mission, Part 1: Ocean Color Instrument, *Front. Earth Sci.*, 7, 152, doi:10.3389/feart.2019.00152, 2019.
- Román, R., Torres, B., Fuertes, D., Cachorro, V. E., Dubovik, O., Toledano, C., Cazorla, A., Barreto, A., Bosch, J. L., Lapyonok,
1500 T., González, R., Goloub, P., Perrone, M. R., Olmo, F. J., de Frutos, A. and Alados-Arboledas, L.: Remote sensing of lunar
aureole with a sky camera: Adding information in the nocturnal retrieval of aerosol properties with GRASP code, *Remote
Sens. Environ.*, 196, 238–252, doi:10.1016/J.RSE.2017.05.013, 2017.
- Ross, J.: *The radiation regime and architecture of plant stands*, Dr W. Junk Publishers., The Hague, Netherlands., 1981.
- Sato, M., Hansen, J., Koch, D., Lacis, A., Ruedy, R., Dubovik, O., Holben, B., Chin, M. and Novakov, T.: Global atmospheric
1505 black carbon inferred from AERONET., *Proc. Natl. Acad. Sci. U. S. A.*, 100(11), 6319–6324,
doi:10.1073/pnas.0731897100, 2003.
- Sayer, A. M., Hsu, N. C., Bettenhausen, C. and Jeong, M.-J.: Validation and uncertainty estimates for MODIS Collection 6
“Deep Blue” aerosol data, *J. Geophys. Res. Atmos.*, 118(14), 7864–7872, doi:10.1002/jgrd.50600, 2013.
- Sayer, A. M., Munchak, L. A., Hsu, N. C., Levy, R. C., Bettenhausen, C. and Jeong, M.-J.: MODIS Collection 6 aerosol
1510 products: Comparison between Aqua’s e-Deep Blue, Dark Target, and “merged” data sets, and usage recommendations, *J.
Geophys. Res. Atmos.*, 119(24), 13,965–13,989, doi:10.1002/2014JD022453, 2014.
- Sayer, A. M., Hsu, N. C., Bettenhausen, C., Jeong, M. J. and Meister, G.: Effect of MODIS Terra radiometric calibration
improvements on Collection 6 Deep Blue aerosol products: Validation and Terra/Aqua consistency, *J. Geophys. Res.
Atmos.*, 120(23), doi:10.1002/2015JD023878, 2015.
- 1515 Sayer, A. M., Hsu, N. C., Lee, J., Kim, W. V., Dubovik, O., Dutcher, S. T., Huang, D., Litvinov, P., Lyapustin, A., Tackett, J. L.
and Winker, D. M.: Validation of SOAR VIIRS Over Water Aerosol Retrievals and Context Within the Global Satellite
Aerosol Data Record, *J. Geophys. Res. Atmos.*, 123(23), 2018JD029465, doi:10.1029/2018JD029465, 2018.
- Sayer, A. M., Hsu, N. C., Lee, J., Kim, W. V. and Dutcher, S. T.: Validation, Stability, and Consistency of MODIS Collection
6.1 and VIIRS Version 1 Deep Blue Aerosol Data Over Land, *J. Geophys. Res. Atmos.*, 124(8), 4658–4688,
1520 doi:10.1029/2018JD029598, 2019.
- Schoeberl, M. R., Douglass, A. R., Hilsenrath, E., Bhartia, P. K., Beer, R., Waters, J. W., Gunson, M. R., Froidevaux, L., Gille,
J. C., Barnett, J. J., Levelt, P. F. and DeCola, P.: Overview of the EOS aura mission, *IEEE Trans. Geosci. Remote Sens.*,
44(5), 1066–1072, doi:10.1109/TGRS.2005.861950, 2006.
- Schuster, G. L., Espinosa, W. R., Ziemba, L. D., Beyersdorf, A. J., Rocha-Lima, A., Anderson, B. E., Martins, J. V., Dubovik,



- 1525 O., Ducos, F., Fuertes, D., Lapyonok, T., Shook, M., Derimian, Y. and Moore, R. H.: A Laboratory Experiment for the Statistical Evaluation of Aerosol Retrieval (STEAR) Algorithms, *Remote Sens.*, 11(5), 498, doi:10.3390/rs11050498, 2019.
- Schutgens, N., Tsyro, S., Gryspeerdt, E., Goto, D., Weigum, N., Schulz, M. and Stier, P.: On the spatio-temporal representativeness of observations, *Atmos. Chem. Phys.*, 17, 9761–9780, doi:10.5194/acp-17-9761-2017, 2017.
- 1530 Sinyuk, A., Holben, B., Eck, T., Giles, D., Slutsker, I., Korkin, S., Schafer, J., Smirnov, A., Sorokin, M. and Lyapustin, A.: The AERONET Version 3 aerosol retrieval algorithm, associated uncertainties and comparisons to Version 2, *Atmos. Meas. Tech.*, 13, 3375–3411, doi: 10.5194/amt-13-3375-2020, 2020.
- Smirnov, A., Holben, B. N., Eck, T. F., Dubovik, O. and Slutsker, I.: Cloud-Screening and Quality Control Algorithms for the AERONET Database, *Remote Sens. Environ.*, 73(3), 337–349, doi:10.1016/S0034-4257(00)00109-7, 2000.
- 1535 Sogacheva, L., Popp, T., Sayer, A. M., Dubovik, O., Garay, M. J., Heckel, A., Hsu, N. C., Jethva, H., Kahn, R. A., Kolmonen, P., Kosmale, M., de Leeuw, G., Levy, R. C., Litvinov, P., Lyapustin, A., North, P., Torres, O. and Arola, A.: Merging regional and global aerosol optical depth records from major available satellite products, *Atmos. Chem. Phys.*, 20(4), 2031–2056, doi:10.5194/acp-20-2031-2020, 2020.
- Tan, Y., Li, E., Zhang, Z., Lin, X., Chi, Y., Zhou, L., Wu, C. and Wang, Q.: Validation of POLDER-3/GRASP aerosol products using AERONET measurements over China, *Atmos. Environ.*, 215, 116893, doi:10.1016/j.atmosenv.2019.116893, 2019.
- 1540 Tanré, D., Kaufman, Y. J., Herman, M. and Mattoo, S.: Remote sensing of aerosol properties over oceans using the MODIS/EOS spectral radiances, *J. Geophys. Res. Atmos.*, 102(D14), 16971–16988, doi:10.1029/96JD03437, 1997.
- Tanré, D., Bréon, F. M., Deuzé, J. L., Dubovik, O., Ducos, F., François, P., Goloub, P., Herman, M., Lifermann, A. and Waquet, F.: Remote sensing of aerosols by using polarized, directional and spectral measurements within the A-Train: the PARASOL mission, *Atmos. Meas. Tech.*, 4(7), 1383–1395, doi:10.5194/amt-4-1383-2011, 2011.
- 1545 Titos, G., Ealo, M., Román, R., Cazorla, A., Sola, Y., Dubovik, O., Alastuey, A. and Pandolfi, M.: Retrieval of aerosol properties from ceilometer and photometer measurements: long-term evaluation with in situ data and statistical analysis at Montsec (southern Pyrenees), *Atmos. Meas. Tech.*, 12(6), 3255–3267, doi:10.5194/amt-12-3255-2019, 2019.
- Torres, B., Dubovik, O., Fuertes, D., Schuster, G., Cachorro, V. E., Lapyonok, T., Goloub, P., Blarel, L., Barreto, A., Mallet, M., Toledano, C. and Tanré, D.: Advanced characterisation of aerosol size properties from measurements of spectral optical depth using the GRASP algorithm, *Atmos. Meas. Tech.*, 10(10), 3743–3781, doi:10.5194/amt-10-3743-2017, 2017.
- 1550 Tsekeri, A., Lopatin, A., Amiridis, V., Marinou, E., Iglhoffstein, J., Siomos, N., Solomos, S., Kokkalis, P., Engelmann, R., Baars, H., Gratsea, M., Raptis, P. I., Biniotoglou, I., Mihalopoulos, N., Kalivitis, N., Kouvarakis, G., Bartsotas, N., Kallos, G., Basart, S., Schuettmeyer, D., Wandinger, U., Ansmann, A., Chaikovsky, A. P. and Dubovik, O.: GARRLiC and LIRIC:



- 1555 strengths and limitations for the characterization of dust and marine particles along with their mixtures, *Atmos. Meas. Tech.*, 10(12), 4995–5016, doi:10.5194/amt-10-4995-2017, 2017.
- Wagner, F. and Silva, A. M.: Some considerations about Ångström exponent distributions, *Atmos. Chem. Phys.*, 8(3), 481–489, doi:10.5194/acp-8-481-2008, 2008.
- 1560 Waquet, F., Cairns, B., Knobelspiesse, K., Chowdhary, J., Travis, L. D., Schmid, B. and Mishchenko, M. I.: Polarimetric remote sensing of aerosols over land, *J. Geophys. Res. Atmos.*, 114(1), doi:10.1029/2008JD010619, 2009.
- Wei, J., Peng, Y., Mahmood, R., Sun, L. and Guo, J.: Intercomparison in spatial distributions and temporal trends derived from multi-source satellite aerosol products, *Atmos. Chem. Phys.*, 19, 7183–7207, doi:10.5194/acp-19-7183-2019, 2019.
- Wei, Y., Li, Z., Zhang, Y., Chen, C., Dubovik, O., Zhang, Y., Xu, H., Li, K., Chen, J., Wang, H., Ge, B. and Fan, C.: Validation of POLDER GRASP Aerosol Optical Retrieval Over China Using SONET Observations, *J. Quant. Spectrosc. Radiat. Transf.*, 246, 106931, doi:10.1016/j.jqsrt.2020.106931, 2020.
- 1565 Winker, D. M., Pelon, J., Coakley, J. A., Ackerman, S. A., Charlson, R. J., Colarco, P. R., Flamant, P., Fu, Q., Hoff, R. M., Kittaka, C., Kubar, T. L., Le Treut, H., McCormick, M. P., Mégie, G., Poole, L., Powell, K., Trepte, C., Vaughan, M. A. and Wielicki, B. A.: The CALIPSO Mission: A Global 3D View of Aerosols and Clouds, *Bull. Am. Meteorol. Soc.*, 91(9), 1211–1230, doi:10.1175/2010BAMS3009.1, 2010.
- 1570 Yu, H., Kaufman, Y. J., Chin, M., Feingold, G., Remer, L. A., Anderson, T. L., Balkanski, Y., Bellouin, N., Boucher, O., Christopher, S., Decola, P., Kahn, R., Koch, D., Loeb, N., Reddy, M. S., Schulz, M., Takemura, T. and Zhou, M.: A review of measurement-based assessments of the aerosol direct radiative effect and forcing, *Atmos. Chem. Phys.*, 6, 613–666, 2006.
- Zhang, Y. and Li, Z.: Remote sensing of atmospheric fine particulate matter (PM_{2.5}) mass concentration near the ground from satellite observation, *Remote Sens. Environ.*, 160, 252–262, doi:10.1016/j.rse.2015.02.005, 2015.
- 1575

1580



1585

1590

Table 1. List of aerosol parameters in PARASOL/GRASP products

Parameters	Dimension	Description
AOD	(λ , Latitude, Longitude)	Aerosol optical depth
AExp	(Latitude, Longitude)	AE (670/865 nm)
AODF	(λ , Latitude, Longitude)	Fine mode AOD
AODC	(λ , Latitude, Longitude)	Coarse mode AOD
AAOD	(λ , Latitude, Longitude)	Aerosol absorption optical depth
SSA	(λ , Latitude, Longitude)	Single scattering albedo
RealRefIndSpect	(λ , Latitude, Longitude)	Real part of refractive index
ImagRefIndSpect	(λ , Latitude, Longitude)	Imaginary part of refractive index
SizeDistrLogNormBin	(5, Latitude, Longitude)	5 Bins of size distribution
SphereFraction	(Latitude, Longitude)	Sphere fraction
VertProfileHeight	(Latitude, Longitude)	Aerosol scale height (unit: m)
LandPercentage	(Latitude, Longitude)	Land percentage (%)
ResidualRelative	(Latitude, Longitude)	Relative residual

$\lambda = 443, 490, 565, 670, 865, \text{ and } 1020 \text{ nm}$

1595

Table 2. Strategies used to select quality assured PARASOL and MODIS aerosol products

		Land	Ocean
POLDER	GRASP/Optimized	"ResidualRelative"<0.05	"ResidualRelative"<0.1
	GRASP/HP	"ResidualRelative"<0.05	"ResidualRelative"<0.1
	GRASP/Models	"ResidualRelative"<1.0	"ResidualRelative"<1.0
	Operational	0.8≤Quality Index≤1.0	0.8≤Quality Index≤1.0
MODIS	DT	QA Flag = 3	QA Flag = 3
	DB	QA Flag = 3	₋₁
	MAIAC	QA = '0000'	₋₂

¹ DB aerosol product is not available over ocean.

² MAIAC aerosol product is presently only available for tiles containing land, so the ocean retrievals are not considered in this study.



1600 Table 3. Global statistics of PARASOL/GRASP spectral AOD vs. AERONET AOD over land and ocean. The best performing of three approaches by each metric is labelled in bold.

Land/Ocean	Band (nm)	Products	R	Slope	Offset	RMSE	GCOS (%)	BIAS	BIAS $\tau < 0.2$	BIAS $0.2 \leq \tau \leq 0.7$	BIAS $\tau > 0.7$
Land	443	Optimized (41268)	0.900	0.867	0.104	0.179	26.7	0.06	0.09	0.06	-0.06
		HP (42202)	0.915	0.981	0.072	0.181	32.7	0.07	0.07	0.07	0.05
		Models (28449)	0.932	1.013	0.003	0.140	49.3	0.01	0.01	0.00	0.02
	490	Optimized (41268)	0.892	0.879	0.099	0.171	26.8	0.06	0.08	0.06	-0.04
		HP (42202)	0.909	1.000	0.069	0.174	33.2	0.07	0.07	0.07	0.07
		Models (28449)	0.929	1.025	0.003	0.131	51.6	0.01	0.01	0.01	0.03
	550	Optimized (41268)	0.876	0.847	0.101	0.162	27.5	0.06	0.08	0.05	-0.08
		HP (42202)	0.898	0.973	0.074	0.163	34.0	0.07	0.07	0.07	0.04
		Models (28449)	0.922	1.023	0.005	0.123	54.2	0.01	0.01	0.01	0.03
	565	Optimized (41268)	0.877	0.877	0.096	0.161	27.3	0.06	0.08	0.06	-0.05
		HP (42202)	0.898	1.004	0.069	0.165	34.0	0.07	0.07	0.07	0.07
		Models (28449)	0.920	1.011	0.006	0.120	54.4	0.01	0.01	0.00	0.02
	670	Optimized (41268)	0.858	0.823	0.099	0.152	28.4	0.06	0.08	0.05	-0.10
		HP (42202)	0.886	0.955	0.077	0.153	35.0	0.07	0.07	0.07	0.02
		Models (28449)	0.911	0.954	0.016	0.108	58.6	0.01	0.01	-0.01	-0.03
	865	Optimized (41268)	0.816	0.785	0.093	0.142	31.3	0.05	0.07	0.03	-0.15
		HP (42202)	0.856	0.932	0.074	0.142	37.6	0.06	0.06	0.07	-0.02
		Models (28449)	0.880	0.935	0.018	0.105	60.3	0.01	0.02	-0.01	-0.04
1020	Optimized (40148)	0.791	0.772	0.089	0.139	32.8	0.05	0.07	0.02	-0.17	
	HP (41016)	0.837	0.924	0.073	0.138	38.8	0.06	0.06	0.06	-0.03	
	Models (27551)	0.856	0.943	0.023	0.109	59.5	0.01	0.02	0.00	-0.04	
Ocean	443	Optimized (1495)	0.938	1.028	0.049	0.084	40.5	0.05	0.05	0.07	0.03
		HP (1551)	0.939	1.043	0.046	0.083	41.2	0.05	0.05	0.06	0.05
		Models (2064)	0.940	0.970	0.026	0.066	60.6	0.02	0.02	0.03	-0.06
	490	Optimized (1495)	0.939	1.064	0.041	0.079	43.2	0.05	0.04	0.07	0.05
		HP (1551)	0.942	1.077	0.039	0.079	43.1	0.05	0.05	0.07	0.09
		Models (2064)	0.946	0.969	0.023	0.057	65.1	0.02	0.02	0.02	-0.05
	550	Optimized (1495)	0.936	1.060	0.035	0.071	48.4	0.05	0.04	0.06	0.04
		HP (1551)	0.940	1.083	0.036	0.074	46.4	0.05	0.04	0.07	0.11
		Models (2064)	0.950	0.960	0.019	0.050	70.3	0.01	0.01	0.01	-0.05
	565	Optimized (1495)	0.939	1.090	0.033	0.072	48.5	0.05	0.04	0.07	0.05
		HP (1551)	0.943	1.105	0.033	0.074	46.7	0.05	0.04	0.07	0.12
		Models (2064)	0.950	0.939	0.020	0.048	71.2	0.01	0.01	0.00	-0.07
	670	Optimized (1495)	0.936	1.071	0.030	0.064	55.8	0.04	0.04	0.06	0.02
		HP (1551)	0.943	1.099	0.032	0.068	50.9	0.05	0.04	0.07	0.11
		Models (2064)	0.951	0.876	0.021	0.043	77.3	0.00	0.01	-0.02	-0.13



865	Optimized (1495)	0.931	1.077	0.020	0.053	66.0	0.03	0.03	0.05	0.15
	HP (1551)	0.942	1.129	0.024	0.060	58.3	0.04	0.03	0.06	0.17
	Models (2064)	0.955	0.852	0.015	0.038	82.1	0.00	0.00	-0.03	-0.13
1020	Optimized (1431)	0.927	1.063	0.017	0.049	71.3	0.02	0.02	0.04	0.15
	HP (1501)	0.940	1.143	0.021	0.058	60.9	0.04	0.03	0.07	0.18
	Models (2002)	0.957	0.865	0.013	0.035	84.6	0.00	0.00	-0.03	-0.11



Table 4. Global statistics of PARASOL/GRASP AE vs. AERONET AE (440/870) over land and ocean.

The best performing of three approaches by each metric is labelled in bold.

		R	Slope	Offset	RMSE	BIAS
Land	Optimized (18594)	0.797	0.680	0.213	0.358	-0.10
	HP (19093)	0.843	0.716	0.139	0.336	-0.14
	Models (11468)	0.681	0.415	0.511	0.420	-0.04
Ocean	Optimized (363)	0.935	0.773	0.199	0.210	0.01
	HP (391)	0.949	0.817	0.092	0.193	-0.05
	Models (522)	0.958	0.620	0.451	0.292	0.16

1605



Table 5. Global statistics of PARASOL/GRASP AODF vs. AERONET SDA AODF at 550 nm over land and ocean. The best performing of three approaches by each metric is labelled in bold.

		R	Slope	Offset	RMSE	GCOS Fraction (%)	BIAS	BIAS $\tau_{r(550)} < 0.2$	BIAS $0.2 \leq \tau_{r(550)} \leq 0.7$	BIAS $\tau_{r(550)} > 0.7$
Land	Optimized (31902)	0.922	0.840	0.044	0.100	54.9	0.02	0.03	0.01	-0.16
	HP (32973)	0.924	0.892	0.029	0.098	60.9	0.01	0.02	0.01	-0.10
	Models (23653)	0.868	0.662	0.028	0.094	64.5	-0.02	0.00	-0.07	-0.37
Ocean	Optimized (1074)	0.901	0.958	0.042	0.058	56.7	0.04	0.04	0.05	-0.24
	HP (1155)	0.908	0.932	0.028	0.043	76.3	0.02	0.02	0.03	-0.27
	Models (1338)	0.834	0.746	0.035	0.048	77.5	0.02	0.02	-0.03	-0.33

Table 6. Global statistics of PARASOL/GRASP AODC vs. AERONET SDA AODC at 550 nm over land and ocean. The best performing of three approaches by each metric is labelled in bold.

		R	Slope	Offset	RMSE	GCOS Fraction (%)	BIAS	BIAS $\tau_{c(550)} < 0.2$	BIAS $0.2 \leq \tau_{c(550)} \leq 0.7$	BIAS $\tau_{c(550)} > 0.7$
Land	Optimized (31903)	0.686	0.744	0.062	0.117	43.1	0.04	0.05	-0.03	-0.18
	HP (32973)	0.742	0.933	0.057	0.124	47.7	0.05	0.05	0.03	-0.02
	Models (23651)	0.571	0.653	0.040	0.112	64.3	0.02	0.03	-0.08	-0.28
Ocean	Optimized (1076)	0.871	0.942	0.009	0.046	77.6	0.01	0.00	0.01	0.03
	HP (1156)	0.915	1.119	0.015	0.051	70.0	0.02	0.02	0.06	0.20
	Models (1337)	0.922	0.754	0.010	0.036	84.8	-0.01	0.00	-0.06	-0.09



Table 7. Global statistics of PARASOL/GRASP spectral SSA vs. AERONET SSA stratified by PARASOL AOD (565 nm) levels. The best performing at each wavelength of three approaches by each metric is labelled in bold.

AOD Level	Band (nm)	Products	R	Slope	Offset	RMSE	BIAS
All L3 data	443	Optimized (7192)	0.285	0.292	0.631	0.051	-0.01
		HP (7450)	0.254	0.266	0.666	0.051	0.00
		Models (6095)	0.348	0.349	0.582	0.047	-0.01
	670	Optimized (7192)	0.511	0.608	0.324	0.065	-0.04
		HP (7450)	0.536	0.648	0.299	0.056	-0.03
		Models (6095)	0.321	0.334	0.602	0.057	-0.02
	865	Optimized (7192)	0.566	0.667	0.267	0.068	-0.04
		HP (7450)	0.594	0.698	0.253	0.058	-0.03
		Models (6095)	0.360	0.347	0.597	0.059	-0.01
	1020	Optimized (7192)	0.596	0.705	0.230	0.072	-0.04
		HP (7450)	0.627	0.730	0.223	0.060	-0.03
		Models (6095)	0.372	0.334	0.615	0.062	0.00
AOD>0.5	443	Optimized (3695)	0.315	0.312	0.619	0.045	-0.01
		HP (4235)	0.242	0.242	0.691	0.047	0.00
		Models (2424)	0.413	0.345	0.594	0.037	0.00
	670	Optimized (3695)	0.534	0.612	0.327	0.056	-0.04
		HP (4235)	0.552	0.642	0.307	0.051	-0.03
		Models (2424)	0.455	0.355	0.592	0.042	-0.01
	865	Optimized (3695)	0.593	0.668	0.274	0.059	-0.04
		HP (4235)	0.615	0.699	0.254	0.052	-0.03
		Models (2424)	0.535	0.387	0.571	0.043	0.00
	1020	Optimized (3695)	0.627	0.703	0.240	0.061	-0.04
		HP (4235)	0.647	0.726	0.228	0.054	-0.03
		Models (2424)	0.564	0.376	0.586	0.046	0.00
AOD>1.0	443	Optimized (715)	0.478	0.459	0.499	0.034	0.00
		HP (976)	0.398	0.366	0.587	0.037	0.00
		Models (463)	0.585	0.457	0.499	0.027	0.01
	670	Optimized (715)	0.674	0.712	0.252	0.036	-0.02
		HP (976)	0.664	0.687	0.277	0.036	-0.02
		Models (463)	0.665	0.464	0.497	0.031	-0.01
	865	Optimized (715)	0.702	0.699	0.264	0.039	-0.02
		HP (976)	0.704	0.692	0.272	0.037	-0.02
		Models (463)	0.737	0.487	0.483	0.033	0.00
	1020	Optimized (715)	0.715	0.694	0.268	0.042	-0.02
		HP (976)	0.723	0.699	0.265	0.040	-0.02
		Models (463)	0.757	0.453	0.519	0.038	0.01
AOD>1.5	443	Optimized (212)	0.544	0.536	0.430	0.030	0.00
		HP (317)	0.527	0.518	0.459	0.031	0.00
		Models (116)	0.639	0.491	0.472	0.022	0.00
	670	Optimized (212)	0.734	0.752	0.220	0.030	-0.01
		HP (317)	0.752	0.804	0.171	0.029	-0.01
		Models (116)	0.814	0.567	0.402	0.023	0.00
	865	Optimized (212)	0.760	0.688	0.283	0.032	-0.01
		HP (317)	0.770	0.738	0.235	0.030	-0.01
		Models (116)	0.876	0.602	0.375	0.025	0.00
	1020	Optimized (212)	0.770	0.666	0.303	0.035	-0.01
		HP (317)	0.779	0.716	0.256	0.034	-0.01
		Models (116)	0.889	0.556	0.423	0.032	0.01



Table 8. Global statistics of PARASOL/GRASP spectral AAOD vs. AERONET AAOD. The best performing at each wavelength of three approaches by each metric is labelled in bold

Band (nm)	Products	R	Slope	Offset	RMSE	BIAS
443	Optimized (7192)	0.486	0.475	0.040	0.046	0.01
	HP (7450)	0.498	0.536	0.034	0.047	0.00
	Models (8046)	0.538	0.509	0.035	0.042	0.00
670	Optimized (7192)	0.480	0.571	0.033	0.034	0.02
	HP (7450)	0.517	0.673	0.028	0.034	0.02
	Models (8046)	0.480	0.492	0.023	0.026	0.01
865	Optimized (7192)	0.393	0.476	0.029	0.028	0.02
	HP (7450)	0.438	0.574	0.024	0.028	0.01
	Models (8046)	0.444	0.439	0.017	0.020	0.00
1020	Optimized (7192)	0.343	0.430	0.026	0.025	0.01
	HP (7450)	0.394	0.526	0.022	0.025	0.01
	Models (8046)	0.414	0.409	0.015	0.018	0.00



1620 Table 9. Statistics of PARASOL and MODIS AOD products against collocated AERONET AOD at 550 nm over land and ocean

		Reference: AERONET AOD (τ_{550})								
		R	Slope	Offset	RMSE	GCOS Fraction (%)	BIAS	BIAS $\tau_{550} < 0.2$	BIAS $0.2 \leq \tau_{550} \leq 0.7$	BIAS $\tau_{550} > 0.7$
Land	GRASP/Optimized (3647)	0.875	0.780	0.098	0.150	28.8	0.04	0.07	0.02	-0.13
	GRASP/HP (4777)	0.908	0.938	0.078	0.157	32.4	0.06	-0.07	0.06	0.02
	GRASP/Models (3111)	0.924	0.989	0.005	0.121	53.2	0.00	0.01	-0.01	0.02
	DT (6858)	0.898	0.988	0.021	0.120	46.1	0.02	0.02	0.02	0.00
	DB (8409)	0.870	0.841	0.026	0.126	48.8	-0.01	0.01	-0.04	-0.14
	MAIAC_0.1 (8164)	0.895	0.793	0.007	0.112	52.8	-0.03	-0.01	-0.08	-0.19
	MAIAC_0.01 (9054)	0.874	0.796	0.014	0.125	48.1	-0.03	0.00	-0.08	-0.19
Ocean	GRASP/Optimized (116)	0.950	1.145	0.033	0.089	42.4	0.06	0.05	0.09	0.17
	GRASP/HP (154)	0.947	1.074	0.054	0.092	26.6	0.07	0.06	0.08	0.13
	GRASP/Models (205)	0.963	0.965	0.024	0.061	62.9	0.02	0.02	0.02	-0.04
	Operational (207)	0.954	1.165	-0.009	0.077	52.2	0.03	0.01	0.04	0.18
	DT (218)	0.952	0.974	0.037	0.081	55.0	0.03	0.03	0.04	0.00



Table 10. Statistics of PARASOL and MODIS AOD products against collocated AERONET AOD at 550 nm classified by NDVI. In each individual NDVI level, the best performing metric is indicated in bold. The number of matched pairs is included in brackets.

		Reference: AERONET AOD (τ_{550})								
		R	Slope	Offset	RMSE	GCOS Fraction (%)	BIAS	BIAS $\tau_{550} < 0.2$	BIAS $0.2 \leq \tau_{550} \leq 0.7$	BIAS $\tau_{550} > 0.7$
Land NDVI<0.2	GRASP/Optimized (1055)	0.892	0.711	0.105	0.153	23.0	0.02	0.08	-0.01	-0.20
	GRASP/HP (1410)	0.915	0.860	0.104	0.155	26.0	0.06	0.09	0.05	-0.03
	GRASP/Models (786)	0.873	0.888	0.023	0.159	39.8	-0.01	0.01	-0.03	0.01
	DT (99)	0.792	0.878	0.073	0.216	44.4	0.05	0.04	0.12	-0.04
	DB (1327)	0.845	0.790	0.044	0.153	44.2	-0.01	0.03	-0.05	-0.16
	MAIAC_0.1 (1853)	0.883	0.734	0.032	0.139	42.4	-0.03	0.02	-0.09	-0.22
	MAIAC_0.01 (2087)	0.853	0.734	0.041	0.155	35.7	-0.03	0.03	-0.09	-0.22
Land 0.2≤NDVI<0.4	GRASP/Optimized (1106)	0.881	0.777	0.101	0.161	31.9	0.04	0.07	0.03	-0.16
	GRASP/HP (1479)	0.928	0.911	0.074	0.145	39.4	0.05	0.05	0.06	-0.03
	GRASP/Models (1020)	0.953	1.062	-0.014	0.125	52.7	0.00	0.00	-0.01	0.04
	DT (1847)	0.895	0.947	0.029	0.145	40.6	0.02	0.03	0.01	-0.05
	DB (2204)	0.888	0.883	0.010	0.142	46.3	-0.02	0.00	-0.05	-0.09
	MAIAC_0.1 (2049)	0.901	0.825	-0.005	0.133	53.9	-0.04	-0.01	-0.11	-0.18
	MAIAC_0.01 (2363)	0.896	0.826	0.002	0.134	51.5	-0.04	0.00	-0.10	-0.18
Land 0.4≤NDVI<0.6	GRASP/Optimized (958)	0.880	0.868	0.083	0.138	31.7	0.05	0.07	0.03	-0.02
	GRASP/HP (1249)	0.903	1.069	0.047	0.173	33.2	0.07	0.06	0.07	0.12
	GRASP/Models (1074)	0.920	0.952	0.014	0.086	61.5	0.00	0.01	0.00	-0.04
	DT (2702)	0.907	0.994	0.012	0.112	46.6	0.01	0.01	0.02	-0.01
	DB (2718)	0.866	0.808	0.030	0.120	50.0	-0.01	0.01	-0.03	-0.20
	MAIAC_0.1 (2193)	0.911	0.821	-0.009	0.093	53.5	-0.04	-0.03	-0.07	-0.19
	MAIAC_0.01 (2530)	0.899	0.827	-0.002	0.097	50.5	-0.03	-0.02	-0.07	-0.17
Land NDVI≥0.6	GRASP/Optimized (194)	0.832	0.932	0.108	0.145	23.7	0.09	0.10	0.08	0.09
	GRASP/HP (287)	0.853	1.001	0.107	0.160	21.3	0.11	0.10	0.11	0.10
	GRASP/Models (231)	0.910	1.115	0.011	0.083	61.9	0.03	0.02	0.07	0.06
	DT (943)	0.910	1.118	-0.005	0.076	55.0	0.01	0.01	0.03	0.17
	DB (907)	0.855	0.884	0.015	0.076	60.2	0.00	0.01	-0.04	0.07
	MAIAC_0.1 (651)	0.826	0.837	-0.005	0.063	66.2	-0.02	-0.02	-0.06	-0.04
	MAIAC_0.01 (669)	0.840	0.929	-0.013	0.074	61.3	-0.02	-0.02	-0.04	0.10



1625 **Table 11. Statistics of PARASOL and MODIS AE products against collocated AERONET AE over land and ocean, with a threshold of satellite AOD (550 nm) > 0.2.**

		Reference: AERONET AE				
		R	Slope	Offset	RMSE	BIAS
Land	GRASP/Optimized (2035)	0.745	0.641	0.168	0.435	-0.19
	GRASP/HP (2791)	0.772	0.654	0.122	0.425	-0.21
	GRASP/Models (1253)	0.686	0.407	0.507	0.443	-0.06
	DT (2589)	0.390	0.372	0.514	0.599	-0.31
	DB (3279)	0.563	0.650	0.444	0.573	0.04
Ocean	GRASP/Optimized (55)	0.840	0.724	0.183	0.279	-0.02
	GRASP/HP (80)	0.890	0.810	0.051	0.229	-0.08
	GRASP/Models (92)	0.949	0.625	0.431	0.291	0.20
	Operational (57)	0.891	0.812	0.841	0.782	0.75
	DT (106)	0.832	0.610	0.317	0.305	0.08



Table 12. Statistics of PARASOL and MODIS AODF products against collocated AERONET AODF over land and ocean

		Reference: AERONET AODF (τ_{f550})								
		R	Slope	Offset	RMSE	GCOS Fraction (%)	BIAS	BIAS $\tau_{f(550)} < 0.2$	BIAS $0.2 \leq \tau_{f(550)} \leq 0.7$	BIAS $\tau_{f(550)} > 0.7$
Land	GRASP/Optimized (2634)	0.923	0.762	0.043	0.104	58.0	0.00	0.02	-0.01	-0.23
	GRASP/HP (3507)	0.926	0.828	0.036	0.106	59.5	0.01	0.02	0.00	-0.17
	GRASP/Models (2795)	0.868	0.587	0.035	0.124	63.8	-0.02	0.00	-0.08	-0.46
	Operational (2619)	0.886	0.546	0.052	0.162	50.5	-0.04	0.00	-0.08	-0.45
Ocean	GRASP/Optimized (91)	0.893	1.397	0.023	0.079	40.7	0.06	0.05	0.10	--
	GRASP/HP (129)	0.924	1.118	0.018	0.049	75.2	0.03	0.03	0.05	--
	GRASP/Models (168)	0.866	1.046	0.028	0.054	65.5	0.03	0.03	0.02	--
	Operational (82)	0.780	1.082	0.017	0.061	67.1	0.02	0.02	0.00	--
	DT (119)	0.808	0.887	0.048	0.067	56.3	0.04	0.04	-0.01	--

Table 13. Statistics of PARASOL and MODIS AODC products against collocated AERONET AODC over land and ocean

		Reference: AERONET AODC (τ_{c550})								
		R	Slope	Offset	RMSE	GCOS Fraction (%)	BIAS	BIAS $\tau_{c(550)} < 0.2$	BIAS $0.2 \leq \tau_{c(550)} \leq 0.7$	BIAS $\tau_{c(550)} > 0.7$
Land	GRASP/Optimized (2634)	0.700	0.678	0.058	0.114	45.6	0.03	0.04	-0.06	-0.24
	GRASP/HP (3506)	0.771	0.912	0.060	0.127	45.8	0.05	0.06	0.02	0.00
	GRASP/Models (2795)	0.536	0.596	0.043	0.125	63.7	0.01	0.03	-0.12	-0.28
	DT (1472)	0.501	0.912	0.246	0.332	11.8	0.24	0.24	0.22	0.06
Ocean	GRASP/Optimized (91)	0.936	1.033	0.021	0.062	59.3	0.03	0.02	0.05	0.03
	GRASP/HP (129)	0.961	1.113	0.033	0.070	45.0	0.05	0.04	0.07	0.20
	GRASP/Models (168)	0.966	0.827	0.008	0.040	81.5	-0.01	0.00	-0.05	-0.09
	Operational (82)	0.936	0.971	0.014	0.045	74.4	0.01	0.01	-0.01	--
	DT (119)	0.911	0.806	0.025	0.045	68.9	0.00	0.01	-0.03	-0.11

1630



Table 14. Pixel to pixel ($0.2^\circ \times 0.2^\circ$) statistical metrics between PARASOL/Operational and PARASOL/GRASP aerosol products; the statistics for only AERONET pixels are presented in brackets.

			Reference: PARASOL/Operational							
			R	Slope	Offset	RMSE	BIAS	BIAS $\tau/\tau_r/\tau_c < 0.2$	BIAS $0.2 \leq \tau/\tau_r/\tau_c \leq 0.7$	BIAS $\tau/\tau_r/\tau_c > 0.7$
Land	AODF	GRASP/HP 8 209 015 (7801)	0.88 (0.91)	1.22 (1.13)	0.03 (0.02)	0.13 (0.13)	0.06 (0.05)	0.04 (0.04)	0.10 (0.05)	0.29 (0.18)
		GRASP/Models 8 117 246 (7427)	0.85 (0.83)	0.94 (0.74)	0.03 (0.04)	0.10 (0.13)	0.02 (-0.01)	0.03 (0.01)	0.02 (-0.04)	-0.05 (-0.19)
Ocean	AOD	GRASP/HP 5 702 109 (93)	0.88 (0.98)	1.19 (1.22)	0.04 (0.04)	0.10 (0.16)	0.06 (0.11)	0.06 (0.08)	0.10 (0.10)	0.22 (0.38)
		GRASP/Models 5 988 842 (91)	0.94 (0.99)	1.09 (1.14)	0.00 (0.01)	0.04 (0.09)	0.01 (0.05)	0.01 (0.04)	0.03 (0.03)	0.10 (0.24)
	AE	GRASP/HP 5 703 282 (93)	0.59 (0.67)	0.53 (0.62)	-0.04 (-0.18)	0.62 (0.77)	-0.48 (-0.66)	--	--	--
		GRASP/Models 5 988 842 (91)	0.38 (0.53)	0.24 (0.40)	0.69 (0.41)	0.44 (0.53)	-0.03 (-0.34)	--	--	--
	AODF	GRASP/HP 5 704 665 (126)	0.63 (0.41)	0.52 (0.24)	0.05 (0.12)	0.07 (0.15)	0.02 (0.00)	0.03 (0.05)	-0.12 (-0.09)	-0.40 (-0.64)
		GRASP/Models 5 991 408 (125)	0.73 (0.74)	0.57 (0.58)	0.04 (0.09)	0.06 (0.11)	0.01 (0.02)	0.02 (0.05)	-0.12 (-0.06)	-0.31 (-0.23)
AODC	GRASP/HP 2 692 908 (--)	0.68 (--)	1.08 (--)	0.04 (--)	0.10 (--)	0.05 (--)	0.04 (--)	0.17 (--)	0.53 (--)	
	GRASP/Models 2 949 016 (--)	0.70 (--)	0.69 (--)	0.02 (--)	0.06 (--)	0.00 (--)	0.00 (--)	-0.01 (--)	0.04 (--)	



Table 15. Pixel to pixel ($0.1^\circ \times 0.1^\circ$) statistical metrics between AOD (550 nm) products based on references of GRASP/Models (Land and Ocean) and MAIAC AOD (Land); the statistics for only AERONET pixels are presented in brackets.

		Reference: GRASP/Models AOD							
		R	Slope	Offset	RMSE	BIAS	BIAS $\tau_{550} < 0.2$	BIAS $0.2 \leq \tau_{550} \leq 0.7$	BIAS $\tau_{550} > 0.7$
Land	GRASP/HP AOD	0.85 (0.90)	0.81 (0.84)	0.11 (0.12)	0.19 (0.19)	0.06 (0.06)	0.07 (0.08)	0.06 (0.06)	-0.07 (-0.02)
	53 656 407 (8564)								
	DT AOD	0.85 (0.90)	0.84 (1.01)	0.00 (0.06)	0.15 (0.18)	-0.04 (0.06)	0.00 (0.04)	-0.07 (0.07)	-0.15 (0.07)
	13 069 294 (3 432)								
	DB AOD	0.76 (0.89)	0.69 (0.89)	0.06 (0.03)	0.18 (0.16)	-0.01 (0.00)	0.03 (0.02)	-0.04 (-0.02)	-0.26 (-0.06)
36 348 953 (4 972)									
MAIAC AOD	0.77 (0.89)	0.66 (0.84)	0.05 (0.02)	0.18 (0.15)	-0.03 (-0.02)	0.02 (0.01)	-0.08 (-0.04)	-0.29 (-0.11)	
64 921 447 (10 830)									
Ocean	GRASP/HP AOD	0.94 (0.97)	1.10 (1.04)	0.04 (0.05)	0.09 (0.10)	0.05 (0.06)	0.05 (0.05)	0.07 (0.06)	0.16 (0.11)
	65 551 501 (300)								
	DT AOD	0.92 (0.97)	0.88 (0.99)	0.01 (-0.01)	0.05 (0.05)	-0.01 (-0.01)	0.00 (-0.02)	-0.04 (-0.01)	-0.06 (-0.04)
	32 486 105 (130)								
	DB AOD	--	--	--	--	--	--	--	--
MAIAC AOD	--	--	--	--	--	--	--	--	
		Reference: MAIAC AOD							
Land	GRASP/HP AOD	0.81 (0.90)	0.91 (0.91)	0.10 (0.11)	0.20 (0.17)	0.08 (0.08)	0.08 (0.09)	0.10 (0.09)	0.00 (0.02)
	54 693 580 (8 679)								
	DT AOD	0.91 (0.93)	1.05 (1.07)	0.01 (0.06)	0.10 (0.15)	0.02 (0.08)	0.01 (0.05)	0.01 (0.11)	0.07 (0.12)
	21 272 908 (5 836)								
	DB AOD	0.86 (0.93)	0.92 (0.98)	0.04 (0.03)	0.13 (0.12)	0.02 (0.02)	0.03 (0.02)	0.02 (0.02)	-0.05 (0.00)
53 758 759 (7 681)									

1640

1645



Table 16. Pixel to pixel ($0.1^\circ \times 0.1^\circ$) statistical metrics between AOD products based on reference of GRASP/Models over land pixels with four classes of surface ($NDVI < 0.2$, $0.2 \leq NDVI < 0.4$, $0.4 \leq NDVI < 0.6$, and $NDVI \geq 0.6$); the statistics for only AERONET pixels are presented in brackets.

		Reference: GRASP/Models AOD							
		R	Slope	Offset	RMSE	BIAS	BIAS $\tau_{550} < 0.2$	BIAS $0.2 \leq \tau_{550} \leq 0.7$	BIAS $\tau_{550} > 0.7$
Land NDVI < 0.2	GRASP/HP AOD 31 341 330 (2069)	0.78 (0.81)	0.68 (0.66)	0.15 (0.19)	0.20 (0.28)	0.06 (0.08)	0.09 (0.12)	0.07 (0.09)	-0.20 (-0.21)
	DT AOD 542 625 (38)	0.74 (0.88)	0.95 (1.27)	0.09 (0.16)	0.17 (0.31)	0.09 (0.24)	0.09 (0.18)	0.07 (0.26)	0.12 (0.47)
	DB AOD 17 834 405 (1013)	0.66 (0.82)	0.59 (0.74)	0.11 (0.08)	0.22 (0.21)	0.01 (0.00)	0.06 (0.05)	-0.02 (-0.03)	-0.33 (-0.17)
	MAIAC AOD 31 329 712 (2357)	0.67 (0.79)	0.60 (0.68)	0.08 (0.08)	0.21 (0.21)	-0.01 (-0.01)	0.04 (0.05)	-0.06 (-0.04)	-0.32 (-0.26)
Land $0.2 \leq NDVI < 0.4$	GRASP/HP AOD 11 667 461 (3596)	0.90 (0.93)	0.84 (0.91)	0.08 (0.08)	0.16 (0.16)	0.04 (0.04)	0.05 (0.06)	0.05 (0.05)	-0.06 (0.00)
	DT AOD 3 784 302 (1547)	0.81 (0.89)	0.86 (0.99)	0.01 (0.09)	0.16 (0.21)	-0.02 (0.08)	0.01 (0.06)	-0.06 (0.10)	-0.08 (0.08)
	DB AOD 7 767 588 (1911)	0.85 (0.92)	0.78 (0.95)	0.03 (0.02)	0.14 (0.16)	-0.01 (0.00)	0.01 (0.01)	-0.04 (0.00)	-0.15 (-0.03)
	MAIAC AOD 13 927 469 (4133)	0.87 (0.92)	0.69 (0.89)	0.04 (0.02)	0.15 (0.15)	-0.03 (-0.02)	0.01 (0.01)	-0.08 (-0.04)	-0.26 (-0.08)
Land $0.4 \leq NDVI < 0.6$	GRASP/HP AOD 7 879 243 (2641)	0.92 (0.93)	0.98 (0.95)	0.07 (0.08)	0.16 (0.14)	0.06 (0.06)	0.06 (0.07)	0.05 (0.06)	0.06 (0.06)
	DT AOD 5 431 789 (1605)	0.86 (0.91)	0.83 (1.01)	-0.01 (0.04)	0.16 (0.14)	-0.06 (0.04)	-0.02 (0.04)	-0.08 (0.05)	-0.17 (0.05)
	DB AOD 7 146 072 (1763)	0.88 (0.91)	0.80 (0.89)	0.01 (0.02)	0.13 (0.13)	-0.03 (-0.01)	0.00 (0.01)	-0.07 (-0.02)	-0.16 (-0.06)
	MAIAC AOD 12 624 553 (3660)	0.88 (0.92)	0.74 (0.90)	0.01 (0.00)	0.14 (0.11)	-0.05 (-0.03)	-0.01 (-0.01)	-0.10 (-0.05)	-0.24 (-0.08)
Land $NDVI \geq 0.6$	GRASP/HP AOD 2 766 521 (258)	0.94 (0.89)	1.00 (0.90)	0.10 (0.10)	0.19 (0.13)	0.10 (0.08)	0.08 (0.09)	0.11 (0.07)	0.13 (0.01)
	DT AOD 3 305 544 (242)	0.91 (0.89)	0.86 (0.85)	-0.01 (0.01)	0.13 (0.09)	-0.05 (-0.02)	-0.02 (0.00)	-0.08 (-0.04)	-0.17 (-0.15)
	DB AOD 3 598 331 (285)	0.90 (0.77)	0.72 (0.55)	0.00 (0.02)	0.12 (0.10)	-0.05 (-0.05)	-0.02 (-0.02)	-0.11 (-0.12)	-0.25 (-0.28)
	MAIAC AOD 7 029 548 (680)	0.90 (0.85)	0.73 (0.71)	0.00 (0.00)	0.14 (0.10)	-0.06 (-0.05)	-0.02 (-0.03)	-0.11 (-0.10)	-0.28 (-0.30)



1650 **Table 17.** The same as Table 16, but for reference of MAIAC AOD

		Reference: MAIAC AOD							
		R	Slope	Offset	RMSE	BIAS	BIAS $\tau_{550}<0.2$	BIAS $0.2 \leq \tau_{550} \leq 0.7$	BIAS $\tau_{550}>0.7$
Land NDVI<0.2	GRASP/HP AOD	0.78 (0.86)	0.80 (0.83)	0.12 (0.13)	0.20 (0.18)	0.08 (0.08)	0.08 (0.09)	0.08 (0.10)	-0.11 (-0.08)
	32 768 635 (2207)								
	DT AOD	0.77 (0.71)	1.28 (1.43)	0.05 (0.33)	0.15 (0.51)	0.08 (0.42)	0.07 (0.34)	0.14 (0.56)	0.33 (0.72)
	885 841 (83)								
Land 0.2≤NDVI<0.4	DB AOD	0.85 (0.89)	0.86 (0.96)	0.06 (0.02)	0.15 (0.16)	0.04 (0.01)	0.04 (0.02)	0.03 (-0.01)	-0.09 (0.00)
	26 151 234 (1500)								
	GRASP/HP AOD	0.85 (0.91)	1.03 (0.92)	0.06 (0.09)	0.17 (0.17)	0.07 (0.07)	0.06 (0.07)	0.09 (0.08)	0.08 (0.02)
	11 919 986 (3641)								
Land 0.4≤NDVI<0.6	DT AOD	0.88 (0.94)	1.03 (1.05)	0.00 (0.08)	0.11 (0.17)	0.01 (0.10)	0.01 (0.06)	0.00 (0.13)	0.08 (0.13)
	5 857 865 (2314)								
	DB AOD	0.87 (0.94)	1.02 (1.00)	0.01 (0.02)	0.12 (0.13)	0.01 (0.02)	0.01 (0.02)	0.02 (0.04)	0.05 (0.01)
	11 668 355 (2922)								
Land NDVI≥0.6	GRASP/HP AOD	0.87 (0.91)	1.09 (0.96)	0.09 (0.11)	0.21 (0.17)	0.11 (0.10)	0.09 (0.10)	0.14 (0.10)	0.17 (0.08)
	7 489 541 (2526)								
	DT AOD	0.92 (0.94)	1.03 (1.06)	0.00 (0.05)	0.10 (0.13)	0.01 (0.07)	0.01 (0.05)	0.00 (0.09)	0.05 (0.12)
	8 401 731 (2416)								
Land NDVI≥0.6	DB AOD	0.88 (0.95)	0.97 (0.95)	0.02 (0.04)	0.11 (0.09)	0.02 (0.03)	0.02 (0.03)	0.01 (0.03)	0.00 (0.00)
	10 298 915 (2628)								
	GRASP/HP AOD	0.88 (0.84)	1.13 (.94)	0.14 (0.15)	0.26 (0.18)	0.17 (0.14)	0.13 (0.14)	0.24 (0.13)	0.26 (0.08)
	2 512 741 (305)								
Land NDVI≥0.6	DT AOD	0.94 (0.94)	1.10 (1.06)	0.00 (0.02)	0.09 (0.07)	0.02 (0.03)	0.01 (0.02)	0.04 (0.05)	0.09 (0.05)
	5 539 285 (548)								
	DB AOD	0.88 (0.78)	0.91 (0.73)	0.02 (0.03)	0.09 (0.06)	0.01 (0.00)	0.01 (0.01)	-0.02 (-0.05)	-0.07 (-0.27)
	5 253 920 (520)								



Table 18. Pixel to pixel statistical metrics between AE products based on references of GRASP/HP; the statistics for only AERONET

1660 **pixels are presented in brackets.**

		Reference: GRASP/HP AE				
		R	Slope	Offset	RMSE	BIAS
Land	GRASP/Models AE 27 385 356 (5 517)	0.70 (0.68)	0.51 (0.43)	0.45 (0.47)	0.39 (0.39)	0.12 (-0.05)
	DT AE 6 017 122 (2 335)	0.31 (0.30)	0.32 (0.29)	0.84 (0.64)	0.66 (0.59)	0.11 (-0.15)
	DB AE 19 317 232 (3 121)	0.40 (0.43)	0.53 (0.49)	0.39 (0.68)	0.67 (0.65)	0.09 (0.21)
Ocean	GRASP/Models AE 49 987 062 (285)	0.74 (0.88)	0.52 (0.68)	0.63 (0.47)	0.45 (0.33)	0.35 (0.23)
	DT AE 18 564 876 (123)	0.46 (0.55)	0.49 (0.78)	0.55 (0.82)	0.53 (0.83)	0.25 (0.60)

1665

1670



Table 19. Pixel to pixel statistical metrics between AE products based on references of GRASP/HP over land pixels with four classes of surface (NDVI<0.2, 0.2≤NDVI<0.4, 0.4≤NDVI<0.6, and NDVI≥0.6)

		Reference: GRASP/HP AE				
		R	Slope	Offset	RMSE	BIAS
Land NDVI<0.2	GRASP/Models AE 15 916 616 (1205)	0.40 (0.53)	0.38 (0.48)	0.49 (0.48)	0.42 (0.42)	0.23 (0.24)
	DT AE 203 121 (25)	0.16 (0.36)	0.14 (0.15)	0.71 (0.47)	0.65 (0.48)	0.32 (-0.30)
	DB AE 12 223 721 (764)	0.12 (0.35)	0.21 (0.60)	0.37 (0.40)	0.65 (0.65)	0.02 (0.21)
Land 0.2≤NDVI<0.4	GRASP/Models AE 5 220 459 (2425)	0.79 (0.69)	0.54 (0.41)	0.42 (0.47)	0.35 (0.39)	0.05 (-0.11)
	DT AE 1 923 619 (1168)	0.30 (0.33)	0.30 (0.27)	0.79 (0.58)	0.69 (0.59)	0.16 (-0.20)
	DB AE 3 157 768 (1256)	0.21 (0.24)	0.23 (0.26)	0.86 (0.98)	0.77 (0.71)	0.24 (0.24)
Land 0.4≤NDVI<0.6	GRASP/Models AE 4 516 281 (1743)	0.80 (0.65)	0.57 (0.48)	0.38 (0.43)	0.34 (0.37)	-0.11 (-0.16)
	DT AE 2 723 494 (1024)	0.28 (0.26)	0.30 (0.29)	0.90 (0.71)	0.65 (0.58)	0.08 (-0.12)
	DB AE 2 896 017 (999)	0.23 (0.27)	0.21 (0.30)	1.04 (1.00)	0.64 (0.58)	0.15 (0.19)
Land NDVI≥0.6	GRASP/Models AE 1 730 292 (144)	0.76 (0.73)	0.57 (0.67)	0.41 (0.24)	0.31 (0.29)	-0.08 (-0.14)
	DT AE 1 166 000 (118)	0.19 (-0.01)	0.22 (-0.01)	1.00 (1.30)	0.65 (0.60)	0.09 (0.14)
	DB AE 1 039 192 (102)	0.18 (-0.07)	0.16 (-0.11)	1.21 (1.44)	0.59 (0.63)	0.25 (0.17)



Table 20: Pixel to pixel statistical metrics between GRASP/HP AODF with other AODF products; the statistics for only AERONET pixels are presented in brackets.

		Reference: GRASP/HP AODF				
		R	Slope	Offset	RMSE	BIAS
Land	GRASP/Models AODF 53 656 407 (8 564)	0.87 (0.91)	0.75 (0.68)	0.02 (0.03)	0.10 (0.15)	-0.01 (-0.06)
Ocean	GRASP/Models AODF 65 551 501 (300)	0.89 (0.67)	0.78 (0.90)	0.02 (0.03)	0.05 (0.11)	0.00 (0.01)
	DT AODF 17 513 511 (116)	0.86 (0.70)	0.66 (0.64)	0.02 (0.04)	0.06 (0.09)	-0.02 (-0.03)

1680 **Table 21: The same as Table 20, but for AODC**

		Reference: GRASP/HP AODC				
		R	Slope	Offset	RMSE	BIAS
Land	GRASP/Models AODC 53 656 407 (8 564)	0.71 (0.63)	0.65 (0.67)	0.02 (0.06)	0.16 (0.18)	-0.04 (0.00)
Ocean	GRASP/Models AODC 65 551 501 (300)	0.89 (0.98)	0.56 (0.64)	0.00 (0.01)	0.09 (0.14)	-0.05 (-0.07)
	DT AODC 17 513 511 (116)	0.84 (0.90)	0.58 (0.69)	0.01 (0.00)	0.08 (0.10)	-0.04 (-0.04)



Table 22: Pixel to pixel statistical metrics between AODF products based on references of GRASP/HP over land pixels with four classes of surface ($NDVI < 0.2$, $0.2 \leq NDVI < 0.4$, $0.4 \leq NDVI < 0.6$, and $NDVI \geq 0.6$); the statistics for only AERONET pixels are presented in brackets.

		Reference: GRASP/HP AODF				
		R	Slope	Offset	RMSE	BIAS
Land $NDVI < 0.2$	GRASP/Models AODF 31 340 947 (2069)	0.68 (0.82)	0.91 (0.84)	0.02 (0.03)	0.09 (0.12)	0.00 (0.01)
Land $0.2 \leq NDVI < 0.4$	GRASP/Models AODF 11 667 461 (3596)	0.90 (0.93)	0.79 (0.68)	0.02 (0.03)	0.09 (0.16)	-0.02 (-0.07)
Land $0.4 \leq NDVI < 0.6$	GRASP/Models AODF 7 879 243 (2641)	0.93 (0.92)	0.73 (0.67)	0.01 (0.02)	0.13 (0.16)	-0.06 (-0.09)
Land $NDVI \geq 0.6$	GRASP/Models AODF 2 766 521 (258)	0.94 (0.88)	0.76 (0.71)	-0.01 (-0.01)	0.16 (0.12)	-0.09 (-0.08)

1690 **Table 23: The same as Table 22, but for AODC**

		Reference: GRASP/HP AODC				
		R	Slope	Offset	RMSE	BIAS
Land $NDVI < 0.2$	GRASP/Models AODC 31 340 947 (2069)	0.69 (0.67)	0.64 (0.72)	0.01 (-0.01)	0.18 (0.23)	-0.07 (-0.08)
Land $0.2 \leq NDVI < 0.4$	GRASP/Models AODC 11 667 461 (3596)	0.77 (0.64)	0.75 (0.69)	0.01 (0.08)	0.13 (0.18)	-0.02 (0.03)
Land $0.4 \leq NDVI < 0.6$	GRASP/Models AODC 7 879 243 (2641)	0.76 (0.60)	0.69 (0.69)	0.04 (0.06)	0.13 (0.13)	0.01 (0.03)
Land $NDVI \geq 0.6$	GRASP/Models AODC 2 766 521 (258)	0.77 (0.65)	0.66 (0.70)	0.04 (0.03)	0.14 (0.08)	-0.01 (0.01)

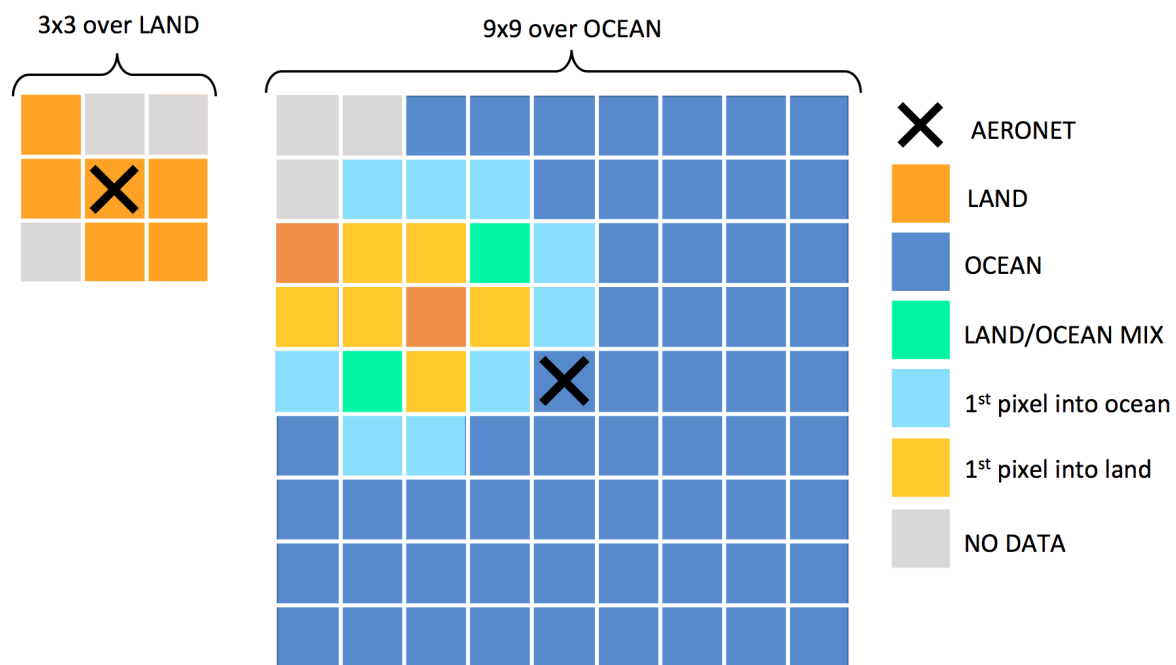
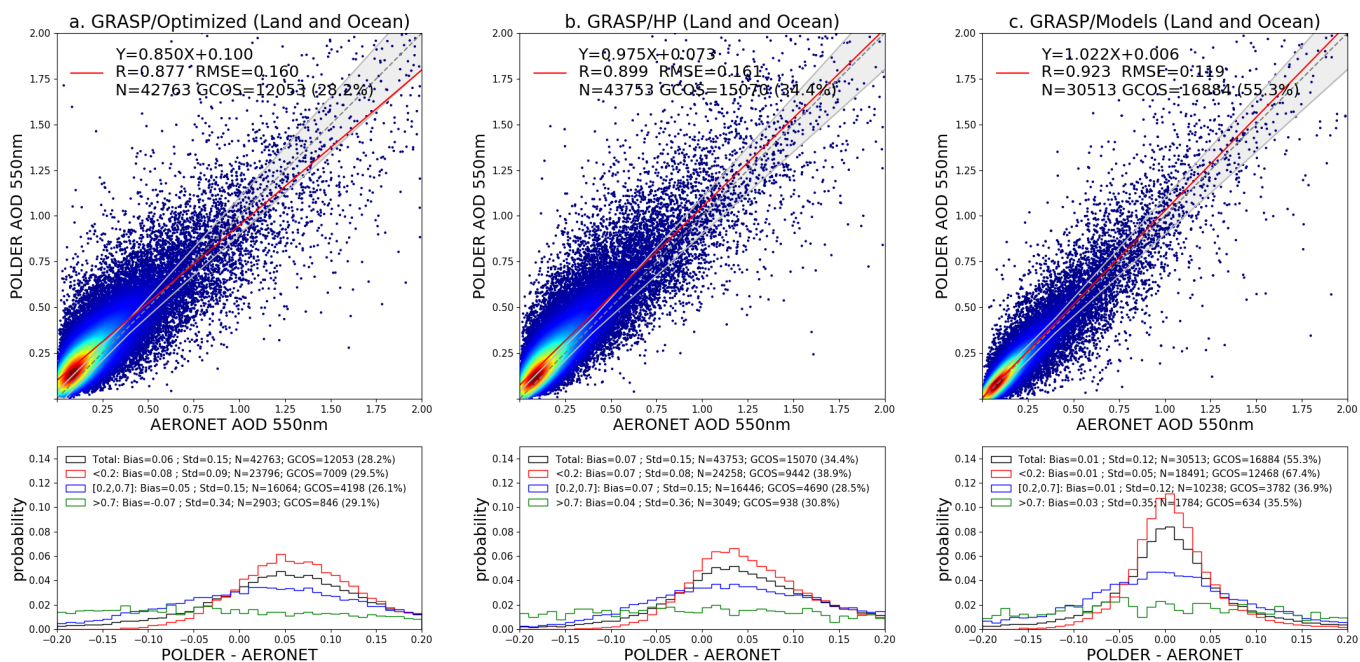
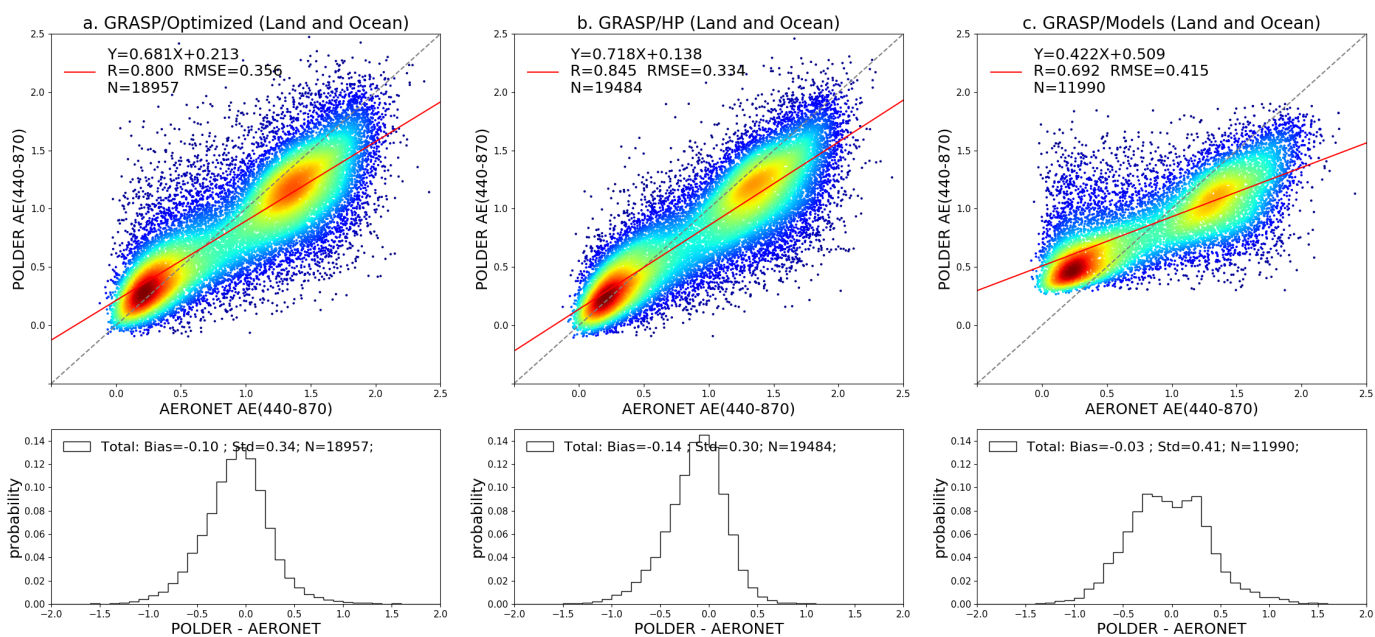


Figure 1: Schematic diagram for satellite data selection over (left) land and (right) ocean.

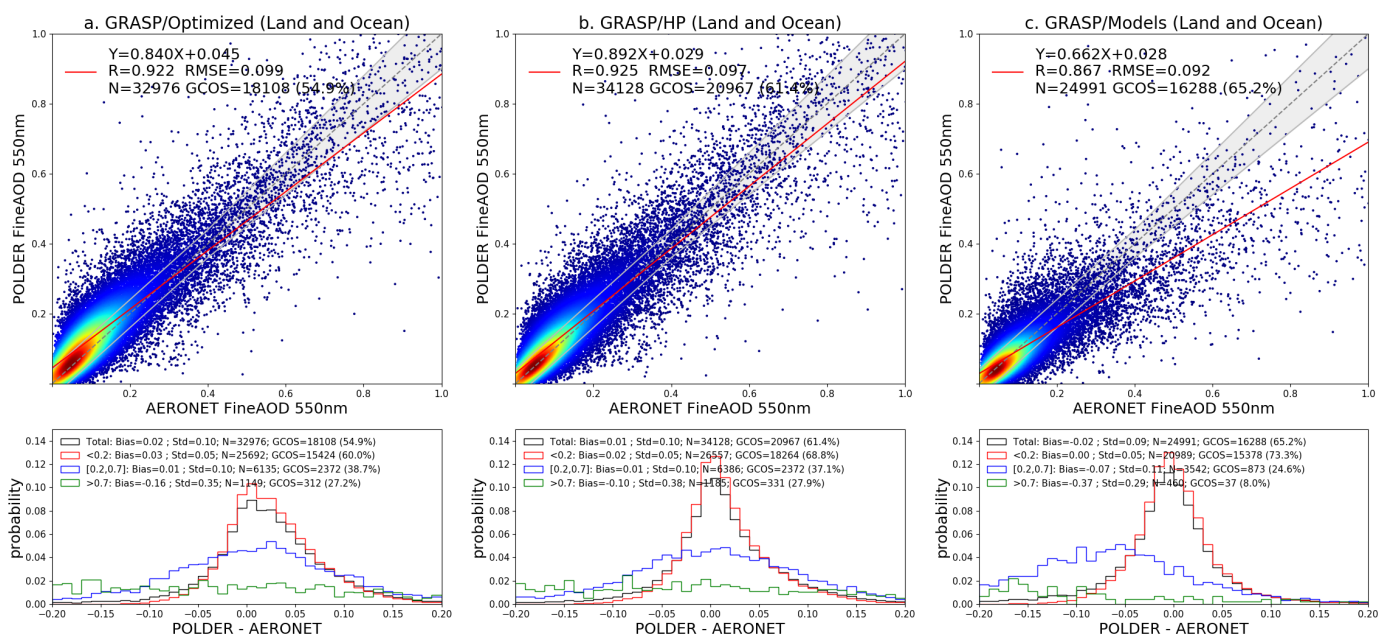


1695 **Figure 2: Evaluation of three archives PARASOL/GRASP AOD at 550 nm against AERONET, (a) GRASP/Optimized; (b) GRASP/HP; (c) GRASP/Models.** The gray dashed line and the red solid line are the 1:1 reference line and the linear regression line. The gray envelope indicates GCOS requirement: max (0.04 or 0.1AOD). The probability density functions of differences (POLDER-AERONET) are present in the lower panel. The black, red, blue and green solid lines indicate all AOD conditions: any AOD, AOD<0.2, 0.2≤AOD≤0.7 and AOD>0.7 respectively.



1700

Figure 3: Evaluation of all archive PARASOL/GRASP AE (440/870) against AERONET, (a) GRASP/Optimized; (b) GRASP/HP; (c) GRASP/Models. The gray dashed line and the red solid line are the 1:1 reference line and the linear regression line. The probability density functions of differences (POLDER-AERONET) are present in the lower panel.



1705 **Figure 4: Evaluation of all archive PARASOL/GRASP AODF at 550 nm with AERONET SDA AODF, (a) GRASP/Optimized; (b) GRASP/HP; (c) GRASP/Models. The gray dashed line and the red solid line are the 1:1 reference line and the linear regression line. The gray envelope indicates GCOS requirement applied for AODF: max (0.04 or 0.1AODF). The probability density functions of differences (POLDER-AERONET) are present in the lower panel. The black, red, blue and green solid lines indicate all AODF conditions: any AODF, AODF<0.2, 0.2≤AODF≤0.7 and AODF>0.7 respectively.**

1710

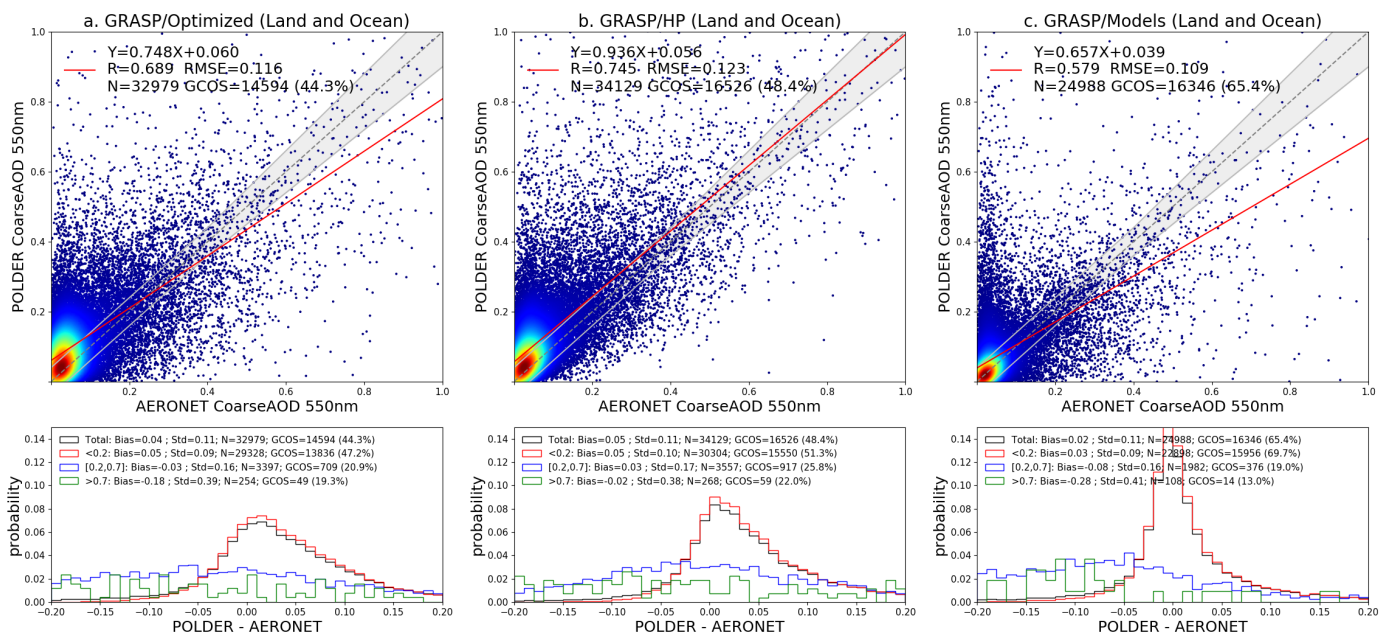


Figure 5: The same as Figure 4, but for AODC at 550 nm.

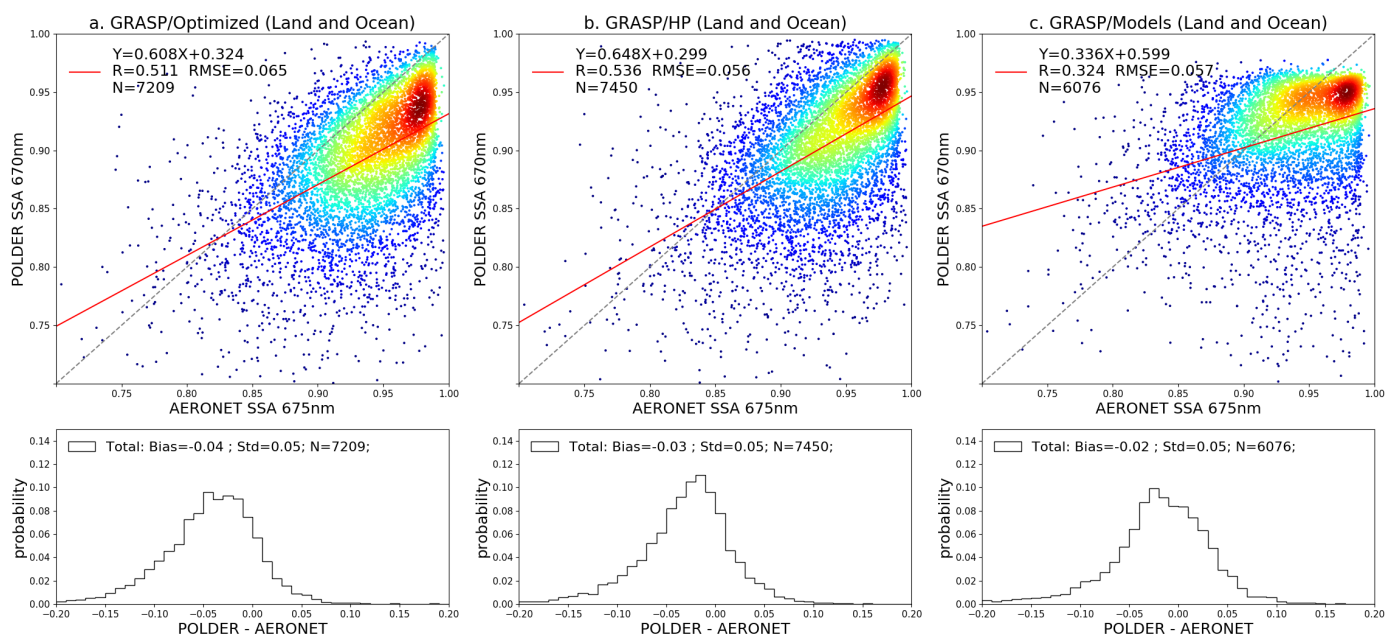


Figure 6: Evaluation of all archive PARASOL/GRASP SSA at 670 nm with AERONET SSA at 675 nm, (a) GRASP/Optimized; (b) GRASP/HP; (c) GRASP/Models. The gray dashed line and the red solid line are the 1:1 reference line and the linear regression line.

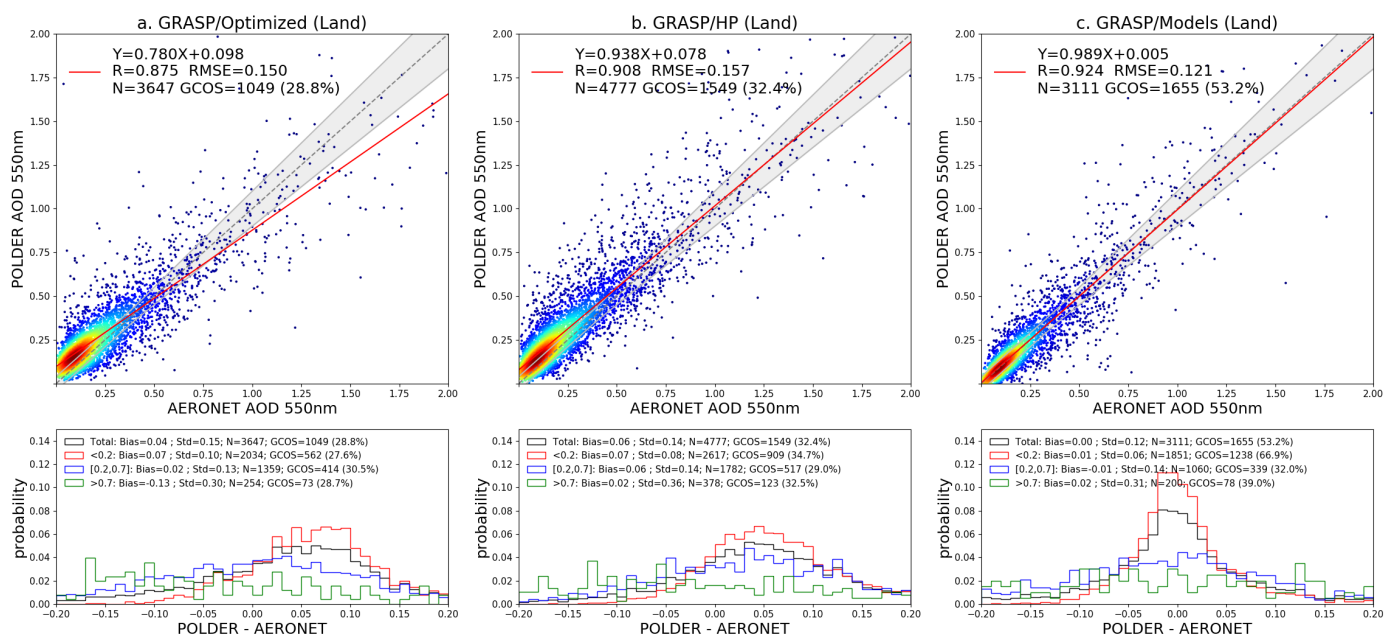


Figure 7: Validation of PARASOL/GRASP AOD at 550 nm over land in 2008, (a) GRASP/Optimized; (b) GRASP/HP; (c) GRASP/Models. The gray dashed line and the red solid line are the 1:1 reference line and the linear regression line. The gray envelope indicates GCOS requirement: max (0.04 or 0.1AOD). The probability density functions of differences (POLDER-AERONET) are present in the lower panel. The black, red, blue and green solid lines indicate all AOD conditions: any AOD, $AOD < 0.2$, $0.2 \leq AOD \leq 0.7$ and $AOD > 0.7$ respectively.

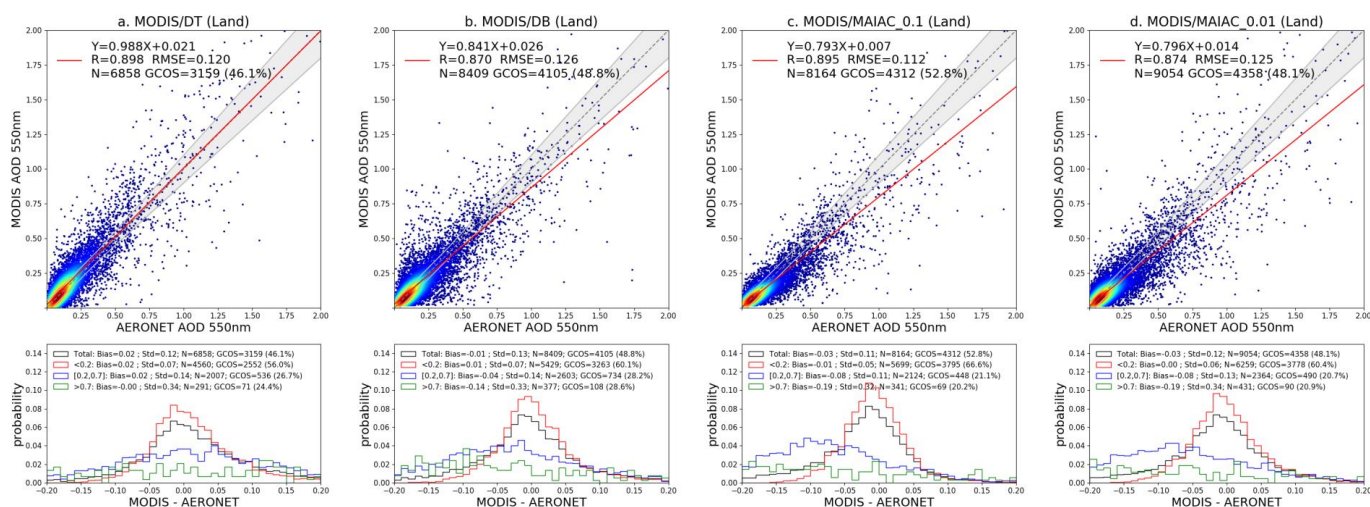
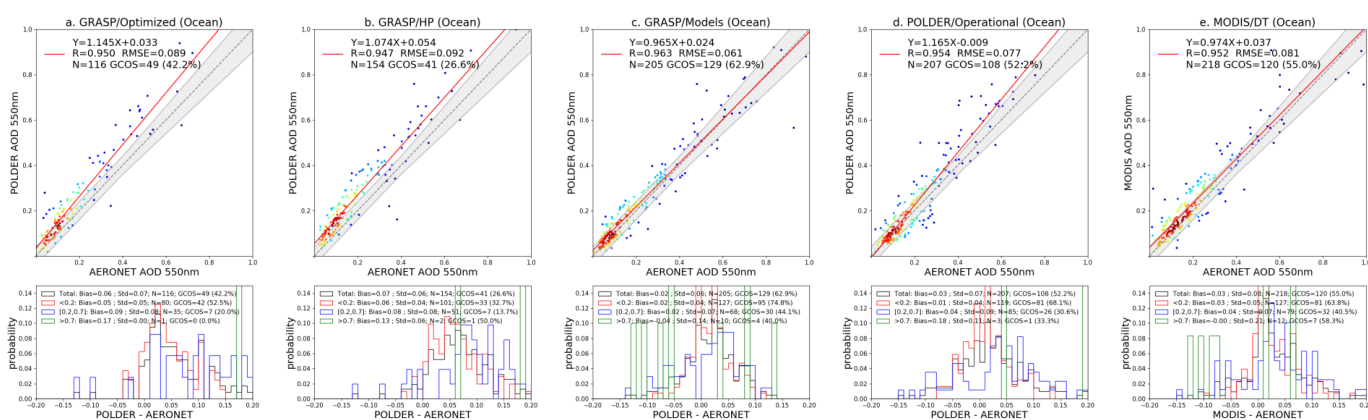
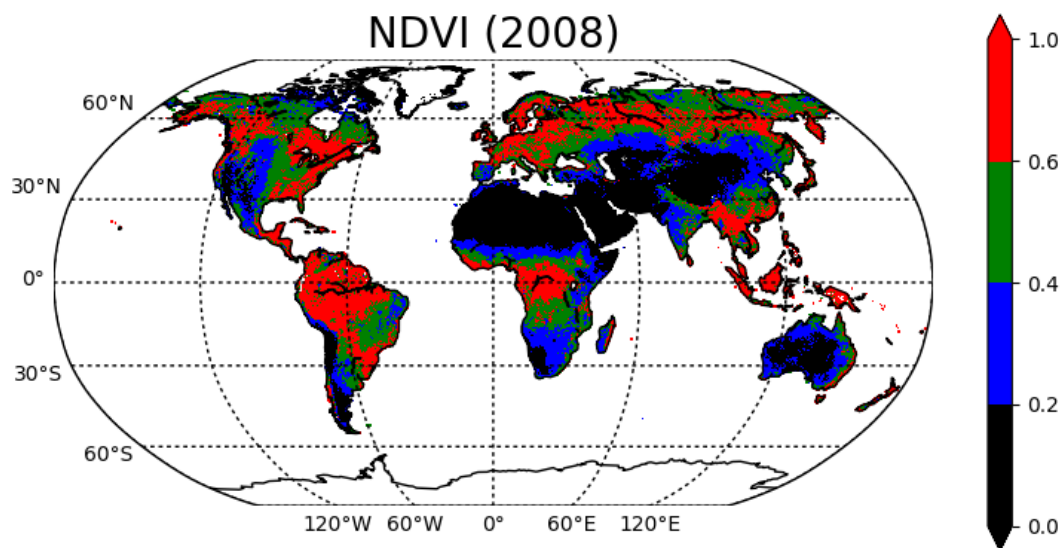


Figure 8: Validation of MODIS AOD at 550 nm over land in 2008, (a) DT; (b) DB; (c) MAIAC_0.1; (d) MAIAC_0.01. The gray dashed line and the red solid line are the 1:1 reference line and the linear regression line. The gray envelope indicates GCOS requirement: max (0.04 or 0.1AOD). The probability density functions of differences (MODIS-AERONET) are present in the lower panel. The black, red, blue and green solid lines indicate all AOD conditions: any AOD, AOD<0.2, 0.2≤AOD≤0.7 and AOD>0.7 respectively.



1730 **Figure 9: Validation of PARASOL/GRASP, PARASOL/Operational and MODIS/DT AOD at 550 nm over ocean in 2008. (a) GRASP/Optimized; (b) GRASP/HP; (c) GRASP/Models; (d) Operational; (e) DT. The gray dashed line and the red solid line are the 1:1 reference line and the linear regression line. The gray envelope indicates GCOS requirement: max (0.04 or 0.1AOD). The probability density functions of differences (Satellite-AERONET) are present in the lower panel. The black, red, blue and green solid lines indicate all AOD conditions: any AOD, $AOD < 0.2$, $0.2 \leq AOD \leq 0.7$ and $AOD > 0.7$ respectively.**



1735

Figure 10: Spatial distribution of annual mean NDVI for 2008 from GRASP/Models L3 products.

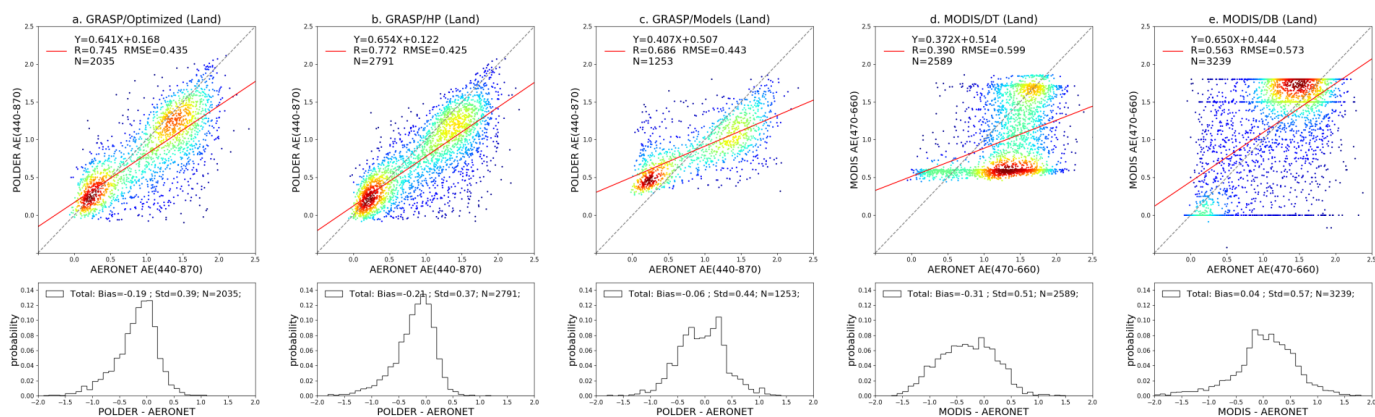


Figure 11: Validation of PARASOL/GRASP (a. GRASP/Optimized, b. GRASP/HP and c. GRASP/Models) and MODIS (d. DT and e. DB) AE over land in 2008. The gray dashed line and the red solid line are the 1:1 reference line and the linear regression line. The 1740 probability density functions of differences (Satellite-AERONET) are present in the lower panel.

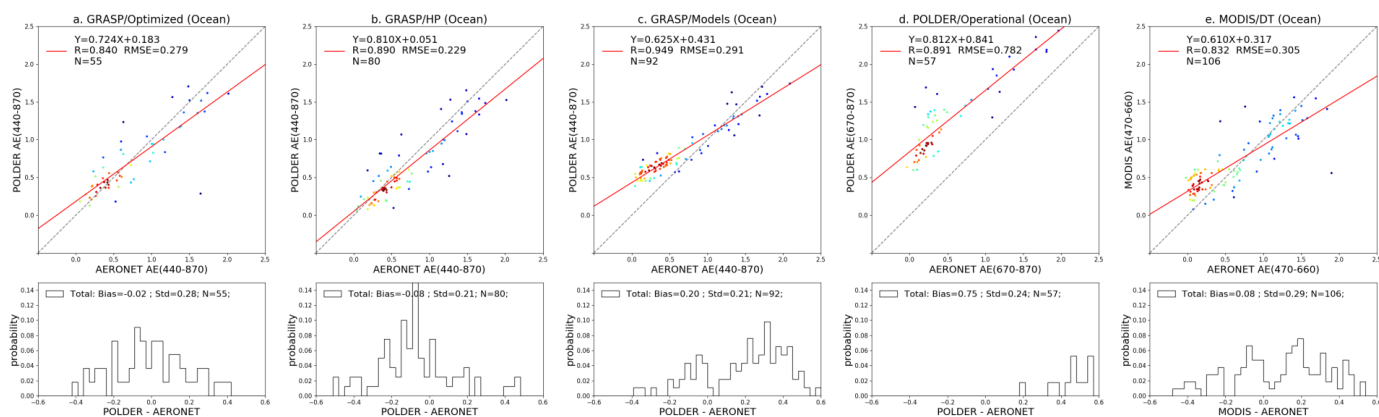


Figure 12: Validation of PARASOL/GRASP (a. GRASP/Optimized; b. GRASP/HP and c. GRASP/Models), (d) PARASOL/Operational and (e) MODIS/DT AE over ocean in 2008. The gray dashed line and the red solid line are the 1:1 reference line and the linear regression line. The probability density functions of differences (Satellite-AERONET) are present in the lower panel.

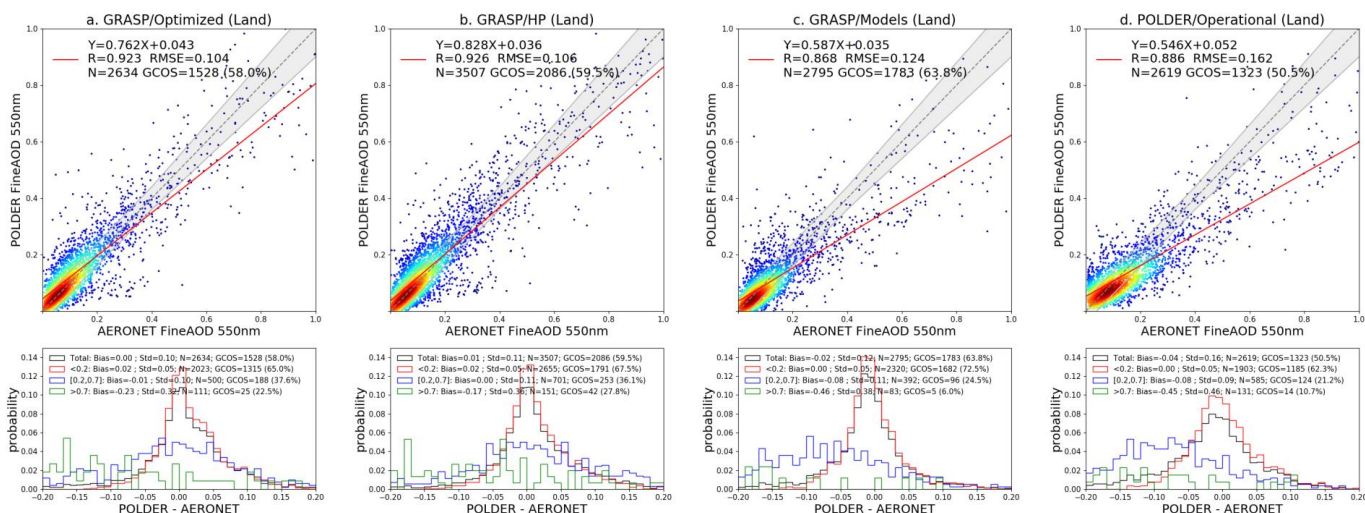
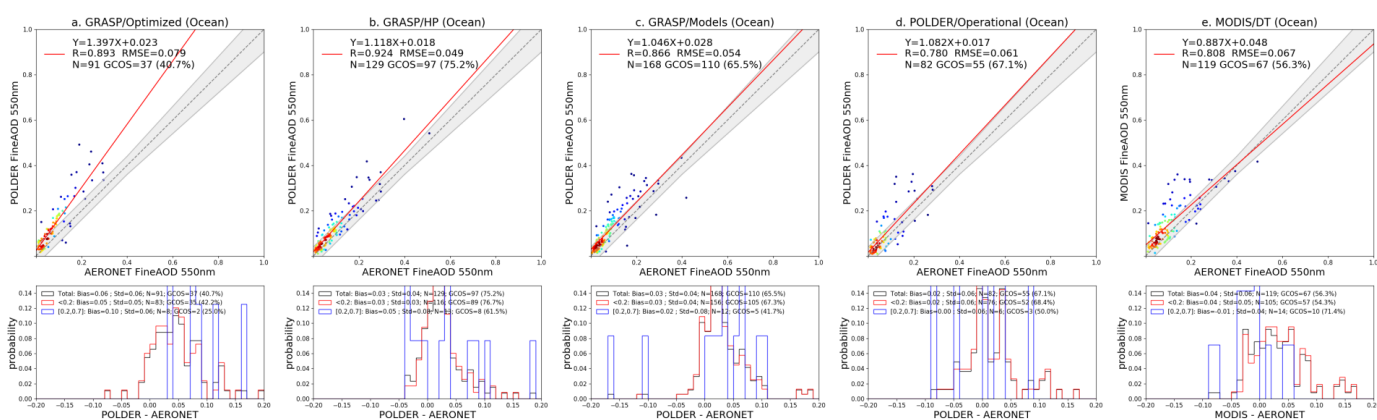


Figure 13: Validation of PARASOL/GRASP (a. GRASP/Optimized; b. GRASP/HP and c. GRASP/Models) and (d) PARASOL/Operational fine mode AOD at 550 nm over land in 2008. The gray envelope indicates GCOS requirement applied for AODF: max (0.04 or 0.1AODF). The probability density functions of differences (POLDER-AERONET) are present in the lower panel. The black, red, blue and green solid lines indicate all AODF conditions: any AODF, $AODF < 0.2$, $0.2 \leq AODF \leq 0.7$ and $AODF > 0.7$ respectively.



1755

Figure 14: Validation of PARASOL/GRASP (a. GRASP/Optimized; b. GRASP/HP and c. GRASP/Models), (d) PARASOL/Operational and (e) MODIS/DT fine mode AOD at 550 nm over ocean in 2008. The gray envelope indicates GCOS requirement applied for AODF: max (0.04 or 0.1AODF). The probability density functions of differences (Satellite-AERONET) are present in the lower panel. The black, red, blue and green solid lines indicate all AODF conditions: any AODF, AODF<0.2, 0.2≤AODF≤0.7 and AODF>0.7 respectively.

1760

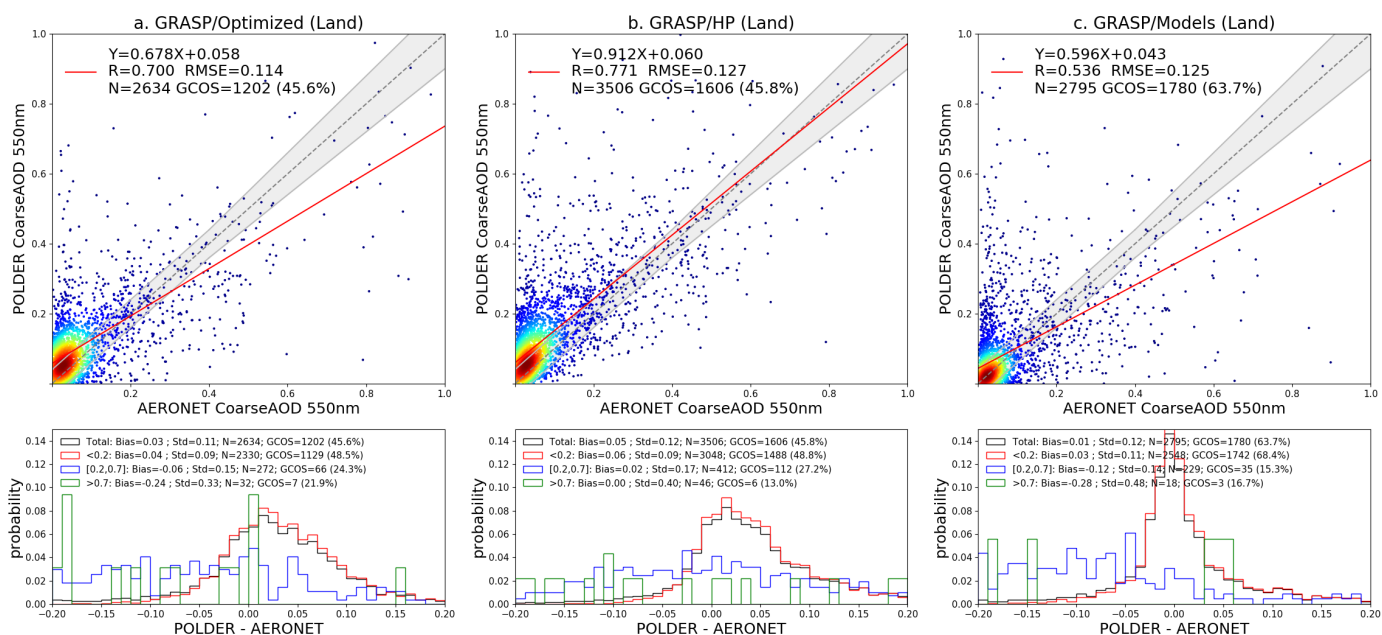


Figure 15: Validation of PARASOL/GRASP (a. GRASP/Optimized; b. GRASP/HP and c. GRASP/Models) coarse mode AOD at 550 nm over land in 2008. The gray envelope indicates GCOS requirement applied for AODC: max (0.04 or 0.1AODC). The probability density functions of differences (POLDER-AERONET) are present in the lower panel. The black, red, blue and green solid lines indicate all 1765 AODC conditions: any AODC, AODC<0.2, 0.2≤AODC≤0.7 and AODC>0.7 respectively.

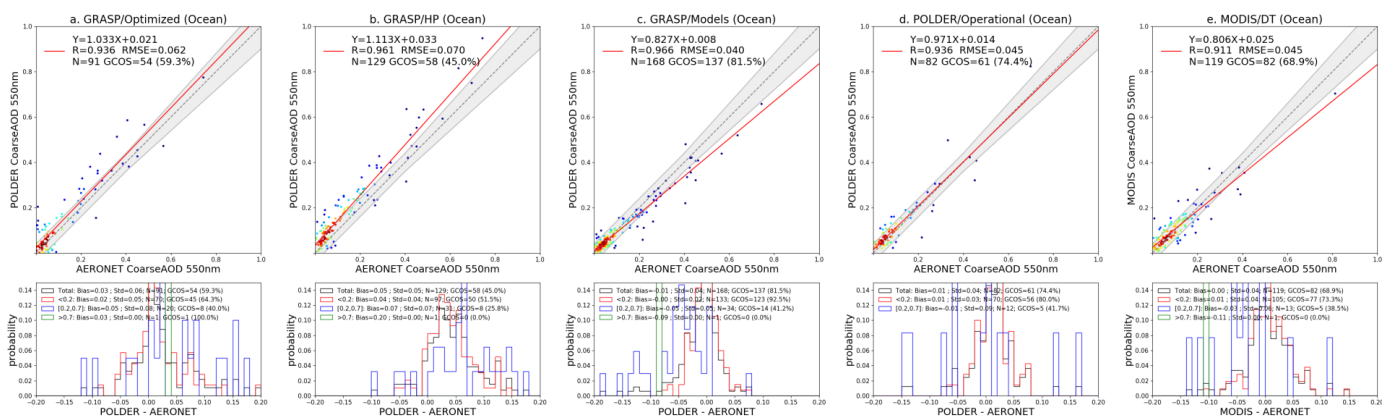
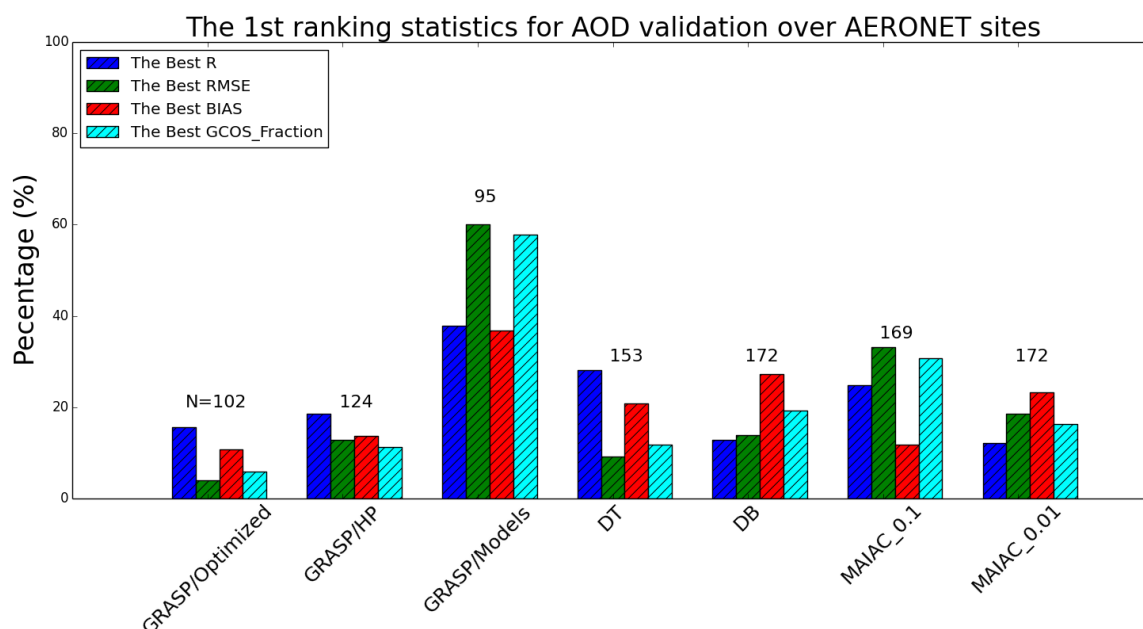
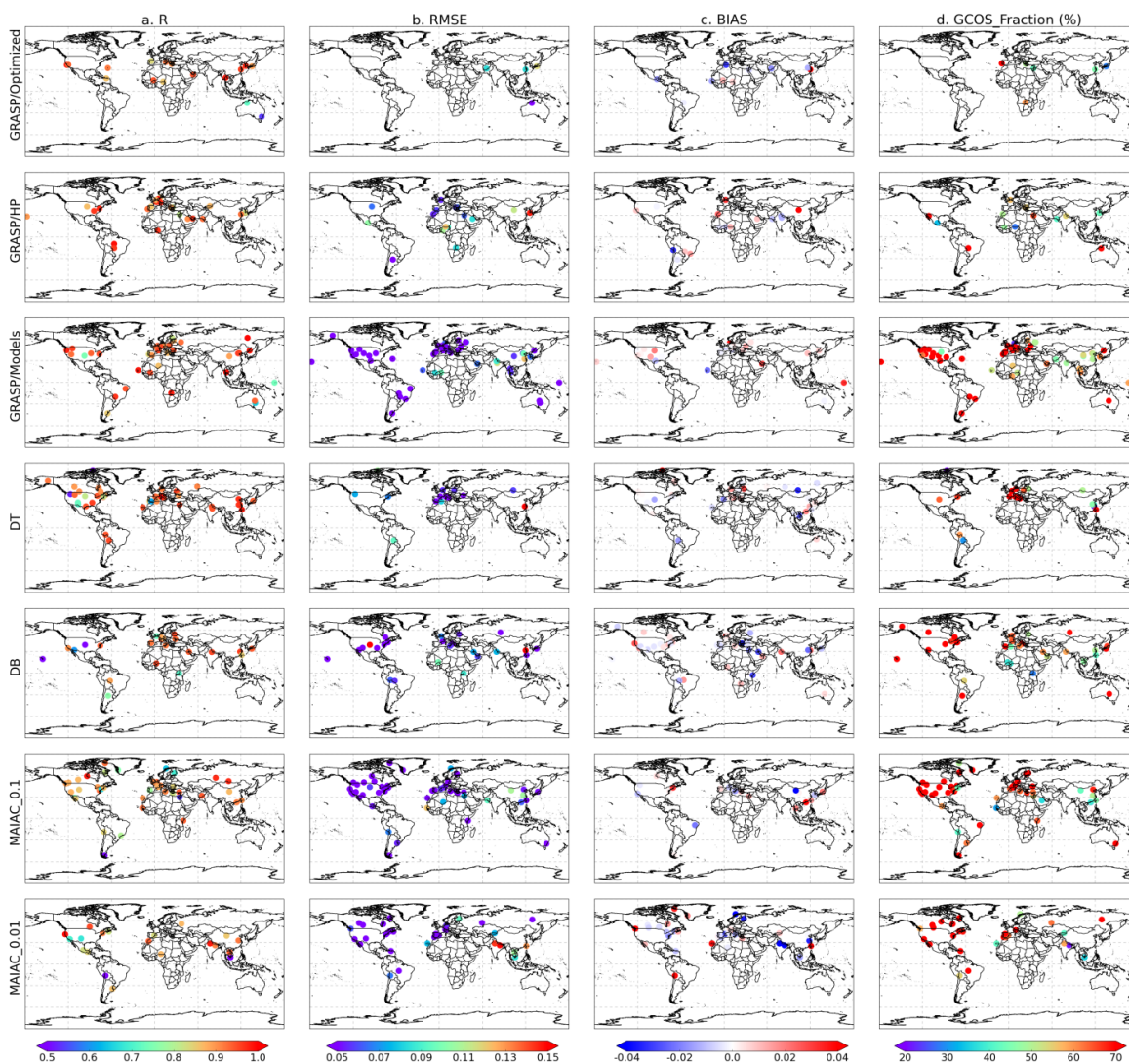


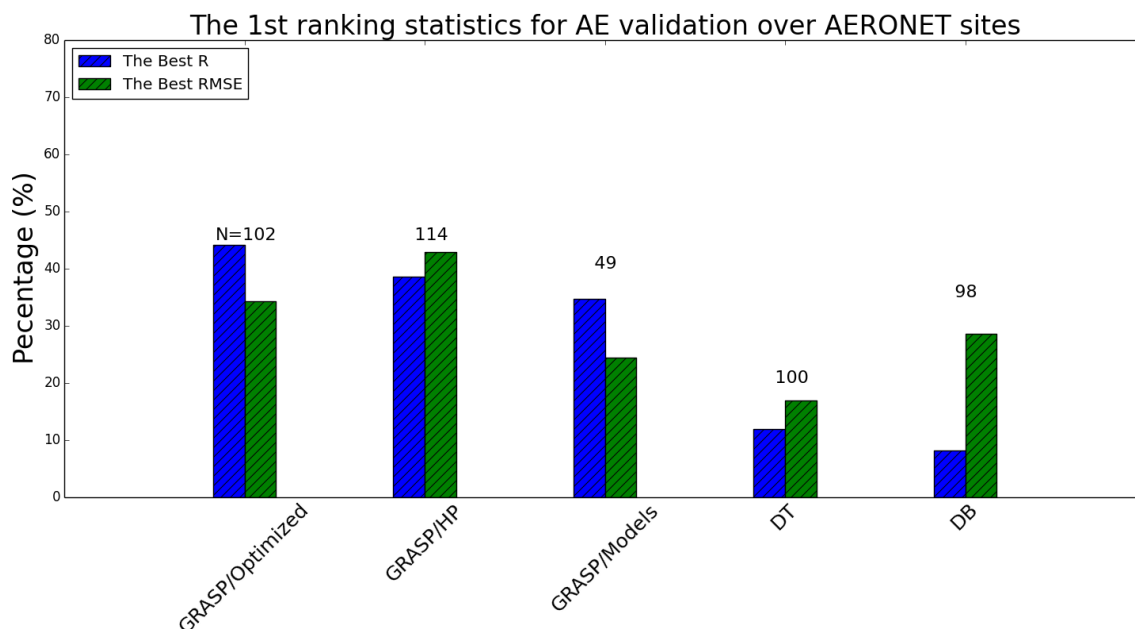
Figure 16: Validation of PARASOL/GRASP (a. GRASP/Optimized; b. GRASP/HP and c. GRASP/Models), (d) PARASOL/Operational and (e) MODIS/DT coarse mode AOD at 550 nm over ocean in 2008. The gray envelope indicates GCOS requirement applied for AODC: max (0.04 or 0.1AODC). The probability density functions of differences (POLDER-AERONET) are present in the lower panel. The black, red, blue and green solid lines indicate all AODC conditions: any AODC, $AODC < 0.2$, $0.2 \leq AODC \leq 0.7$ and $AODC > 0.7$ respectively.



1775 **Figure 17: Percentage of the AERONET sites where each product shows the best statistical metric (R, RMSE, BIAS and GCOS Fraction) between 7 PARASOL/GRASP and MODIS AOD products. The number on top of each product is the number of sites where this product has sufficient matchup points for the comparison.**



1780 **Figure 18:** Maps showing statistical metrics (a) R; (b) RMSE; (c) BIAS; (d) GCOS Fraction (%) for the best performed AOD products (1st ranking statistics among 7 PARASOL/GRASP and MODIS products) over each AERONET site. Note that only the 1st ranking statistics over each site are present in the maps.



1785 **Figure 19: Percentage of the AERONET sites where each product shows the best statistical metric (R and RMSE) between 5 PARASOL/GRASP and MODIS AE products. The number on top of each product is the number of sites where this product has sufficient matchup points for the comparison.**

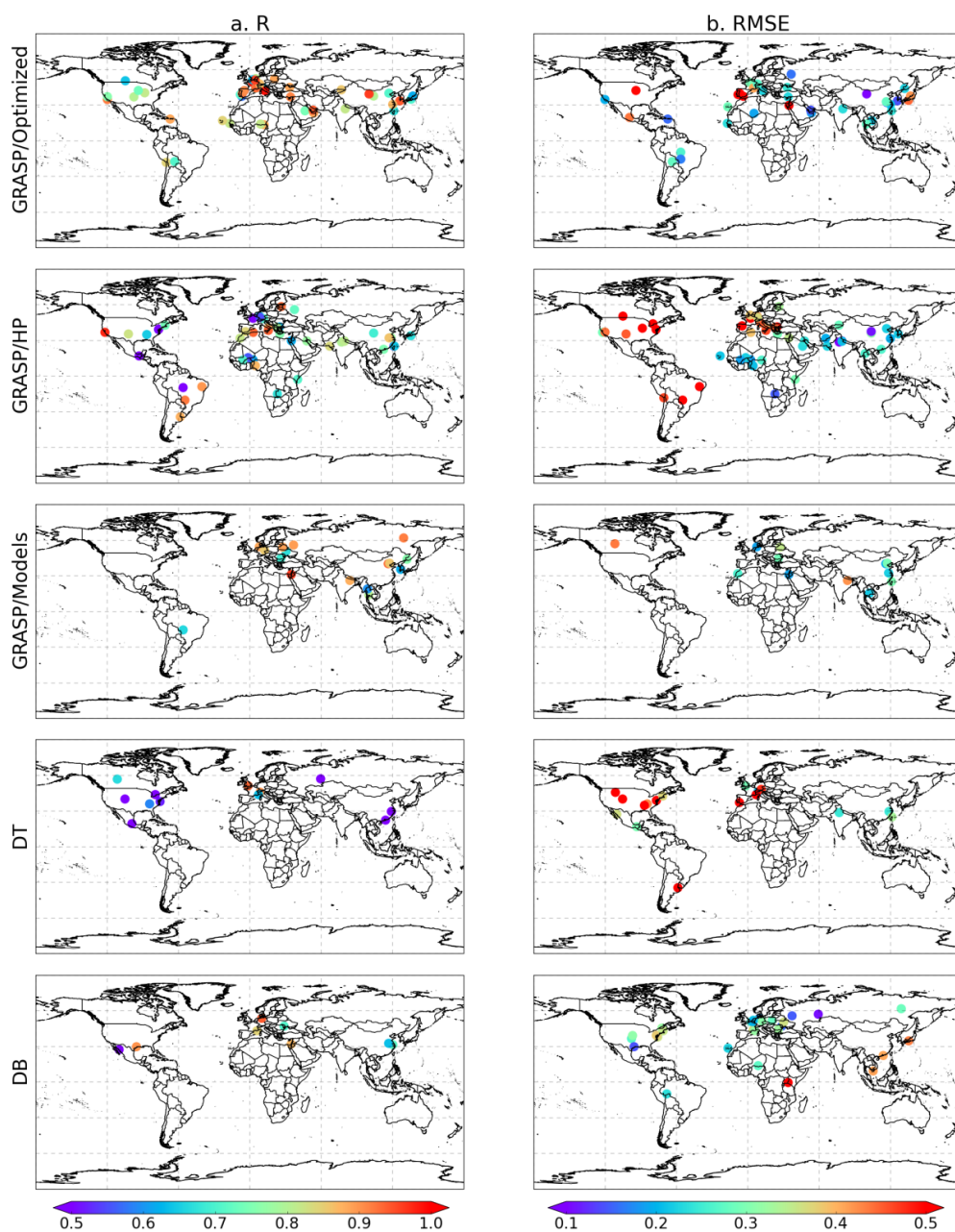


Figure 20: Maps showing statistical metrics (a) R; (b) RMSE; for the best performed AE products 1790 (1st ranking statistics among 5 PARASOL/GRASP and MODIS products) over each AERONET site. Note that only the 1st ranking statistics over each site are present in the maps.

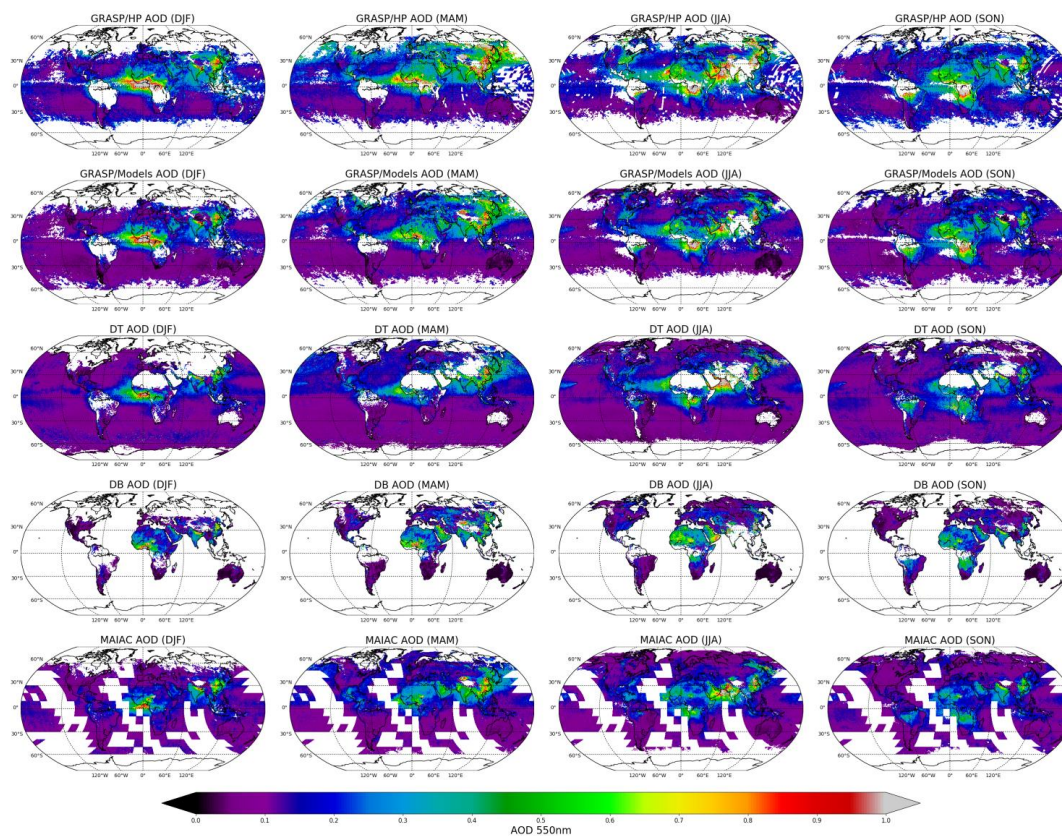


Figure 21: Spatial distribution of $0.1^\circ \times 0.1^\circ$ seasonal AOD (550 nm) from PARASOL (GRASP/HP and GRASP/Models) and MODIS 1795 (DT, DB, and MAIAC) products. DJF – December / January / February; MAM – March / April / May; JJA – June / July / August; SON – September / October / November.

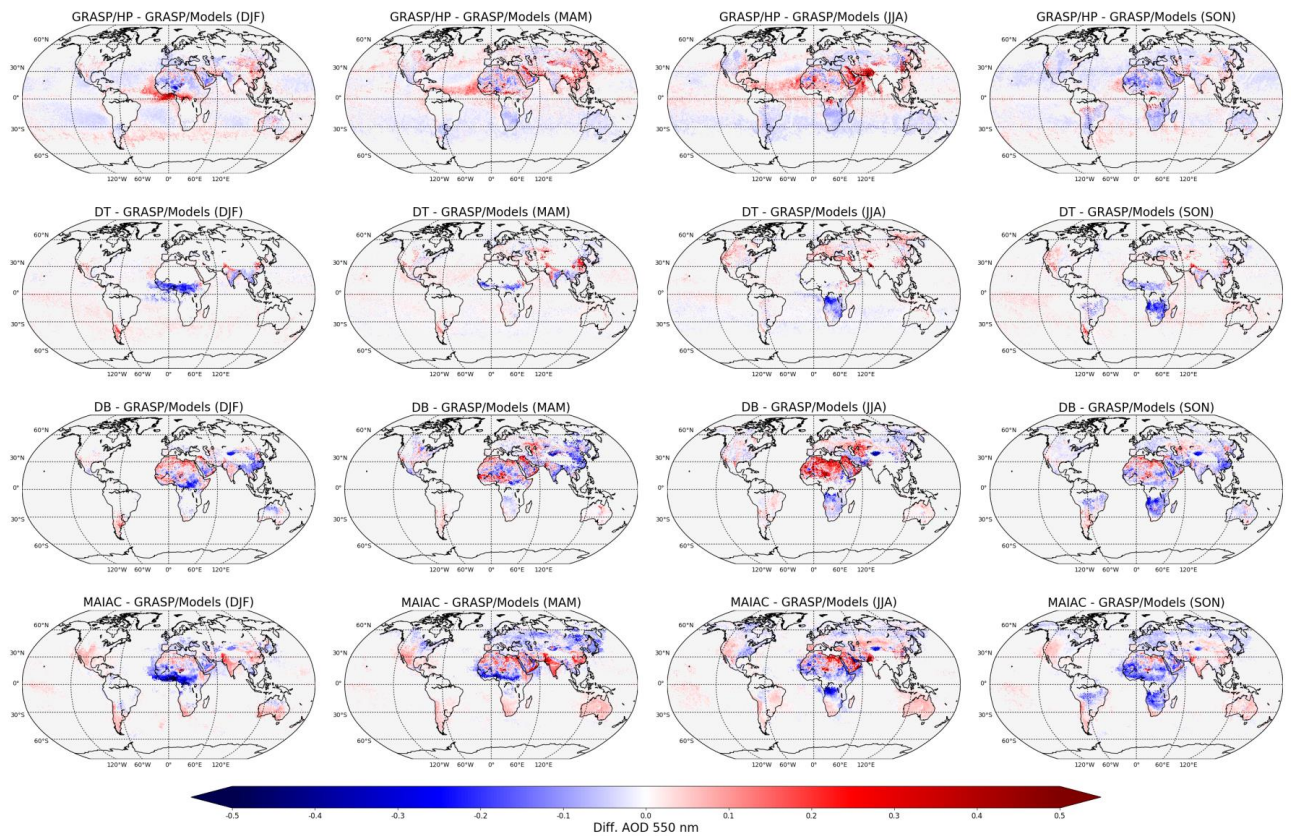
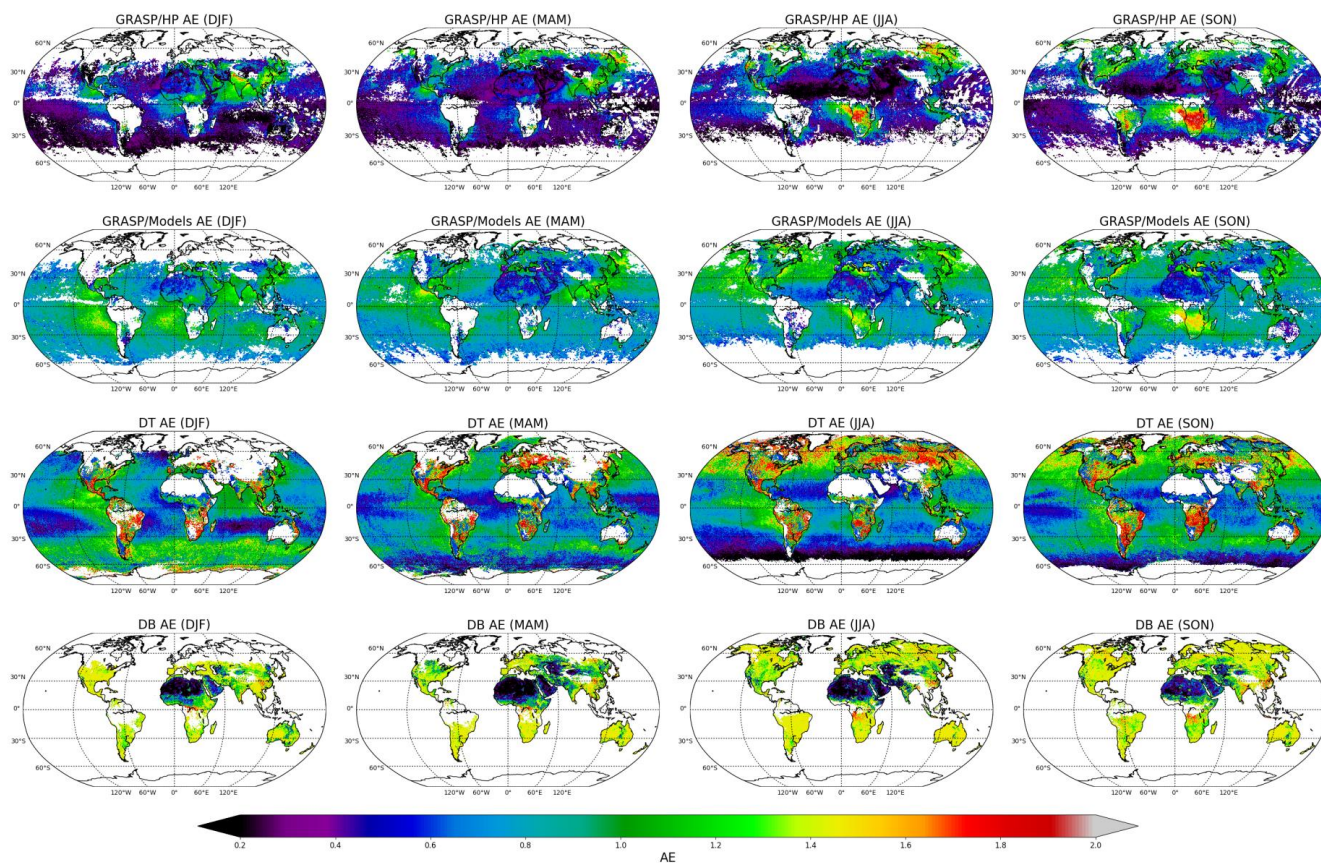


Figure 22: Spatial distribution of $0.1^\circ \times 0.1^\circ$ seasonal AOD (550 nm) differences between PARASOL and MODIS aerosol products, referenced to GRASP/Models.



1800

Figure 23: Spatial distribution of $0.1^\circ \times 0.1^\circ$ seasonal AE from PARASOL (GRASP/HP and GRASP/Models) and MODIS (DT and DB) products.

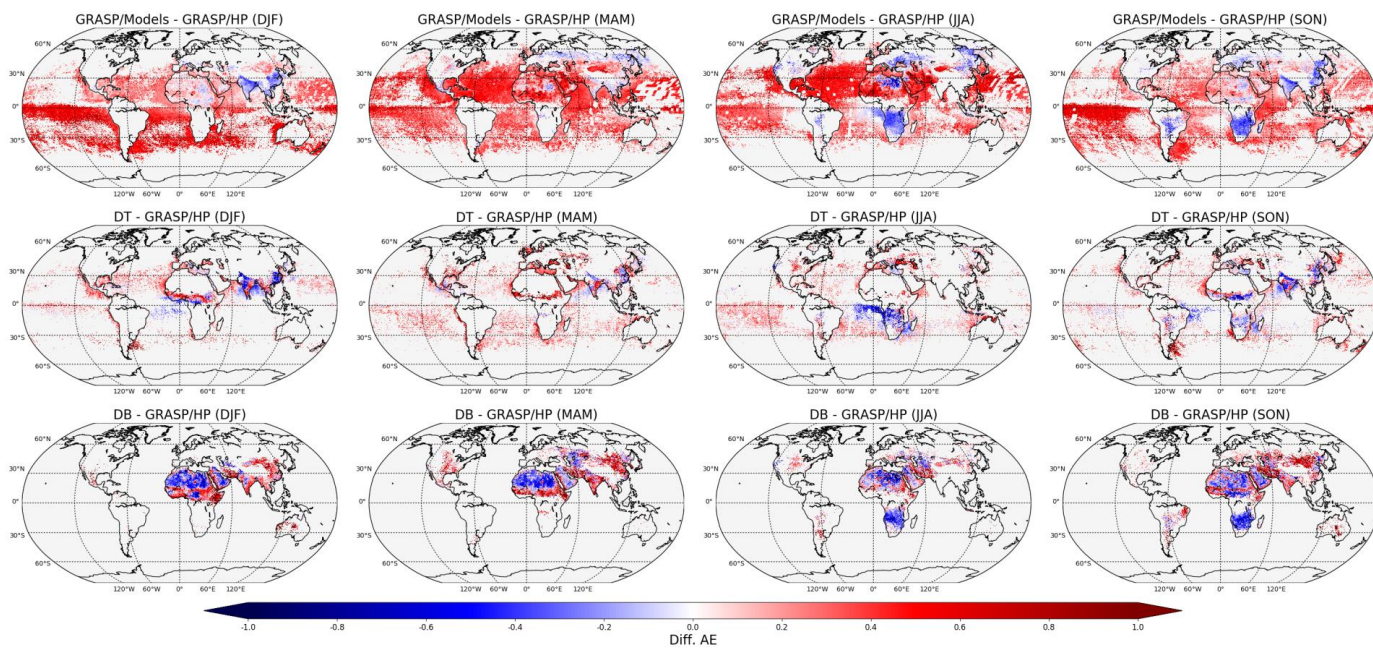
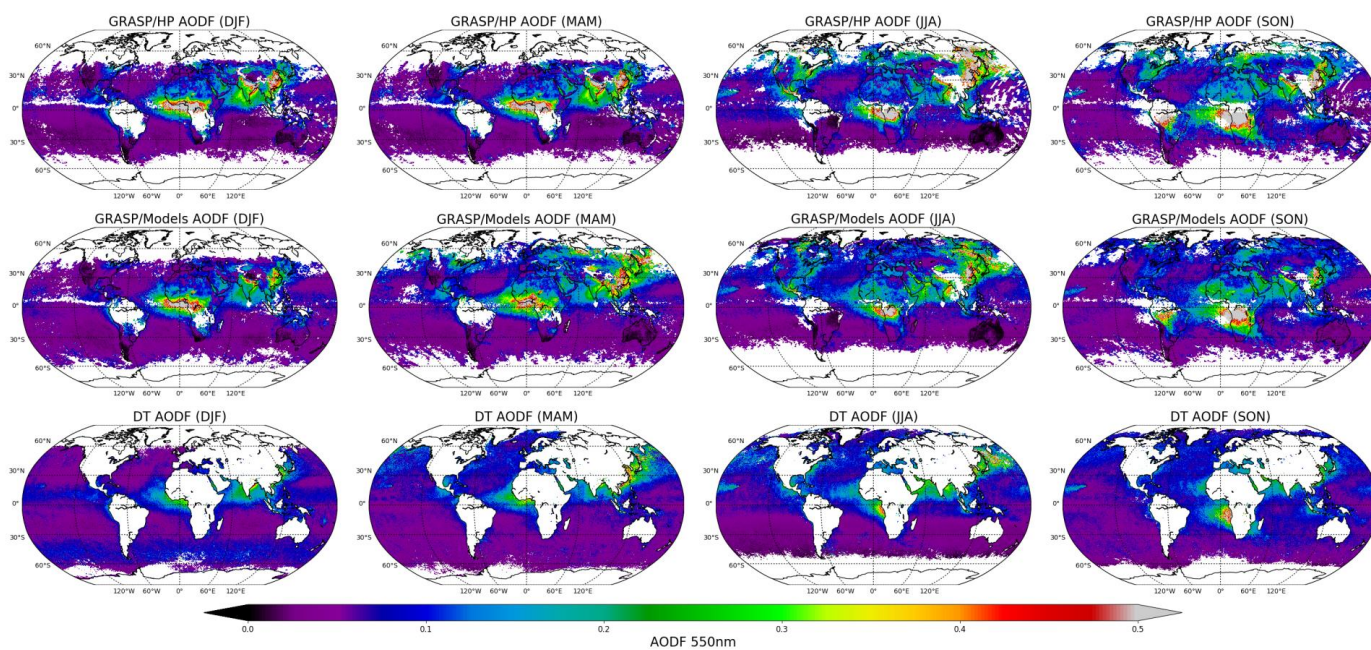


Figure 24: Spatial distribution of seasonal AE differences between PARASOL and MODIS aerosol products, referenced to GRASP/HP.



1805

Figure 25: Spatial distribution of $0.1^\circ \times 0.1^\circ$ seasonal AOD (550 nm) from PARASOL (GRASP/HP and GRASP/Models) and MODIS (DT) products.

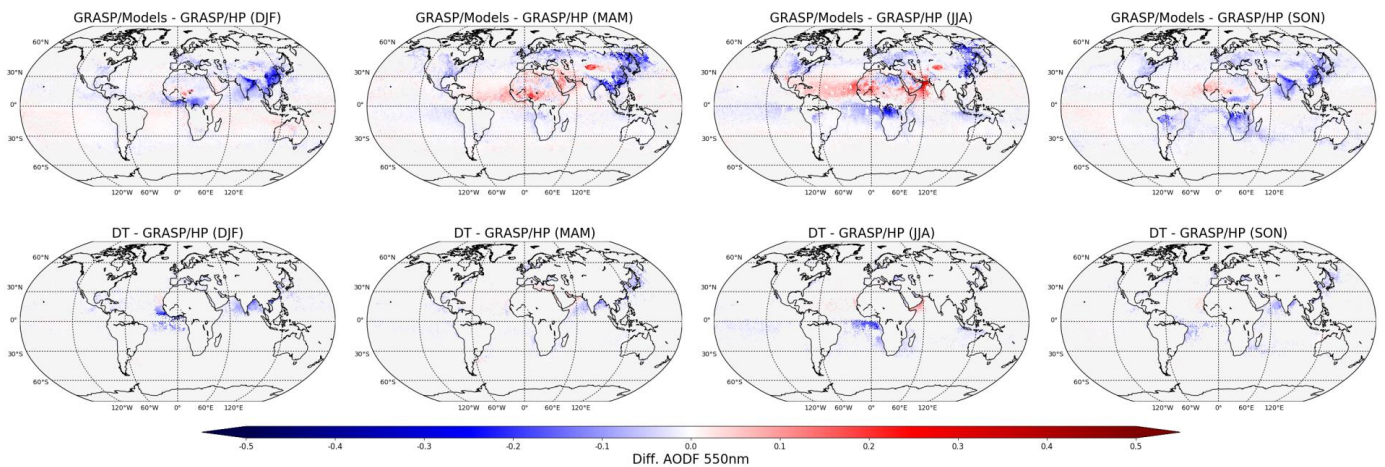


Figure 26: Spatial distribution of seasonal AODF (550 nm) differences between PARASOL and MODIS aerosol products, referenced to 1810 GRASP/HP.

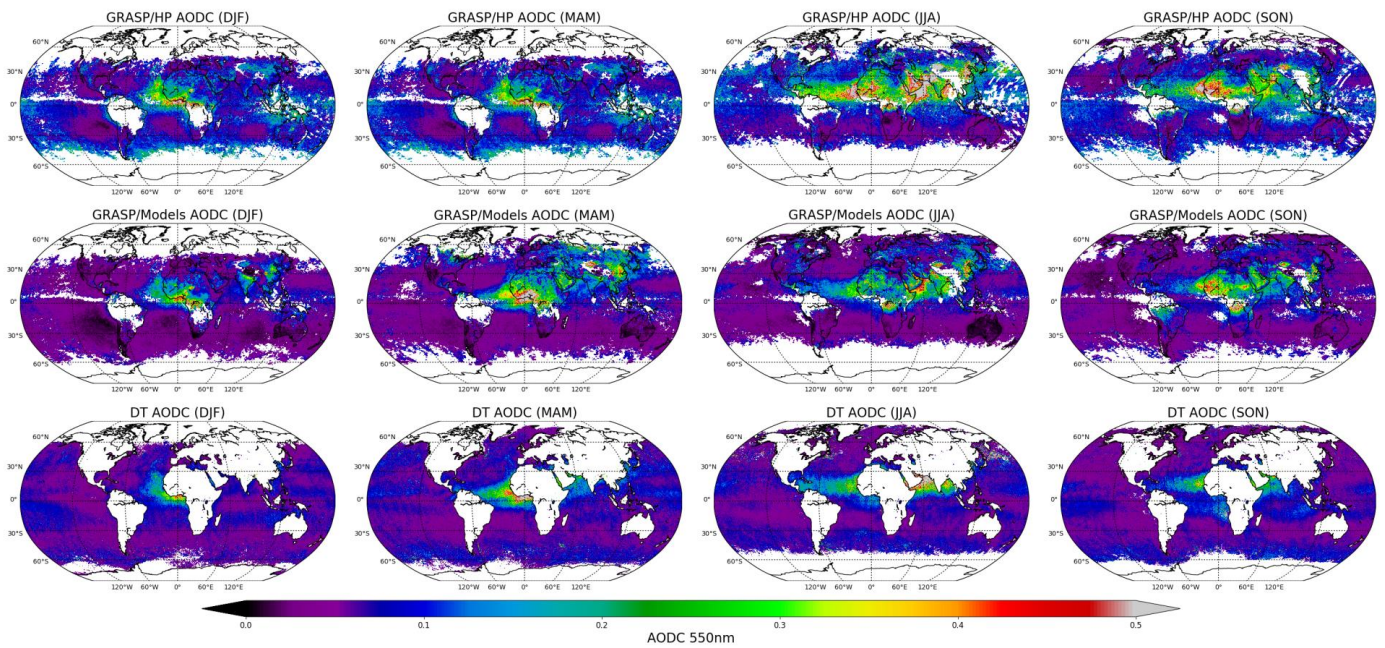


Figure 27: The same as Figure 25, but for AODC (550 nm).

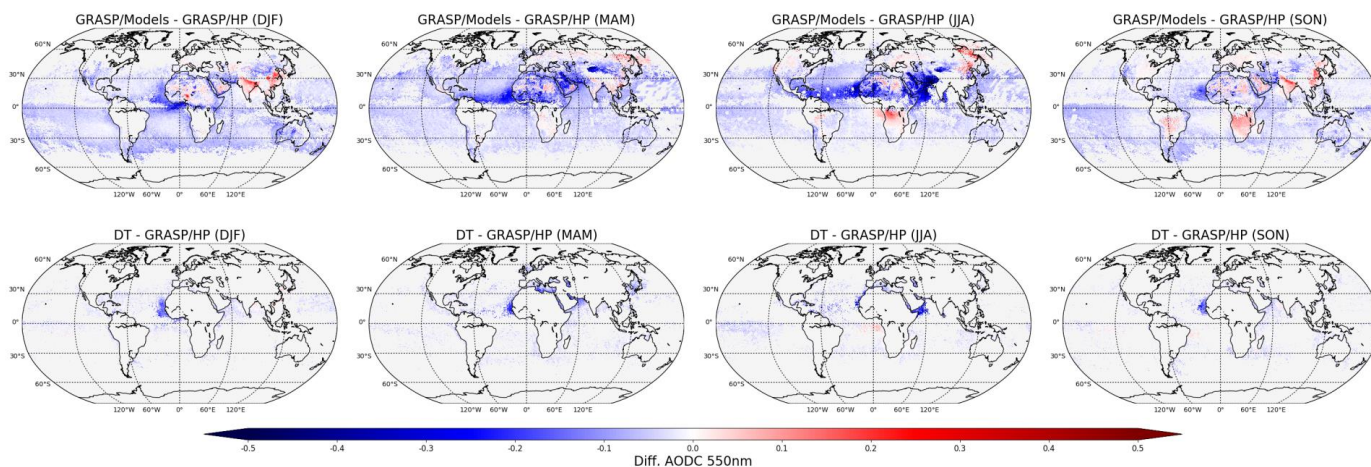


Figure 28: The same as Figure 26, but for AODC (550 nm).

1815